Nuclear quantum effects and geometric isotope effects on small halide-ion-water clusters by path integral molecular dynamics simulations

Qi Wang

June 2013

Nuclear quantum effects and geometric isotope effects on small halide-ion-water clusters by path integral molecular dynamics simulations

Qi Wang

Doctoral Program in Chemistry

Submitted to Graduate School of

Pure and Applied Sciences

in Partial Fulfillment of the Requirements

for the Degree of Doctor of Philosophy in Science

at the

University of Tsukuba

Table of Contents

Chapter 1: General Introduction

The ionic hydrogen bond, which has a stronger intermolecular interaction than typical hydrogen bond, plays an important role at various biological and chemical fields, such as protein folding and proton transport [1-9]. Meanwhile, these hydrogen bonds could help us to understand the important phenomena of ion hydration. Many efforts have been devoted to obtaining the detailed structural information of the halide ion water clusters at molecular level. However, it is often difficult to obtain the accurate ionic hydrogen-bonded structures theoretically, because the ionic hydrogen bonds are coupled with molecular vibration in a complex manner. In addition, the quantum and thermal fluctuation effects, which play important roles in the structures of the ionic hydrogen-bonded clusters, are not taken into count in the conventional molecular orbital calculations.

In this thesis, first, to obtain a potential level with the balance of calculation accuracy and efficiency, I compare the optimized geometries and energetics of fluoride and chloride ion water clusters between semi-empirical methods and high-level *ab initio*/DFT calculations. Next, the PM6-DH+ semi-empirical potential is applied in the following classical molecular dynamics and path integral molecular dynamics simulations. Then nuclear quantum effects and geometric isotope effects on the structures of the ionic hydrogen-bonded clusters are investigated.

1.1. Ionic hydrogen bonded systems

To understand important phenomena of ion hydration at the molecular level, the ionic hydrogen-bonded structure information is indispensable. A typical hydrogen bond is constituted of a proton donor X—H and a proton acceptor Y.

$$X - H \cdots Y \tag{1.1}$$

X or Y should be electronegative atoms, such as the Nitrogen, Oxygen or Fluorine. The hydrogen bonds can occur between molecules, or within different parts of a single molecule.

Many efforts have been devoted to study the strength and energies of hydrogen bonds [10-17].

According to [18], the hydrogen bonds could be approximately classified into three types: strong hydrogen bonds, moderate hydrogen bonds and weak hydrogen bonds. The three types of hydrogen bonds show different binding energies, the H…Y distances and XHY angles, as shown in table 1-1. A strong hydrogen bond has a larger binding energy, shorter H…Y distance, and larger XHY angle. The ionic hydrogen bond is a type of strong hydrogen bonds, which could significantly affect the molecular structure [19, 20]. Thus, in this thesis, I focus on small halide-ion-water clusters as $X^-(H_2O)_n$ (X=F, Cl, n=1-4). For case of X=F, the water molecules are bonded to fluoride ion through strong ionic hydrogen bonds. However, for case of X=Cl, different structures are demonstrated from fluoride case, which is due to the rising cooperation of ion-water and water-water hydrogen bond interactions.

To understand the ionic hydrogen bonded structures at molecular level, there have been many experimental and theoretical studies with respect to halide ion water clusters [21-34]. The neutron diffraction experiments [19, 30, 35, 36] have provided limited structural information of the bond lengths. For example, the average distance between fluoride/chloride and oxygen is 2.6~2.9Å/3.1~3.5Å. In addition, the infrared (IR) spectroscopy has provided very useful information on the vibration motions of the small halide ion water clusters [37-40].

On the other hand, there are many studies on the equilibrium structure and harmonic vibrational analysis with *ab initio* molecular orbital (MO) calculations [22, 31, 41, 42]. The obtained optimized stable structures have been utilized to understand the corresponding experiments. However, it is often difficult to deal with the ionic hydrogen bonded systems with anharmonic and floppy vibrations, because the quantum and thermal fluctuations are not taken into account in conventional MO calculations. Furthermore, the H/D isotopic substitution effect plays important roles in the structure of the hydrogen-bonded systems. For example, the macroscopic properties of water, such as the melting point and the temperature of maximum density (TMD), are increased by 3.8K and 7.2K in D_2O compared with H_2O, respectively. From the microscopic point of view, the neutron diffraction experiments show that intramolecular r(O-D) distance is shorter than r(O-H) by about 0.5%. In addition, the experimental phenomena, such as the redshift in vibrational frequencies, change in reaction rate and the Ubbelohde effect [43, 51], could not be explained by the conventional MO calculations. Instead, the theoretical methods, which consider the nuclear quantum effects, should be applied to understand the H/D substitution effects, such as the geometric isotope effects

induced by the substitution of proton (H) with deuteron (D). The most common used methods are the multi-component molecular orbital (MC_MO) method [52-56], the quantum Monte Carlo (QMC) method [57-68] and the path integral (PI) method [69-87].

The MC_MO method enables us to analyze the nuclear quantum effects in molecular systems, because it simultaneously determines the electronic and nuclear wavefunctions and directly express the H/D isotope effects. The nuclear basis function is assumed to take the form of Gaussian-type functions (GTF), which could be obtained by optimizing the exponent and center of the nuclear GTF using a vibrational procedure to minimize the system energy. For the QMC scheme, under the Born–Oppenheimer (BO) approximation, the nuclear wavefunction is numerically solved on the potential energy surface (PES). Also under BO approximation, the PI simulation combines the PI technique and statistical sampling methods, such as molecular dynamics (MD) and Monte Carlo (MC). Different from MC_MO and QMC, the temperature effects of the system are naturally taken into account by the PI technique, which will be discussed in detail in the next subsection. The PI simulations have the advantage of inclusion both the nuclear quantum effects and the thermal effects, which are important in ionic hydrogen bonded structures. In this thesis, I apply the PI simulations to study the nuclear quantum effects and geometric isotope effects of the small halide-ion-water clusters.

1.2. Path integral formulism

To obtain the physical nature of the quantum systems, an intuitional approach is to solve the Schrödinger equations. The evolution of the wave functions could be calculated with the given Hamiltonian and initial conditions of the system. However, it becomes a formidable task for large dimensional many-body systems due to the increasing difficulties in calculating the eigenvalues for the Hamiltonian. As an alternative solution, a statistical approach was developed by R. P. Feynman in 1948 [79], which is widely known as the PI method.

The PI formulation is a description of quantum theory which generalizes the action principle of classical mechanics. It replaces the classical notion of a single, unique trajectory for a system with a sum over all the possible trajectories to compute the quantum amplitude [88]. In this subsection, I will present the brief

outline of the PI formulation.

In the canonical ensemble, which is also called NVT ensemble, the density matrix in the position presentation takes the form,

$$\rho(\boldsymbol{r},\boldsymbol{r}';\beta) =< \boldsymbol{r}|e^{-\beta \boldsymbol{H}}|\boldsymbol{r}' >, \tag{1.2}$$

where β=1/kT, **r** and **r**' represents the initial and final position of the particle. **H** is the Hamiltonian.

Then the partition function Z(β), which determines the thermodynamics of the system, is expressed as the trace of the density matrix at finite temperature T,

$$Z(\beta) = Tr(\rho) = \int d\boldsymbol{r} < \boldsymbol{r}|e^{-\beta \boldsymbol{H}}|\boldsymbol{r} >, \tag{1.3}$$

Now let us consider a single quantum particle, which has mass m, momentum **p**, and coordinate **r**. The Hamiltonian reads,

$$\boldsymbol{H} = \boldsymbol{K} + \boldsymbol{V} = \frac{\boldsymbol{p}^2}{2m} + V(\boldsymbol{r}) \tag{1.4}$$

where **K** and **V** are kinetic and potential operators, respectively. Then the partition function could be expressed as,

$$Z(\beta) = \int d\boldsymbol{r} < \boldsymbol{r}|e^{-\beta(\boldsymbol{K}+\boldsymbol{V})}|\boldsymbol{r} > \tag{1.5}$$

Generally, the operators **K** and **V** do not commute with each other, so that the exponential exp[-β(**K**+**V**)] could not be calculated directly. However, by using the famous Trotter theorem [18, 99-101], any two operators have the following rule,

$$e^{\lambda(\boldsymbol{A}+\boldsymbol{B})} = \lim_{P\to\infty}\left(e^{\frac{\lambda}{2P}\boldsymbol{B}} e^{\frac{\lambda}{P}\boldsymbol{A}} e^{\frac{\lambda}{2P}\boldsymbol{B}}\right)^P \tag{1.6}$$

For simplicity, let us define a new operator,

$$\boldsymbol{\Omega} = e^{-\frac{\lambda}{2P}\boldsymbol{V}} e^{-\frac{\lambda}{P}\boldsymbol{K}} e^{-\frac{\lambda}{2P}\boldsymbol{V}} \tag{1.7}$$

By applying the completeness relation of the coordinate **r**,

$$I = \int d\boldsymbol{r}|\boldsymbol{r} >< \boldsymbol{r}| \tag{1.8}$$

The partition function can be rewritten as,

$$\begin{aligned} Z(\beta) &= \lim_{P\to\infty} \int d\boldsymbol{r} < \boldsymbol{r}|\Omega^P|\boldsymbol{r} > \\ &= \lim_{P\to\infty} \int d\boldsymbol{r}_1 \cdots \boldsymbol{r}_P \left[\prod_{i=1}^{P} < \boldsymbol{r}_i|\Omega|\boldsymbol{r}_{i+1} >\right]_{\boldsymbol{r}_{i+1}=\boldsymbol{r}_1} \end{aligned} \tag{1.9}$$

Here the condition $\boldsymbol{r}_{i+1} = \boldsymbol{r}_1$ is as a result of the trace. The partition function $Z(\beta)$ could be determined by the evaluating the matrix elements of $< \boldsymbol{r}_i|\Omega|\boldsymbol{r}_{i+1} >$.

By using the completeness relation of the momentum **p**,

$$I = \int d\boldsymbol{p}|\boldsymbol{p} >< \boldsymbol{p}| \tag{1.10}$$

And the relation for the inner product of coordinate and momentum eigen-states,

$$< \boldsymbol{r}|\boldsymbol{p} >= (2\pi\hbar)^{-\frac{3}{2}} e^{i\boldsymbol{p}\cdot\boldsymbol{r}/\hbar} \tag{1.11}$$

The expression for the matrix elements could be derived as,

$$< \boldsymbol{r}_i|\Omega|\boldsymbol{r}_{i+1} >= \left(\frac{mP}{2\pi\hbar^2\beta}\right)^{3/2} exp[-\frac{mP}{2\hbar^2\beta}(\boldsymbol{r}_{i+1} - \boldsymbol{r}_i)^2 - \frac{\beta}{2P}(V(\boldsymbol{r}_{i+1}) + V(\boldsymbol{r}_i))] \tag{1.12}$$

Finally, the partition function of canonical systems for single quantum particle is obtained as

$$Z(\beta) = \lim_{P\to\infty} \left(\frac{mP}{2\pi\hbar^2\beta}\right)^{\frac{3P}{2}} \int d\boldsymbol{r}_1 \cdots \boldsymbol{r}_P \, exp\left\{-\beta \sum_{i=1}^{P} \left[\frac{mP}{2\hbar^2\beta^2}(\boldsymbol{r}_{i+1} - \boldsymbol{r}_i)^2 + \frac{1}{P}V(\boldsymbol{r}_i)\right]\right\} \tag{1.13}$$

For the case of Boltzmann statistics, the exchange terms could be safely ignored. The above equation could be easily generalized into N particles in three dimensions with the following Hamiltonian,

$$\boldsymbol{H} = \sum_{k=1}^{N} \frac{\boldsymbol{p}_k^2}{2m_k} + V(\boldsymbol{r}_1, \boldsymbol{r}_2, \cdots, \boldsymbol{r}_N) \tag{1.14}$$

The partition function of canonical systems for N quantum particle takes the form,

$$Z(N,V,T) = \lim_{P\to\infty} Z_P = \lim_{P\to\infty} \prod_{k=1}^{N} \left(\frac{m_k P}{2\pi\hbar^2\beta}\right)^{3P/2} \int \prod_{k=1}^{N} d\,\boldsymbol{r}_k^1 \cdots \boldsymbol{r}_k^P \, exp\{-\beta\Phi\}, \tag{1.15}$$

Here let k index the particles and i index the imaginary-time intervals. The effective potential Φ takes

the form,

$$\Phi = \sum_{k=1}^{N}\sum_{i=1}^{P}\frac{m_k P}{2\hbar^2\beta^2}(\boldsymbol{r}_k^{i+1} - \boldsymbol{r}_k^{i})^2 + \frac{1}{P}\sum_{i=1}^{P} V(\boldsymbol{r}_1^{i}, \cdots, \boldsymbol{r}_N^{i}), \tag{1.16}$$

From the above equation, the effective potential Φ is composed of two parts. The first term corresponds to a cyclic polymer, which are connected by harmonic springs. Since the cyclic polymer resembles a necklace, its P points are also referred to as "beads". The second term represents the interactions of the nucleus. Note that only beads with the same imaginary-time index on different chains interact with each other. The schematic illustration of the interaction pattern between two quantum particles is shown in Fig. 1-1 [92].

Since it is usually difficult to obtain the analytical results of Z_P caused by the complex interactions in molecular systems, the numerical implement of PI with finite number of beads P is quite necessary. The MD or MC method could be applied to make sampling of the canonical ensemble. Next, the numerical evaluation of PI will be realized through the MD approach. By recasting the prefactor in Z_P as a set of Gaussian integrals for $\mathbf{p_1}$, …, $\mathbf{p_N}$, the form of the classical canonical partition function will be obtained,

$$Z_P = \prod_{i=1}^{P}\int\prod_{k=1}^{N} d\,\boldsymbol{r}_k^1 \cdots \boldsymbol{r}_k^P \int\prod_{k=1}^{N} d\,\boldsymbol{p}_k^1 \cdots \boldsymbol{p}_k^P exp\{-\beta \mathrm{H}_{eff}\}, \tag{1.17}$$

Where the effective potential takes the form,

$$H_{eff} = \sum_{i=1}^{P}\frac{\boldsymbol{p_i^2}}{2m_i'} + \Phi \tag{1.18}$$

Here the parameter *m'* appearing in Gaussian integrals is given by $m' = mP/(2\pi\hbar)^2$. Note that the index of *m'* is from 1 to P, which is different from Eq. (1.15). Thus the equilibrium properties of quantum system could be simulated using the classical equations of motion

$$\begin{aligned} \frac{d\boldsymbol{r}_i}{dt} &= \frac{\partial H_{eff}}{\partial \boldsymbol{p}_i} = \frac{\boldsymbol{p}_i}{m_i'} \\ \frac{d\boldsymbol{p}_i}{dt} &= -\frac{\partial H_{eff}}{\partial \boldsymbol{r}_i} = -\frac{m_i P}{\hbar^2\beta^2}(2\boldsymbol{r}_i - \boldsymbol{r}_{i+1} - \boldsymbol{r}_{i-1}) - \frac{1}{P}\frac{\partial \Phi}{\partial \boldsymbol{r}_i}, \end{aligned} \tag{1.19}$$

The equations of motion could be integrated with a given initial state. If the system is ergodic, the

averages of estimators over these ergodic trajectories could give the corresponding thermodynamical properties of the quantum system.

For example, the average of total energy <E> could be obtained through a primitive estimator,

$$< E >_{primitive} = -\frac{1}{Z_P}\frac{\partial Z_P}{\partial \beta}$$
$$= \frac{3NP}{2\beta} + < \sum_{k=1}^{N}\sum_{i=1}^{P} -\frac{m_k P}{2\hbar^2\beta^2}(\boldsymbol{r}_k^{i+1} - \boldsymbol{r}_k^i)^2 + \frac{1}{P}\sum_{i=1}^{P} V(\boldsymbol{r}_1^i, \cdots, \boldsymbol{r}_N^i) > \quad (1.20)$$

On the other hand, it is better to make the energy estimator be independent of number of beads P for numerical calculations. Thus the virial estimator [76, 93] for total energy could be used,

$$< E >_{virial} = \frac{3N}{2\beta} + \frac{1}{P} < \sum_{k=1}^{N}\sum_{i=1}^{P} \frac{1}{2}(\boldsymbol{r}_k^i - \boldsymbol{r}_k^c) \cdot \nabla_k^i V(\boldsymbol{r}_1^i, \cdots, \boldsymbol{r}_N^i) + \frac{1}{P}\sum_{i=1}^{P} V(\boldsymbol{r}_1^i, \cdots, \boldsymbol{r}_N^i) > \quad (1.21)$$

For the simulation of molecular systems, it is reasonable to apply the Born-Oppenheimer (BO) approximation to separate the electronic and nuclear motions. The electronic ground state potential and its derivative could be evaluated by *ab initio* MO calculations. Then the nuclear motion could be simulated on the electronic ground state potential surface within the framework of PI presentations. This method called as *ab initio* path integral (AIPI) technique, which are discussed in detail in [70, 74, 75, 94, 95]. With the increasing development of modern parallel calculation technique, the PI formulation has been successfully implemented into the molecular systems with light mass atoms [92].

From the numerical point of view, finite number of beads P is applied. The above obtained partition function and the corresponding effective potential are retained to the second order expansion of Eq. (1.6) by Trotter theorem. High-order PI schemes have also been discussed in [77, 96, 97]. However, additional calculations for Hessian matrix are required, which may dramatically increase the computational cost. Thus the second order PI scheme is applied in my study. On the other hand, the normal mode transformation could be applied to the coordinate **r** to decouple the coupling terms in the effective potential [78, 98-101]. The transformation increases the efficiency of simulating the ergodicity of the system. The Nosé-Hoover chain technique [102-105] is applied to control the temperature of the canonical ensemble. The flow chart of the PIMD algorithm is shown in Fig. 1-2.

1.3. The contents of the thesis

There have been AIPI simulations with respect to the geometric isotope effects on fluoride ion water clusters in the previous study [97]. However, the chloride ion water clusters show quite different structural feature from the case of fluoride due to its relative weaker ionic hydrogen bonds, which are close to the water-water hydrogen bond interactions. Thus, in this thesis, I applied classical MD and PIMD simulations to study the nuclear quantum effects and geometric isotope effects on the ionic hydrogen bonded structures of small halide-ion-water clusters. The thesis is organized as follows.

In the chapter 2, the optimized geometries and stabilization energies of fluoride and chloride ion water clusters are compared between semi-empirical methods and high-level *ab initio*/DFT calculations. Despite the successful application of *ab initio*/DFT PIMD simulations into small charged clusters, it is still a forbidden task for systems with large size or with floppy structures, which require long simulation time to reach statistical convergence. As a compromise solution, the semi-empirical potentials could be applied for the sake of calculation efficiency. First, the global minima structures are examined. For X=F, the semi-empirical PM6-DH+ method shows that the global minima are close to $HF(OH)^-(H_2O)_{n-1}$ structures, which are different from *ab initio*/DFT calculations. However, the topological characteristics for the global minima of X=Cl obtained by semi-empirical method have the same symmetries with *ab initio*/DFT calculations. On the other hand, the PM6-DH+ method show consistent results of stabilization energies with high-level *ab initio*/DFT calculations as well as the corresponding experiments for both X=F and Cl. Thus it is reasonable to use PM6-DH+ potential to investigate the nuclear quantum effects and geometric isotope effects on $Cl^-(H_2O)_n$ clusters by comparison of classical MD and PIMD simulations.

In the chapter 3, the nuclear quantum effects on the rearrangement of single and multi hydration shell structures of $Cl^-(H_2O)_{1-4}$ clusters are discussed. According to the previous studies, the structures of $F^-(H_2O)_{1-4}$ clusters are vibrating near the local minimum of potential energy surfaces, which is due to the formation of strong ionic hydrogen bonds. However, the $Cl^-(H_2O)_{1-4}$ clusters show quite different behavior, since their structures are rather flexible and the rearrangement of ion-water and water-water hydrogen bond network is quite frequent within the simulation time. First, to show the rearrangement of single and multi hydration shell cluster structures, the r^1(Cl…O) coordinate is selected at each time step, which stands for the longest

r(Cl…O) distance in $Cl^-(H_2O)_n$ clusters (n>2). The r^l(Cl…O) distance, which is larger than r_0, can be viewed as an intuitive proof for the existence of multi hydration shell cluster structures. The results show that the probability for the multi shell structures is increasing with cluster size. Second, to describe the changing of bonded H* atom to the chloride ion, I define a new coordinate δ. For the two hydrogen atoms H_1 and H_2 in the same water molecule of the first hydration shell, δ represents the relative position of H_1 and H_2 atoms pointing towards the chloride ion. Since larger δ corresponds to stronger ionic hydrogen bond, it could be viewed as a measure of ionic hydrogen bond strength. The correlations between δ and other cluster vibration motions are also discussed with an emphasis on nuclear quantum effect. The results indicate the vibration motions affected by the ion are weakened by nuclear quantum effect, which results from the preference of water-water hydrogen bond interactions by quantum simulation.

In the chapter 4, the geometric isotope effects on $Cl^-(H_2O)_n$ clusters are discussed through carrying out classical MD and PIMD simulations. The geometric isotope effects are shown to be important in hydrogen-bonded systems, since strong quantum behavior is exhibited for the light atom at low temperature or even at room temperature. First, I show the geometric isotope effects on structural rearrangement of single and multi hydration shell cluster structures. The proportion of single/multi shell structures is decreased/increased for quantum simulations of H and D in comparison of the corresponding classical simulations. However, it is interesting to find that the results of D(qu) are more favored than H(qu) for multi shell structures. The results indicate D(qu) favors water-water hydrogen bond network, which are due to the decrease of zero-point energy (ZPE) corrections by heavier mass of D. Next I show the geometric isotope effects on the two competitive nuclear quantum effects. The intramolecular zero-point energy effect tends to stabilize the hydrogen bond network, while the intermolecular nuclear quantum effect disrupts the hydrogen bond network. Thus they are discussed in the intramolecular r(O-Y*) stretching and intermolecular ion-water wagging motions for single and multi hydration shell structures, respectively. In addition, the geometric isotope effects on the correlations between ion-water stretching motion and other cluster vibration coordinates are discussed for single and multi shell structures, respectively.

Finally, I will draw the general conclusions in Chapter 5.

References in Chapter1:

[1] C. L. Perrin, J. B. Nielson, *Annu. Rev. Phys. Chem.* **48**, 511-544 (1997).

[2] G. C. Pimentel, M. Al, *Annu. Rev. Phys. Chem.* **22**, 347 (1971).

[3] K. M. Lange, R. Konnecke, M. Soldatov, R. Golnak, J. E. Rubensson, A. Soldatov, E. F. Aziz, *Angew. Chem. Int. Ed.* **50**, 10621-10625 (2011).

[4] R. Ludwig, *Angew. Chem. Int. Ed.* **40**, 1808-1827 (2001).

[5] J. M. Ugalde, I. Alkorta, J. Elguero, *Angew. Chem. Int. Ed.* **39**, 717-721 (2000).

[6] K. Liu, J. D. Cruzan, R. J. Saykally, *Science* **271**, 929-933 (1996).

[7] C. Desfrancois, S. Carles, J. P. Schermann, *Chem. Rev.* **100**, 3943-3962 (2000).

[8] S. Rajagopal, S. Vishveshwara, *FEBS J.* **272**, 1819-1832 (2005).

[9] J. Cerny, P. Hobza, *Phys. Chem. Chem. Phys.* **9**, 5291-5303 (2007).

[10] S. J. Grabowski, *J. Mol. Struct.* **562**, 137-143 (2001).

[11] S. J. Grabowski, *Chem. Phys. Lett.* **338**, 361-366 (2001).

[12] B. G. Oliveira, F. S. Pereira, R. De Araujo, M. N. Ramos, *Chem. Phys. Lett.* **427**, 181-184 (2006).

[13] M. M. Deshmukh, S. R. Gadre, L. J. Bartolotti, *J. Phys. Chem. A* **110**, 12519-12523 (2006).

[14] M. Jablonski, A. Kaczmarek, A. J. Sadlej, *J. Phys. Chem. A* **110**, 10890-10898 (2006).

[15] S. J. Grabowski, *J. Phys. Org. Chem.* **17**, 18-31 (2004).

[16] C. L. Sun, C. S. Wang, *J. Mol. Struc.-TheoChem* **956**, 38-43 (2010).

[17] K. Wendler, J. Thar, S. Zahn, B. Kirchner, *J. Phys. Chem. A* **114**, 9529-9536 (2010).

[18] T. Steiner, *Angew. Chem. Int. Ed.* **41**, 48-76 (2002).

[19] H. Ohtaki, T. Radnai, *Chem. Rev.* **93**, 1157-1204 (1993).

[20] Y. Marcus, *Chem. Rev.* **109**, 1346-1370 (2009).

[21] D. D. Kemp, M. S. Gordon, *J. Phys. Chem. A* **109**, 7688-7699 (2005).

[22] J. Kim, H. M. Lee, S. B. Suh, D. Majumdar, K. S. Kim, *J. Chem. Phys.* **113**, 5259-5272 (2000).

[23] W. H. Robertson, M. A. Johnson, *Annu. Rev. Phys. Chem.* **54**, 173-213 (2003).

[24] L. S. Sremaniak, L. Perera, M. L. Berkowitz, *J. Phys. Chem.* **100**, 1350-1356 (1996).

[25] S. Roszak, M. Kowal, R. W. Gora, J. Leszczynski, *J. Chem. Phys.* **115**, 3469-3473 (2001).

[26] H. M. Lee, D. Kim, K. S. Kim, *J. Chem. Phys.* **116**, 5509-5520 (2002).

[27] A. V. Egorov, E. N. Brodskaya, A. Laaksonen, *J. Chem. Phys.* **118**, 6380-6386 (2003).

[28] R. Ayala, J. M. Martinez, R. R. Pappalardo, E. S. Marcos, *J. Chem. Phys.* **119**, 9538-9548 (2003).

[29] D. H. Herce, L. Perera, T. A. Darden, C. Sagui, *J. Chem. Phys.* **122**, 24513 (2005).

[30] J. M. Lisy, *J. Chem. Phys.* **125**, 132302 (2006).

[31] D. Majumdar, J. Kim, K. S. Kim, *J. Chem. Phys.* **112**, 101-105 (2000).

[32] L. Perera, M. L. Berkowitz, *J. Chem. Phys.* **99**, 4222-4224 (1993).

[33] P. Jungwirth, D. J. Tobias, *J. Phys. Chem. B* **106**, 6361-6373 (2002).

[34] A. Tongraar, B. M. Rode, *Phys. Chem. Chem. Phys.* **5**, 357-362 (2003).

[35] Y. Marcus, *Chem. Rev.* **88**, 1475-1498 (1988).

[36] I. Harsanyi, L. Temleitner, B. Beuneu, L. Pusztai, *J. Mol. Liq.* **165**, 94-100 (2012).

[37] J. H. Choi, K. T. Kuwata, Y. B. Cao, M. Okumura, *J. Phys. Chem. A* **102**, 503-507 (1998).

[38] P. Ayotte, G. H. Weddle, J. Kim, M. A. Johnson, *J. Am. Chem. Soc.* **120**, 12361-12362 (1998).

[39] B. F. Yates, H. F. Schaefer, T. J. Lee, J. E. Rice, *J. Am. Chem. Soc.* **110**, 6327-6332 (1988).

[40] W. H. Robertson, E. G. Diken, E. A. Price, J. W. Shin, M. A. Johnson, *Science* **299**, 1367-1372 (2003).

[41] G. M. Chaban, S. S. Xantheas, R. B. Gerber, *J. Phys. Chem. A* **107**, 4952-4956 (2003).

[42] J. Baik, J. Kim, D. Majumdar, K. S. Kim, *J. Chem. Phys.* **110**, 9116-9127 (1999).

[43] T. Strassner, *Angew. Chem. Int. Ed.* **45**, 6420-6421 (2006).

[44] M. Ceriotti, T. E. Markland, *J. Chem. Phys.* **138**, 14112 (2013).

[45] E. G. Noya, C. Vega, L. M. Sese, R. Ramirez, *J. Chem. Phys.* **131**, 124518 (2009).

[46] A. Zeidler, P. S. Salmon, H. E. Fischer, J. C. Neuefeind, J. M. Simonson, T. E. Markland, *J. Phys. Condens. Matter* **24**, 284126 (2012).

[47] C. P. Herrero, R. Ramirez, *J. Chem. Phys.* **134**, 94510 (2011).

[48] R. Ramirez, C. P. Herrero, *J. Chem. Phys.* **133**, 144511 (2010).

[49] C. Vega, M. M. Conde, C. Mcbride, J. Abascal, E. G. Noya, R. Ramirez, L. M. Sese, *J. Chem. Phys.* **132**, 46101 (2010).

[50] M. Tachikawa, M. Shiga, *J. Chem. Phys.* **121**, 5985-5991 (2004).

[51] W. A. Van Hook, *NUKLEONIKA* **56**, 217-240 (2011).

[52] M. Tachikawa, K. Mori, H. Nakai, K. Iguchi, *Chem.l Phys. Lett.* **290**, 437-442 (1998).

[53] T. Ishimoto, M. Tachikawa, U. Nagashima, *Int. J. Quantum Chem.* **108**, 472-481 (2008).

[54] T. Ishimoto, M. Tachikawa, U. Nagashima, *Int. J. Quantum Chem.* **109**, 2677-2694 (2009).

[55] Y. Itou, S. Mori, T. Udagawa, M. Tachikawa, T. Ishimoto, U. Nagashima, *J. Phys. Chem. A* **111**, 261-267 (2006).

[56] T. Ishimoto, M. Tachikawa, U. Nagashima, *J. Chem. Phys.* **128**, 164118 (2008).

[57] D. M. Ceperley, *Adv. Chem. Phys.* **93**, 1-38 (1996).

[58] A. Aspuru-Guzik, W. A. Lester, *Adv. Quantum Chem.* **49**, 209-226 (2005).

[59] A. Luchow, J. B. Anderson, *Annu Rev Phys Chem* **51**, 501-526 (2000).

[60] B. M. Austin, D. Y. Zubarev, W. A. Lester, *Chem Rev* **112**, 263-288 (2012).

[61] P. Galek, N. C. Handy, W. A. Lester, *Mol Phys* **104**, 3069-3085 (2006).

[62] W. Foulkes, L. Mitas, R. J. Needs, G. Rajagopal, *Rev. Mod. Phys.* **73**, 33-83 (2001).

[63] A. Lüchow, *WIREs Comput Mol Sci* **1**, 388-402 (2011).

[64] K. A. L. M. Jindřich, *Rep. Prog. Phys.* **74**, 26502 (2011).

[65] M. A. Morales, J. Mcminis, B. K. Clark, J. Kim, G. E. Scuseria, *J. Chem. Theory Comput.* **8**, 2181-2188 (2012).

[66] M. C. Per, K. A. Walker, S. P. Russo, *J. Chem. Theory Comput.* **8**, 2255-2259 (2012).

[67] E. Coccia, O. Chernomor, M. Barborini, S. Sorella, L. Guidoni, *J. Chem. Theory Comput.* **8**, 1952-1962 (2012).

[68] M. Barborini, S. Sorella, L. Guidoni, *J. Chem. Theory Comput.* **8**, 1260-1269 (2012).

[69] B. J. Berne, D. Thirumalai, *Annu. Rev. Phys. Chem.* **37**, 401-424 (1986).

[70] M. Shiga, M. Tachikawa, S. Miura, *Chem. Phys. Lett.* **332**, 396-402 (2000).

[71] M. H. Muser, *Comput. Phys. Commun.* **147**, 83-86 (2002).

[72] M. J. Gillan, F. Christodoulos, *Int. J. Mod. Phys. C* **4**, 287-297 (1993).

[73] C. Chakravarty, *Int. Rev. Phys. Chem.* **16**, 421-444 (1997).

[74] M. Shiga, M. Tachikawa, S. Miura, *J. Chem. Phys.* **115**, 9149-9159 (2001).

[75] D. Marx, M. Parrinello, *J. Chem. Phys.* **104**, 4077-4082 (1996).

[76] M. F. Herman, E. J. Bruskin, B. J. Berne, *J. Chem. Phys.* **76**, 5150-5155 (1982).

[77] A. Perez, M. E. Tuckerman, *J. Chem. Phys.* **135**, 64104 (2011).

[78] M. E. Tuckerman, B. J. Berne, G. J. Martyna, M. L. Klein, *J. Chem. Phys.* **99**, 2796-2808 (1993).

[79] R. P. Feynman, *Rev. Mod. Phys.* **20**, 367 (1948).

[80] R. Lambert, N. Makri, *J. Chem. Phys.* **137**, 22A-553A (2012).

[81] R. Lambert, N. Makri, *J. Chem. Phys.* **137**, 22A-552A (2012).

[82] S. L. Mielke, D. G. Truhlar, *J. Chem. Theory Comput.* **8**, 1589-1596 (2012).

[83] H. Engel, D. Doron, A. Kohen, D. T. Major, *J. Chem. Theory Comput.* **8**, 1223-1234 (2012).

[84] S. L. Mielke, D. G. Truhlar, *J. Chem. Theory Comput.* **8**, 1589-1596 (2012).

[85] P. Dopieralski, C. L. Perrin, Z. Latajka, *J. Chem. Theory Comput.* **7**, 3505-3513 (2011).

[86] A. Pe Rez, O. A. Von Lilienfeld, *J. Chem. Theory Comput.* **7**, 2358-2369 (2011).

[87] A. Azuri, H. Engel, D. Doron, D. T. Major, *J. Chem. Theory Comput.* **7**, 1273-1286 (2011).

[88] A. R. Hibbs, D. F. Styer, R. P. Feynman *Quantum Mechanics and Path Integrals*; Emended ed.; Dover Publications, (2010).

[89] L. Brualla, K. Sakkos, J. Boronat, J. Casulleras, *J. Chem. Phys.* **121**, 636-643 (2004).

[90] X. Li, J. Q. Broughton, *J. Chem. Phys.* **86**, 5094-5100 (1987).

[91] H. De Raedt, B. De Raedt, *Phys. Rev. A* **28**, 3575-3580 (1983).

[92] M. E. Tuckerman *Statistical Mechanics :Theory and Molecular Simulation*; Oxford University Press, (2010).

[93] M. Parrinello, A. Rahman, *J. Chem. Phys.* **80**, 860-867 (1984).

[94] D. Marx, M. Parrinello, *Z. Phys. B* **95**, 143-144 (1994).

[95] R. Iftimie, P. Minary, M. E. Tuckerman, *PNAS* **102**, 6654-6659 (2005).

[96] M. Ceriotti, G. A. R. Brain, O. Riordan, D. E. Manolopoulos, *Proc. R. Soc. A* **468**, 2-17 (2012).

[97] K. Suzuki, M. Tachikawa, M. Shiga, *J. Chem. Phys.* **132**, 144108 (2010).

[98] J. Cao, G. A. Voth, *J. Chem. Phys.* **100**, 5093-5105 (1994).

[99] J. Cao, G. A. Voth, *J. Chem. Phys.* **100**, 5106-5117 (1994).

[100] J. Cao, G. A. Voth, *J. Chem. Phys.* **101**, 6157-6167 (1994).

[101] J. Cao, G. A. Voth, *J. Chem. Phys.* **101**, 6168-6183 (1994).

[102] G. J. Martyna, M. L. Klein, M. Tuckerman, *J. Chem. Phys.* **97**, 2635-2643 (1992).

[103] J. A. Morrone, T. E. Markland, M. Ceriotti, B. J. Berne, *J. Chem. Phys.* **134**, 14103 (2011).

[104] T. Morishita, *Mol. Phys.* **108**, 1337-1347 (2010).

[105] S. Nose, *J. Chem. Phys.* **81**, 511-519 (1984).

Table 1-1 Classification of strong, moderate and weak hydrogen bonds and the corresponding guiding numerical values [56].

Types of hydrogen bond	Strong	Moderate	Weak
Binding energy (kcal/mol*)	15~40	4~15	<4
H…Y (Å)	1.2~1.5	1.5~2.2	>2.2
XHY (degree)	170~180	>130	>90
Example bonding type	$O^{-}H\cdots F^{-}$	$O^{-}H\cdots O$	$C^{-}H\cdots O$

*(*1kcal/mol=4.184KJ/mol)*

List of figure captions

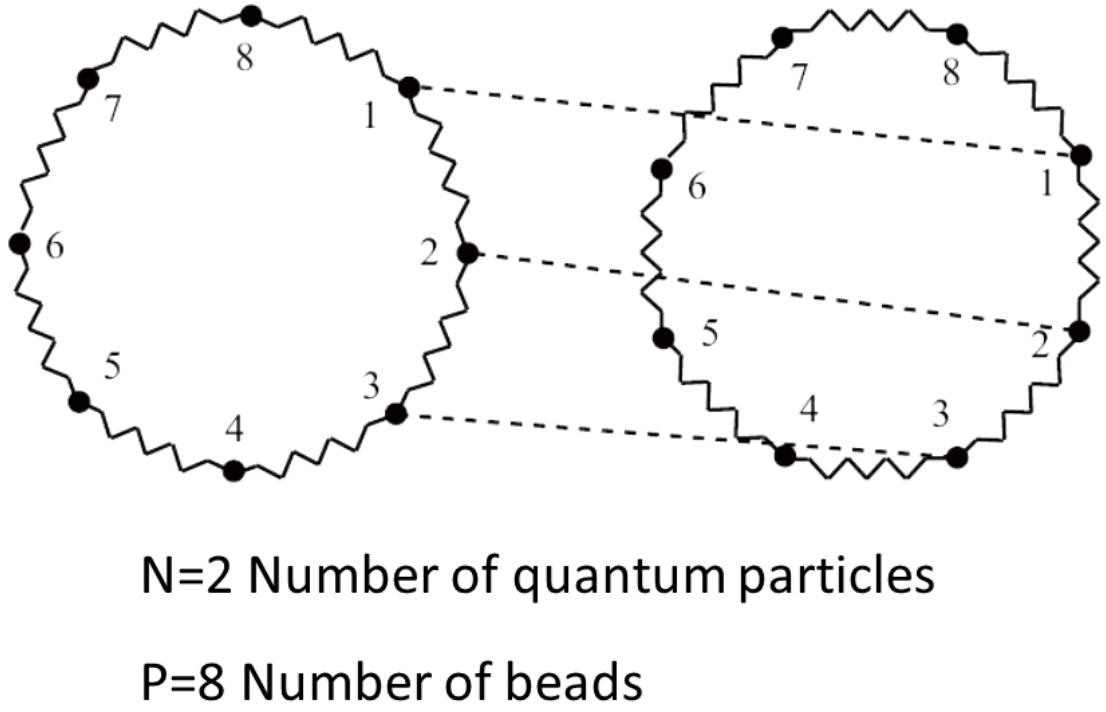

Figure 1-1. Schematic illustration of the interaction pattern between two quantum particles within the discrete path integral framework.

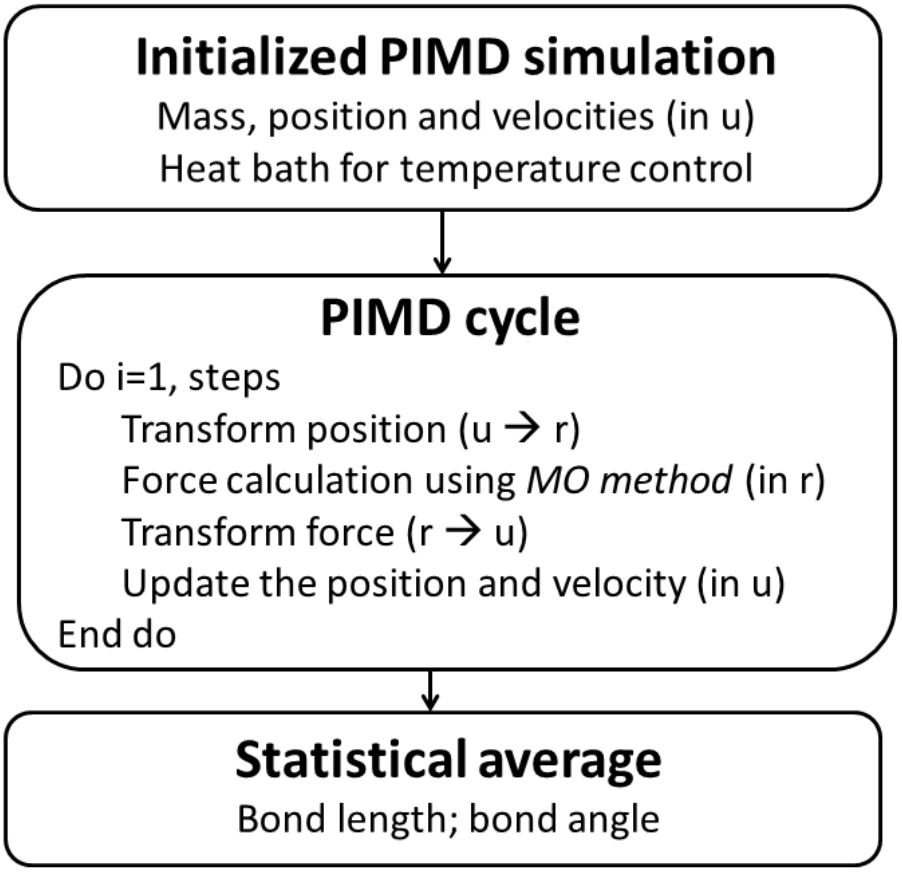

Figure 1-2. Flow chart of the PIMD algorithm. Here u and r represent the normal mode coordinate and real space coordinate, respectively. The theoretical accuracy of the PIMD simulations depends on the choice of molecular orbital (MO) level.

Chapter 2. Semi-empirical Investigations on the Stabilization Energies and Ionic Hydrogen Bonded Structures of $F^-(H_2O)_n$ and $Cl^-(H_2O)_n$ (n=1-4) Clusters

In this chapter, I utilized several semi-empirical methods to analyze the structures and stabilities of $X^-(H_2O)_n$ (X=F, Cl, n=1-4) clusters with respect to the number of water molecules, through comparing with *ab initio* molecular orbital calculations. The results show that the recently developed semi-empirical PM6-DH+ method can provide reasonable binding energies of hydrated fluoride and chloride ion clusters, which are consistent with the corresponding experimental results. For the optimized geometries of X=F, however, the semi-empirical methods show that the global minima are close to $HF(OH)^-(H_2O)_{n-1}$ structures, which are different from *ab initio* calculations. Meanwhile, the topological characteristics for the global minima of X=Cl obtained by semi-empirical methods have the same symmetries as *ab initio* calculations. All calculation levels agree on the trend of decreasing ion-water interactions with the increasing number of water molecules. I also found a new local minimum structure of $Cl^-(H_2O)_4$ with a second hydration shell as a complement of previous studies. Those are very important data for the studies of on-the-fly classical MD and PIMD simulations in the following chapters.

2.1. Introduction

The ionic hydrogen bond, which has stronger intermolecular interaction than typical hydrogen bond, plays significant roles in various biological and chemical processes [1-4], such as protein folding [5] and molecular recognization [6, 7]. Meanwhile, the ionic hydrogen bonded structures provide a powerful lens through which the important phenomena of ion hydration could be further understood [8-11]. Intensive studies [12-15], with experimental techniques [8, 16-22] and theoretical approaches [23-39], have been focused on the detailed structures of the hydrated halide ion clusters.

Experimentally, the formation enthalpies of small hydrated halide ion clusters in the gas phase have been studied by using pulsed electron beam high-pressure mass spectrometer [21]. Diffraction studies [22]

have provided limited structural information on these clusters, for example, the average distance between fluoride/chloride and oxygen is 2.6~2.9Å/3.1~3.5Å. Recently, vibrational spectroscopy using argon predissociation technique has provided more abundant structural information about the fundamentals and first two overtones for $X^-(H_2O)_n$ (X=F, Cl, n=1-4) clusters [8, 16-18].

On the other hand, to understand the ion hydration at molecular level, intensive theoretical works have focused on the structures and binding energies of hydrated ion water clusters [23-26]. For example, Kim and co-workers reported various local minima and transition state structures for these clusters with n=1-6 through high level *ab initio* MO calculations [23-25]. A recent study by Kamp *et. al.* has studied the solvation of fluoride and chloride ion water clusters with $n \leq 20$ by using the effective fragment potential (EFP) method and Monte Carlo simulations [26]. In addition, other theoretical efforts, such as quantum-mechanical/molecular mechanical (QM/MM) [28] and molecular dynamics (MD) with potential including polarization term [29, 30], are also devoted to these clusters. The interaction potentials are essential to the theoretical studies and high level *ab initio* calculations are considered to be the most reliable. However, due to the bottleneck of computational limitations, it is formidable to use such expensive potentials to deal with the energetics and geometries of these clusters with respect to large number of water molecules.

As an alternative solution, semi-empirical potentials have been successfully applied into various systems with extremely cheap computation cost [40, 41]. Recently, the PM6 semi-empirical potential [42, 43] has been successfully applied into the quantum chemistry study of neutral hydrogen bonded systems, such as glycine-water clusters [44] and hydrogen storage material MOF-5 [45]. The PM6 results show reasonable accurate structures and stabilization energies compared to high level *ab initio* calculations. More recently, new semi-empirical potentials of PM6-DH [46], PM6-DH+ [47] and PM6-DH2 [48], which improve PM6 by including two important corrections of dispersion energy and hydrogen bonding, have shown promising results for extended hydrogen bonded complexes. To the best of our knowledge, however, there is still no report on ionic hydrogen bonded systems with PM6 or PM6-DH+ semi-empirical potentials.

In this chapter, thus, I apply the semi-empirical potentials to $X^-(H_2O)_n$ (X=F, Cl, n=1-4) clusters for investigating the various possible geometries. On the other hand, *ab initio* MO and density functional theory (DFT) methods are also utilized to examine the performance of the semi-empirical potentials, with respect to the dependence of the number of water molecules on the energetics and geometries of the ionic hydrogen

bonded clusters.

Those are very important data for study of on-the-fly classical MD and PIMD simulations, as shown in the following chapters.

2.2. Computational details

First, I have explored the optimized energies and geometries of $X^-(H_2O)_n$ (X=F, Cl, n=1-4) clusters by semi-empirical PM6. Then two modified semi-empirical methods, PM6-DH+ and PM6-DH2, were also applied to these clusters. PM6-DH+ was applied to examine both the energies and geometries of the clusters. However, due to the limitation on geometry optimizations of PM6-DH2 [48], I examined the interaction energies of PM6-DH2 on basis of the optimized geometries from PM6. All the semi-empirical calculations were performed using MOPAC2009 program package [49].

On the other hand, I have examined the above obtained semi-empirical results by applying *ab initio* MO and DFT calculations for such ionic hydrogen bonded systems. The *ab initio* calculations were performed with Hartree-Fock (HF) and second order Møller-Plesset perturbation theory (MP2) [50] including electron correlations. The DFT scheme utilized the Becke's three parameters hybrid method using Lee-Yang-Parr correlation function (B3LYP) [51, 52]. The aug-cc-pVDZ basis set was used for all methods for comparison. Of the above mentioned theoretical levels, MP2 is usually considered to be the most reliable method, while it requires the most computational cost. The computations were performed using the Gaussian 09 program package [53].

2.3. Results and discussion

The schematic illustrations of optimized structures for $X^-(H_2O)_{1-4}$ are shown in Fig. 2-1. Here X refers to F or Cl. These topological structures obtained from semi-empirical calculations are consistent with *ab initio* calculations. In addition, the global minimum structures of fluoride clusters, which are optimized by only semi-empirical methods, are shown in Fig. 2-2. The binding energies for fluoride and chloride anion water clusters are listed in Table 2-1 and Table 2-2, respectively. The binding energy is defined as

$$\Delta E = (E_{X^-} + nE_{(H2O)}) - E_{X^-(H2O)n}, \quad (2.1)$$

where E_Z refers to the optimized energy of species Z. The selected bond lengths and bong angles, which represent the ionic hydrogen bond strengths of $X^-(H_2O)_{1-4}$ clusters, are shown in detail at Table 2-3 and Table 2-4 in supplementary data for X=F and X=Cl, respectively. In addition, the values and directions of the imaginary frequencies of the corresponding transition state structures are shown in Table 2-5 and Fig. 2-5, respectively.

I will focus on the performance of semi-empirical methods on the optimized geometries and binding energies of $X^-(H_2O)_n$ clusters with respect to the increasing water number, through comparing with *ab initio* and DFT calculations.

2.3.1. Fluoride anion water clusters

In the $F^-(H_2O)$ cluster, the stable structure takes C_s symmetry and the transition state takes C_{2v} symmetry for all calculation methods. The potential barrier height between the transition state and stable structure is 7.7kcal/mol at PM6 level with zero point vibrational energy (ZPE) correction, which is exactly the same as MP2 level. We note here that the PM6-DH+ and PM6-DH2 show the same stabilization energies as PM6. The ionic hydrogen bonded structures of $F^-(H_2O)_n$ are exhibited through r(F…H_{near}), r(F…O) and θ(F…H-O). In comparison with C_{2v} structure, the semi-empirical results show that the r(F…H_{near}) of C_s structure is shorter and θ(F…H-O) is much larger, which agree well with other calculation levels (see Table 2-3 for details). The results indicate that the ionic hydrogen bond strength in stable structure is stronger than that in transition state structure. However, r(F…O) of C_s structure is slightly longer for the semi-empirical methods, which is just on the contrary at higher calculation levels. Here we have to mention that the r(F…H_{near}) predicted by PM6-DH+ (1.165Å) is much shorter than that of MP2 (1.413Å). The optimized F…H and H…O distances in isolated HF and H_2O molecules are 0.966Å and 0.949Å at PM6-DH+ level, respectively. Thus, the global minimum would be close to $HF(OH^-)$ structure. (See Fig. 2-2)

In the case of $F^-(H_2O)_2$, *ab initio* calculations show that stable and transition state structures take C_2 and C_{2v} symmetries, respectively. The potential barrier height between these two structures is 0.2kcal/mol at MP2 level with ZPE correction. The energy barrier is quite small in comparison of $F^-(H_2O)$ cluster, which indicates

the frequent changes of cluster geometry under certain thermal fluctuations. The semi-empirical methods can also provide such small energy difference (no more than 0.1 kcal/mol) between C_2 and C_{2v} structures. However, the preferred global minimum structure by semi-empirical methods takes C_1 symmetry, rather than C_2 symmetry by *ab initio* calculations. The results indicate that the water-water interaction in $F^-(H_2O)_2$ is not well estimated by semi-empirical methods. In addition, the $2(C_{2v'})$ of $F^-(H_2O)_2$ structure is shown to be a saddle point with the smallest binding energies by semi-empirical as well as *ab initio* and DFT calculations. The $2(C_{2h})$ structure was optimized as a saddle point by MP2/6-311++G** and MP2/TZ(2*df*, *pd*)++ in ref [24], however, by using a larger basis set of aug-cc-pVDZ in this work, it is shown to be a transition state at MP2 level and to be a local minimum at HF and B3LYP levels. The semi-empirical methods support that it is a saddle point structure. On the other hand, the geometry differences of C_2, C_{2v} and C_{2h} structures, such as r(F…H_{near}), r(F…O) and θ(F…H-O), are very close for both semi-empirical and *ab initio* calculations. The results imply that the ionic hydrogen bond strengths in these geometries are very close. Similar as the case of n=1, short r(F…H_{near}) is predicted by PM6-DH+ (1.087Å), the C_1 structure is probably $HF(OH^-)H_2O$.

In the case of $F^-(H_2O)_3$, *ab initio* calculations show that stable structures take C_3 and C_s symmetries and C_3 structure is more stable. It is interesting from the *ab initio* results that when ZPE are included, the energy of the transition state with C_{3h} symmetry could be even lower than that with C_3 symmetry. Unfortunately, this important indication could not be well supported by PM6 or PM6-DH+. Instead, the most stable C_1 structure of $F^-(H_2O)_3$ optimized by semi-empirical methods takes a planar structure similar to C_{3h}. What differs with C_{3h} symmetry is that the fluoride ion locates outside, rather than the inside of the cluster. The semi-empirical results show that the binding energy of C_S structure is higher than that of C_3 structure, which may result from the overestimation of water-water interactions. On the other hand, in agreement with *ab initio* results, semi-empirical methods show that r(F…H_{near}) of C_s structure is the shortest in $F^-(H_2O)_3$ clusters, which is followed by C_{3h} and C_3 symmetry. The largest r(F…O) also appears in C_{3h} structure at PM6 level, while other higher calculation levels favor C_3 structure. The largest θ(F…H-O) appears in C_s structure at PM6 level, while other higher calculation levels prefer C_{3h} symmetry. The C_1 structure, which optimized through PM6-DH+ method, has a very short F…H distance (1.063Å). The results indicate that the structure of $HF(OH^-)(H_2O)_2$ is probably formed instead of $F^-(H_2O)_3$. However, the *ab initio* calculations do not support these results. In addition, both the semi-empirical and *ab initio* calculations show that due to the formation of

second hydration shell in C_s structure, shorter r(F…H_{near}) and larger θ(F…H-O) are obtained in comparison with C_3 symmetry. The results indicate that the ionic hydrogen bond strength in structures with second hydration shell is stronger than that in single hydrogen shell structures, when the water molecule number included in the cluster is the same. More interestingly, the ionic hydrogen bond strength in C_s structure of $F^-(H_2O)_3$ is stronger than that in C_2 structure of $F^-(H_2O)_2$. The result indicates that the ionic hydrogen bond strength is strengthened when additional water molecular is connected via water-water interaction.

In the case of $F^-(H_2O)_4$, PM6 and PM6-DH+ show that the most stable structure takes C_1 symmetry and F^- locates at surface of the clusters. However, in the global minimum optimized by HF and B3LYP, F^- is in the middle of the cluster with C_1 symmetry. Besides, MP2 favors C_s symmetry with 0.4 kcal/mol binding energy higher than C_1 symmetry. The binding energy of C_1 structure by PM6-DH+ is closer to MP2 in comparison of PM6. However, the binding energy differences between C_1 and other symmetries by PM6 or PM6-DH+ are greater than 6kcal/mol, comparing with the differences less than 2kcal/mol by MP2. Since the energy differences between the stable configurations are quite small at MP2 level, the cluster tends to be delocalized and have the coexistence of several configurations. However, the semi-empirical results indicate a more localized structure of C_1 symmetry. In this structure, F…H distance (1.040Å) at PM6-DH+ level is close to the isolated HF bond distance (0.966Å). Thus, the structure of $HF(OH^-)(H_2O)_3$ is probably formed. From the results of *ab initio* and DFT calculations, the longest r(F…H_{near}) and r(F…O) appear in the transition state structure with C_i symmetry. And the largest and smallest θ(F…H-O) appear in C_{4h} symmetry and C_1 structure, respectively. However, the semi-empirical results show that the longest r(F…H_{near}) and r(F…O) appear in C_1 and C_s structure, respectively, while the largest and smallest θ(F…H-O) both appear in C_2 structure. Similar to the case of n=3, *ab initio* and DFT calculations agree that the shortest r(F…H_{near}) and r(F…O) appear in C_s structure, which indicates that the strongest hydrogen bond exits in a second hydration shell structure.

As the water molecular molecules in $F^-(H_2O)_n$ clusters increases from 1 to 4, the semi-empirical methods represent reasonable binding energies of the global minima. However, PM6-DH+ and PM6 probably favor a optimized global minimum structure of $HF(OH^-)(H_2O)_{n-1}$. As n increases from 1 to 4, the F…H distance in the global minimum structure is getting closer to the HF bond distance. (See Fig. 2-2) Similar structures have been optimized by the EFP method as local minima, while they are not global

minima on the potential energy surface. However, $HF(OH^-)(H_2O)_{n-1}$ structures are not optimized by *ab initio* or DFT calculations. As shown in Fig. 2-3, the *ab initio* and DFT calculations show that as n increases from 1 to 4, r(F…H_{near}) and r(F…O) distances of the stable configurations with only one hydration shell increase, and θ(F…H-O) angle decreases. The results imply that the ionic hydrogen bond strength is decreasing with the increase of cluster size. However, the opposite trend emerged for semi-empirical methods. The semi-empirical methods are sufficient to show that the ionic hydrogen bond strength is enhanced when the second hydration shell forms, comparing with the structure without the additional water molecular. However, the semi-empirical methods are not accurate enough to study the structures of small fluoride ion water clusters, where strong ionic hydrogen bond exists.

2.3.2. Chloride anion water clusters

In the $Cl^-(H_2O)$ cluster, all calculations show that the most stable structure takes C_s symmetry. The semi-empirical methods also show C_{2v} symmetry to be a local minimum, though it is supposed to be a transition state by *ab initio* and DFT calculations. The energy difference between C_s and C_{2v} symmetries is 0.4kcal/mol at PM6-DH2 level with ZPE correction, which is slightly lower than that of 1.3kcal/mol at MP2 level. The small energy barrier indicates that the cluster geometry is very flexible. In comparison with C_{2v} structure, C_s structure shows shorter r(Cl…H_{near}) and r(Cl…O) and much larger θ(Cl…H-O) by all calculation levels (see Table 2-4 for details). The results indicate that the ionic hydrogen bond of $Cl^-(H_2O)$ is stronger in asymmetric C_s structure than that of symmetric C_{2v} structure.

In the case of $Cl^-(H_2O)_2$, semi-empirical methods show that the stable and transition state structures take C_1 and C_2 symmetry, respectively. The results are compatible with *ab initio* and DFT calculations. The potential barrier height is 1.7kcal/mol at PM6-DH2 level with ZPE correction, which is higher than that of 0.1kcal/mol for MP2 level. Such small energy difference indicates that the delocalized cluster geometry varies easily under certain thermal fluctuations. The $2(C_{2v})$ and $2(C_{2h})$ for $Cl^-(H_2O)_2$ structures are not obtained by semi-empirical calculations. In addition, the $2(C_{2v'})$ structure is optimized as a local minimum by semi-empirical calculations, while it is a saddle point structure for *ab initio* and DFT methods. Despite the underestimation of θ(Cl…H-O) for C_2 structure, the semi-empirical methods could present the same trend as

ab initio and DFT methods that the bond lengths of r(Cl…H_{near}) and r(Cl…O) in C_2 structure are close to the average of two in C_1 structure. The results imply that the ionic hydrogen bond strength of transition state C_2 structure is between the two ionic hydrogen bond strengths of local minimum C_1 structure.

In the case of $Cl^-(H_2O)_3$, all calculations show that the most stable structure takes C_3 symmetry. By including ZPE correction, it is found that PM6-DH+ and PM6-DH2 could present binding energies very close to MP2 as well as experimental results. From the geometry point of view, the semi-empirical PM6 and PM6-DH+ show that the shortest r(Cl…O) in $Cl^-(H_2O)_3$ clusters is in C_s structure, which is consistent with *ab initio* and DFT methods. The higher calculations also show that shortest r(Cl…H_{near}) and largest θ(Cl…H-O) are in C_s structure, while it takes C_3 symmetry by semi-empirical method. The higher calculation results indicate that the ionic bond strength is weakened in sequence of C_s, C_{3h} and C_3 structure. However, the semi-empirical method PM6 or PM6-DH+ do not show the clear tendency.

In the case of $Cl^-(H_2O)_4$, the semi-empirical methods show that the most stable structure takes C_4 structure, which is consistent with higher calculation results without ZPE corrections. When considering ZPE corrections, B3LYP shows that the C_s structure becomes the most stable, while HF and MP2 still favor C_4 structure. The PM6 and PM6-DH+ methods show that the shortest r(Cl…H_{near}) and r(Cl…O) and largest θ(Cl…H-O) come up in the second hydration shell C_s' structure. The results are consistent with the other calculations and indicate that the strongest ionic hydrogen bond exits in the second hydration shell structure of $Cl^-(H_2O)_4$. The longest r(Cl…H_{near}) and r(Cl…O) appear in C_s structure for semi-empirical methods and in C_2 structure for higher calculations, respectively. The smallest θ(Cl…H-O) is obtained in the stable structure with C_2 symmetry for all calculations. Here we note that C_s' structure of $Cl^-(H_2O)_4$ is reported here for the first time. It is a different configuration from C_s structure found previously. In C_s' structure, it is interesting that strength of the single ionic hydrogen bond is stronger than that of other two symmetric ionic hydrogen bonds, while it is contrary to the case of C_s structure. This new local minimum obtained from PM6 and PM6-DH+ methods could be verified through *ab initio* and DFT results.

The binding energies and topological characteristics of the global minimum structures presented by PM6 and PM6-DH+ are in good agreement of other *ab initio* and DFT results. Thus it is reasonable to apply semi-empirical methods on $Cl^-(H_2O)_n$ clusters for on-the-fly MD studies from both energetic and geometric considerations. Due to the complex coupling of ion-water and water-water interactions, the ionic hydrogen

bond strength is strengthened by the formation of second hydrogen shell. As the number of water molecules in $Cl^-(H_2O)_n$ cluster increases from 1 to 4, the tendency of weakening the ionic hydrogen bond strength with the increasing number of water molecules could be obtained both from semi-empirical and *ab initio* and DFT calculations (See Fig. 2-4). We note that the mean values of r(Cl…H) and θ(Cl…H-O) are adopted for cases of structures with more than one ionic hydrogen bonds. Especially for Cl…H distances, PM6-DH+ shows better results than PM6 as n increases in comparison with MP2.

2.3.3. Comparison of fluoride and chloride clusters

For both fluoride and chloride clusters, PM6-DH+ could substantially improve the binding energies of PM6 in comparison with experiments as well as MP2 results. The semi-empirical methods are sufficient to show the well-known results that the binding energy of fluoride cluster is larger than that of chloride one with similar geometries.

From the geometry point of view, the optimized geometries by PM6 and by PM6-DH+ show little distinction for both X=F and X=Cl. The results show that $HF(OH)^-(H_2O)_{n-1}$ structures are probable to be global minima for X=F. However, the *ab initio* and DFT results all show that F prefer to locate inside of the small $F^-(H_2O)_n$ clusters. The strong ion-water interactions are dominated in these clusters, while they are not well estimated by PM6 or PM6-DH+. On the other hand, the semi-empirical results show that it is quite ubiquitous to find the cooperation of ion-water and water-water interactions in $Cl^-(H_2O)_n$ clusters. The results are compatible with *ab initio* and DFT calculations and that the global minima take the same topological characteristics.

2.4. Summary

I have performed the semi-empirical calculations to analyze the stabilization energies and ionic hydrogen bonded structures of $X^-(H_2O)_n$ (X=F, Cl, n=1-4). The results were also compared with high level *ab initio* and DFT calculations.

For fluoride and chloride clusters, the stabilization energies by PM-DH+ are better than those by PM6

in comparison with MP2 as well as experimental results. On the other hand, PM6-DH+ presents tiny differences in optimized geometries from PM6. In the case of X=F, the optimized global minima are more probable to take $HF(OH)^-(H_2O)_{n-1}$ structures, which are not supported by *ab initio* or DFT calculations. The results may be due to the fact that the strong ion-water interactions are not well estimated by PM6 or PM6-DH+ methods. However, the optimized global minima for X=Cl present the same topological characteristics as MP2, which take C_s, C_1, C_3 and C_4 symmetries for n=1-4, respectively.

As the number of water molecules increases, the ionic hydrogen bond strength becomes weaker for $X^-(H_2O)_n$ clusters. The ionic hydrogen bond strength of fluoride cluster is stronger than that of chloride cluster with similar geometry. It is interesting to find that the emergence of the second hydration shell enhances the ionic hydrogen bond strengths, comparing with the structure that without the additional water molecular. Meanwhile, I have reported new stable structure of $Cl^-(H_2O)_4$ with C_s' symmetry with the second hydration shell. The aforementioned conclusions obtained from semi-empirical methods have been verified by *ab initio* and DFT calculations.

The study of on-the-fly classical MD and PIMD simulation with PM6 or PM6-DH+ potentials will be shown in the following chapters.

References in Chapter 2.

[1] C. L. Perrin, J. B. Nielson, *Annu Rev Phys Chem* **48**, 511 (1997).

[2] T. Steiner, *Angew Chem Int Edit* **41**, 48 (2002).

[3] M. Meot-Ner, *Chem Rev* **105**, 213 (2005).

[4] I. Rozas, *Phys Chem Chem Phys* **9**, 2782 (2007).

[5] E. Shakhnovich, *Chem Rev* **106**, 1559 (2006).

[6] J. Yoon, S. K. Kim, N. J. Singh, K. S. Kim, *Chem Soc Rev* **35**, 355 (2006).

[7] Z. Xu, S. K. Kim, J. Yoon, *Chem Soc Rev* **39**, 1457 (2010).

[8] O. M. Cabarcos, C. J. Weinheimer, J. M. Lisy, S. S. Xantheas, *J Chem Phys* **110**, 5 (1999).

[9] W. H. Robertson, M. A. Johnson, *Annu Rev Phys Chem* **54**, 173 (2003).

[10] K. J. Tielrooij, N. Garcia-Araez, M. Bonn, H. J. Bakker, *Science* **328**, 1006 (2010).

[11] C. G. Zhan, D. A. Dixon, *J Phys Chem A* **108**, 2020 (2004).

[12] B. Hribar, N. T. Southall, V. Vlachy, K. A. Dill, *J Am Chem Soc* **124**, 12302 (2002).

[13] K. D. Collins, G. W. Neilson, J. E. Enderby, *Biophys Chem* **128**, 95 (2007).

[14] Y. Marcus, *Chem Rev* **109**, 1346 (2009).

[15] D. Marx, A. Chandra, M. E. Tuckerman, *Chem Rev* **110**, 2174 (2010).

[16] J. H. Choi, K. T. Kuwata, Y. B. Cao, M. Okumura, *J Phys Chem A* **102**, 503 (1998).

[17] W. H. Robertson, E. G. Diken, E. A. Price, J. W. Shin, M. A. Johnson, *Science* **299**, 1367 (2003).

[18] S. Horvath, A. B. Mccoy, J. R. Roscioli, M. A. Johnson, *J Phys Chem A* **112**, 12337 (2008).

[19] T. Baer, R. C. Dunbar, *J Am Soc Mass Spectr* **21**, 681 (2010).

[20] H. J. Bakker, J. L. Skinner, *Chem Rev* **110**, 1498 (2010).

[21] K. Hiraoka, S. Mizuse, S. J. Yamabe, *J. Chem. Phys.* **92**, 3943 (1988).

[22] H. Ohtaki, T. Radnai, *Chem Rev* **93**, 1157 (1993).

[23] J. Baik, J. Kim, D. Majumdar, K. S. Kim, *J Chem Phys* **110**, 9116 (1999).

[24] J. Kim, H. M. Lee, S. B. Suh, D. Majumdar, K. S. Kim, *J Chem Phys* **113**, 5259 (2000).

[25] H. M. Lee, D. Kim, K. S. Kim, *J Chem Phys* **116**, 5509 (2002).

[26] D. D. Kemp, M. S. Gordon, *J Phys Chem A* **109**, 7688 (2005).

[27] R. Ayala, J. M. Martinez, R. R. Pappalardo, E. S. Marcos, *J Chem Phys* **119**, 9538 (2003).

[28] A. Tongraar, B. M. Rode, *Phys Chem Chem Phys* **5**, 357 (2003).

[29] L. Perera, M. L. Berkowitz, *J Chem Phys* **95**, 1954 (1991).

[30] L. S. Sremaniak, L. Perera, M. L. Berkowitz, *J. Phys. Chem.* **100**, 1350 (1996).

[31] M. Masamura, *J Phys Chem A* **106**, 8925 (2002).

[32] J. E. Combariza, N. R. Kestner, J. Jortner, *Chem Phys Lett* **203**, 423 (1993).

[33] J. E. Combariza, N. R. Kestner, *J. Phys. Chem.* **98**, 3513 (1994).

[34] S. S. Xantheas, *J. Phys. Chem.* **100**, 9703 (1996).

[35] D. Toffoli, M. Sparta, O. Christiansen, *Chem Phys Lett* **510**, 36 (2011).

[36] J. L. Rheinecker, J. M. Bowman, *J Chem Phys* **124**, 131102 (2006).

[37] M. E. Tuckerman, D. Marx, M. L. Klein, M. Parrinello, *Science* **275**, 817N (1997).

[38] J. A. Morrone, R. Car, *Phys Rev Lett* **101**, 17801 (2008).

[39] C. Vega, M. M. Conde, C. Mcbride, J. Abascal, E. G. Noya, R. Ramirez, L. M. Sese, *J Chem Phys* **132**, 46101 (2010).

[40] M. E. Foster, K. Sohlberg, *Phys Chem Chem Phys* **12**, 307 (2010).

[41] K. E. Riley, P. Hobza, *WIREs Comput. Mol. Sci.* **1**, 3 (2011).

[42] J. Stewart, *J Mol Model* **15**, 765 (2009).

[43] J. Stewart, *J Mol Model* **13**, 1173 (2007).

[44] T. Takayanagi, T. Yoshikawa, A. Kakizaki, M. Shiga, M. Tachikawa, *J Mol Struc-Theochem* **869**, 29 (2008).

[45] D. A. Gomez, A. F. Combariza, G. Sastre, *Phys Chem Chem Phys* **11**, 9250 (2009).

[46] J. Rezac, J. Fanfrlik, D. Salahub, P. Hobza, *J. Chem. Theo. Comput.* **5**, 1749 (2009).

[47] M. Korth, *J. Chem. Theo. Compu.* **6**, 3808 (2010).

[48] M. Korth, M. Pitonak, J. Rezac, P. Hobza, *J. Chem. Theo. Compu.* **6**, 344 (2010).

[49] J. J. P. Stewart, Mopac2009, Stewart Computational Chemistry, Colorado Springs, Co, Usa, Http://Openmopac.Net, 2008.

[50] O. M, C. Ller, M. S. Plesset, *Phys. Rev.* **46**, 618 (1934).

[51] A. D. Becke, *J Chem Phys* **98**, 5648 (1993).

[52] C. T. Lee, W. T. Yang, R. G. Parr, *Phys Rev B* **37**, 785 (1988).

[53] M. J. Frisch, G. W. Trucks, H. B. Schlegel, G. E. Scuseria, M. A. Robb, J. R. Cheeseman, G. Scalmani, V. Barone, B. Mennucci, G. A. Petersson, H. Nakatsuji, M. Caricato, X. Li, H. P. Hratchian, A. F. Izmaylov, J. Bloino, G. Zheng, J. L. Sonnenberg, M. Hada, M. Ehara, K. Toyota, R. Fukuda, J. Hasegawa, M. Ishida, T. Nakajima, Y. Honda, O. Kitao, H. Nakai, T. Vreven, J. A. Montgomery, J. E. Peralta, F. Ogliaro, M. Bearpark, J. J. Heyd, E. Brothers, K. N. Kudin, V. N. Staroverov, R. Kobayashi, J. Normand, K. Raghavachari, A. Rendell, J. C. Burant, S. S. Iyengar, J. Tomasi, M. Cossi, N. Rega, J. M. Millam, M. Klene, J. E. Knox, J. B. Cross, V. Bakken, C. Adamo, J. Jaramillo, R. Gomperts, R. E. Stratmann, O. Yazyev, A. J. Austin, R. Cammi, C. Pomelli, J. W. Ochterski, R. L. Martin, K. Morokuma, V. G. Zakrzewski, G. A. Voth, P. Salvador, J. J. Dannenberg, S. Dapprich, A. D. Daniels, Farkas, J. B. Foresman, J. V. Ortiz, J. Cioslowski, D. J. Fox, *Gaussian 09, Revision A.02, Gaussian, Inc., Wallingford CT* (2009).

Table 2-1 Binding energies (kcal/mol) of fluoride anion water clusters

$F^-(H_2O)_n$	Experiment	PM6			PM6-DH+			PM6-DH2			HF/aug-cc-pVDZ			B3LYP/aug-cc-pVDZ			MP2/aug-cc-pVDZ		
		ΔE	ΔE_{ZPE}	IF	ΔE	ΔE_{ZPE}	IF	ΔE	ΔE_{ZPE}	IF	ΔE	ΔE_{ZPE}	IF	ΔE	ΔE_{ZPE}	IF	ΔE	ΔE_{ZPE}	IF
$1(C_s)$	23.3	24.5	23.0	0	24.6	23.0	0	24.6	23.0	0	23.6	22.2	0	27.3	26.5	0	26.8	26.0	0
$1(C_{2v})$		16.8	15.3	1	16.8	15.3	1	16.8	15.3	1	18.0	16.7	1	19.6	18.6	1	19.4	18.3	1
$2(C_2)$	42.5	36.0	32.8	1	36.1	33.0	1	36.2	33.1	1	42.9	39.4	0	48.1	45.3	0	48.1	45.0	0
$2(C_{2v})$		35.2	32.9	1	35.3	32.9	0	35.3	33.0	0	42.7	39.4	1	47.7	45.2	1	47.5	44.8	1
$2(C_{2v'})$		31.1	28.1	3	31.2	28.2	3	31.2	28.2	3	33.7	31.1	3	36.1	33.9	3	36.1	33.9	3
$2(C_{2h})$		35.3	33.1	3	35.4	33.2	2	35.4	33.2	3	42.9	39.6	0	47.8	45.2	0	47.6	44.9	1
$2(C_1)$		43.5	39.3	0	46.5	41.8	0	49.8	45.0	0	-	-	-	-	-	-	-	-	-
$3(C_3)$	57.8	48.5	42.5	2	51.2	44.2	2	50.7	44.3	2	59.0	52.7	0	64.8	59.7	0	66.9	60.4	0
$3(C_s)$		51.1	45.9	1	56.1	48.1	1	54.2	48.7	1	56.5	49.9	0	64.1	58.1	0	65.4	59.3	0
$3(C_{3h})$		44.8	41.5	3	45.2	41.9	3	45.2	42.0	3	58.9	53.5	1	64.8	60.0	1	65.3	60.4	1
$3(C_1)$		57.2	50.7	0	66.6	57.1	0	65.7	58.7	0	-	-	-	-	-	-	-	-	-
$4(C_1)$	71.7	70.6	62.2	0	80.0	70.0	0	84.5	74.6	0	72.8	64.3	0	79.1	70.9	0	82.2	73.7	0
$4(C_2)$		61.8	54.8	0	66.6	58.8	2	65.0	57.3	3	72.5	64.3	0	78.6	70.9	0	81.1	73.2	0
$4(C_4)$		59.7	51.1	3	66.2	55.3	3	64.0	55.0	3	72.0	63.1	0	78.0	69.2	0	82.2	72.8	0
$4(C_s)$		63.4	55.8	1	71.6	61.8	1	68.6	59.8	1	71.5	61.9	0	79.9	70.7	0	83.5	74.1	0
$4(C_i)$		60.7	53.9	1	66.0	58.2	1	64.3	57.0	1	72.0	63.7	0	77.6	69.9	1	80.1	72.2	1
$4(C_{4h})$		52.3	47.8	6	53.2	48.8	5	53.3	48.8	5	71.6	63.9	2	77.4	70.4	2	79.7	72.8	5

ΔE and ΔE_{ZPE} represents for the binding energies without and with ZPE corrections. IF represents the number of imaginary frequencies. The experiment values are taken from Ref. [22].

Table 2-2 Binding energies (kcal/mol) of chloride anion water clusters

$Cl^-(H_2O)_n$	Experiment	PM6			PM6-DH+			PM6-DH2			HF/aug-cc-pVDZ			B3LYP/aug-cc-pVDZ			MP2/aug-cc-pVDZ		
		ΔE	ΔE_{ZPE}	IF	ΔE	ΔE_{ZPE}	IF	ΔE	ΔE_{ZPE}	IF	ΔE	ΔE_{ZPE}	IF	ΔE	ΔE_{ZPE}	IF	ΔE	ΔE_{ZPE}	IF
$1(C_s)$	14.7	15.3	14.2	0	15.3	14.2	0	15.3	14.2	0	11.8	10.5	0	14.3	13.2	0	14.7	13.5	0
$1(C_{2v})$		15.4	13.8	0	15.5	13.9	0	15.4	13.8	0	11	10	1	12.5	11.6	1	13.1	12.2	1
$2(C_1)$	27.7	30.1	26.5	0	32.2	28.1	0	31.5	27.7	0	23.5	19.8	0	28	24.5	0	29.8	26.2	0
$2(C_2)$		29.1	25.6	1	29.5	25.9	1	29.7	26.0	1	23.1	19.7	1	27.5	24.4	1	29.3	26.1	1
$2(C_{2h})$		-	-	-	-	-	-	-	-	-	22.4	19.8	2	26.6	24.2	2	27.6	25.2	3
$2(C_{2v})$		-	-	-	-	-	-	-	-	-	22.3	19.8	3	26.6	24.2	2	27.7	25.2	2
$2(C_{2v'})$		29.6	26.3	0	29.7	26.2	0	29.7	26.4	0	21.0	19.0	4	23.4	21.6	5	24.9	23.1	4
$3(C_3)$	39.5	44.2	37.6	0	48.8	40.8	0	47.2	40.4	0	35.4	28.8	0	42	35.4	0	46.1	39.4	0
$3(C_s)$		41.6	35.4	0	47.0	36.8	1	44.3	37.0	1	33.9	28	0	40.9	35.2	0	43.5	37.6	0
$3(C_{3h})$		41.7	36.7	3	42.0	37.1	3	42.0	37.1	3	32.1	28.2	1	37.8	34.2	1	39.6	36	1
$4(C_2)$	51.1	54.2	46.6	0	58.2	47.8	2	56.3	48.2	2	43.1	35.8	0	50.2	43	0	54.5	47.2	0
$4(C_4)$		57.9	48.3	0	67.7	52.5	0	63.6	53.7	0	46.1	36.9	0	54.6	45.1	0	60.8	51.1	0
$4(C_s')$		54.0	46.0	0	63.7	52.5	0	60.5	51.7	0	44	35.7	0	52.4	44.1	0	57.5	49.1	0
$4(C_s)$		53.1	45.9	2	60.9	49.8	2	57.8	49.6	2	44.9	36.2	1	54	45.3	1	59.3	50.4	1

ΔE and ΔE_{ZPE} represents for the binding energies without and with ZPE corrections. IF represents the number of imaginary frequencies. The experiment values are taken from Ref. [22].

Table 2-3. Comparison of selected optimized distances (Å) and angles (degree) of fluoride anion water clusters.

$F^-(H_2O)_n$	PM6			PM6-DH+			HF/aug-cc-pVDZ			B3LYP/aug-cc-pVDZ			MP2/aug-cc-pVDZ		
	$r(F\cdots H_{near})$	$r(F\cdots O)$	$\theta(F\cdots H\text{-}O)$	$r(F\cdots H_{near})$	$r(F\cdots O)$	$\theta(F\cdots H\text{-}O)$	$r(F\cdots H_{near})$	$r(F\cdots O)$	$\theta(F\cdots H\text{-}O)$	$r(F\cdots H_{near})$	$r(F\cdots O)$	$\theta(F\cdots H\text{-}O)$	$r(F\cdots H_{near})$	$r(F\cdots O)$	$\theta(F\cdots H\text{-}O)$
$1(C_s)$	1.165	2.346	169.0	1.165	2.347	169.0	1.512	2.507	174.1	1.403	2.462	176.7	1.413	2.469	176.8
$1(C_{2v})$	1.856	2.344	107.2	1.856	2.344	107.2	2.096	2.627	113.7	2.015	2.579	114.5	2.020	2.590	115.0
$2(C_2)$	1.370	2.383	156.5	1.371	2.383	156.4	1.596	2.573	173.3	1.516	2.536	176.1	1.527	2.543	173.7
$2(C_{2v})$	1.377	2.392	157.7	1.376	2.391	157.7	1.597	2.573	172.7	1.516	2.536	176.6	1.519	2.539	176.9
$2(C_{2v'})$	1.921	2.397	107.1	1.918	2.394	107.1	2.142	2.664	113.2	2.069	2.618	113.8	2.077	2.633	114.3
$2(C_{2h})$	1.378	2.397	159.0	1.379	2.396	158.7	1.595	2.572	173.4	1.518	2.535	175.6	1.523	2.540	175.9
$2(C_1)$	1.092	2.363	170.6	1.090	2.365	171.2	-	-	-	-	-	-	-	-	-
	3.122	3.632	115.9	3.343	3.739	107.9	-	-	-	-	-	-	-	-	-
$3(C_3)$	1.565	2.459	144.1	1.626	2.467	137.8	1.673	2.633	169.5	1.595	2.596	174.4	1.632	2.613	165.9
$3(C_{3h})$	1.513	2.468	153.8	1.511	2.467	154.0	1.661	2.629	173.9	1.591	2.594	176.1	1.589	2.592	176.8
$3(C_s)$	1.327	2.369	160.8	1.329	2.372	160.8	1.568	2.548	173.6	1.490	2.514	175.2	1.492	2.515	175.3
$3(C_1)$	1.064	2.380	170.7	1.063	2.383	171.8	-	-	-	-	-	-	-	-	-
	2.929	3.802	153.3	2.896	3.738	148.3	-	-	-	-	-	-	-	-	-
	3.276	3.595	102.3	4.135	3.870	67.2	-	-	-	-	-	-	-	-	-
$4(C_4)$	1.720	2.555	139.0	1.865	2.598	128.6	1.755	2.702	167.6	1.712	2.682	165.4	1.711	2.680	165.0
$4(C_2)$	1.327	2.372	161.7	1.325	2.371	161.7	1.702	2.661	171.6	1.631	2.623	172.2	1.620	2.613	172.4
	2.820	3.484	127.6	2.829	3.474	125.8	1.763	2.708	166.7	1.724	2.690	164.6	1.731	2.692	163.5
$4(C_s)$	2.688	3.563	153.2	3.082	3.846	138.9	1.744	2.693	167.5	1.728	2.699	166.4	1.719	2.692	166.9
	1.318	2.364	161.3	1.353	2.404	161.0	1.632	2.595	169.7	1.557	2.560	170.8	1.557	2.559	170.4
$4(C_1)$	1.050	2.395	175.4	1.040	2.412	176.6	1.744	2.686	165.3	1.636	2.629	174.4	1.707	2.667	162.0
	2.911	3.800	156.1	2.949	3.803	150.3	1.755	2.694	164.4	1.716	2.674	161.8	1.713	2.670	161.5
	3.036	3.716	129.7	3.452	3.871	109.6	1.738	2.685	166.9	1.707	2.668	162.3	1.687	2.656	164.7
	3.231	3.602	105.6	4.319	3.990	63.6	1.714	2.672	171.2	1.695	2.663	164.2	1.636	2.629	174.2
$4(C_i)$	1.342	2.374	159.9	1.346	2.379	159.9	1.697	2.659	172.9	1.628	2.621	173.0	1.621	2.615	173.4
	2.820	3.485	127.6	2.820	3.480	127.2	1.808	2.745	164.8	1.771	2.726	162.5	1.762	2.720	163.0
$4(C_{4h})$	1.640	2.578	155.2	1.639	2.578	155.5	1.728	2.689	174.9	1.667	2.658	176.7	1.656	2.648	177.1

Table 2-4. Comparison of selected optimized distances (Å) and angles (degree) of chloride anion water clusters.

$Cl^-(H_2O)_n$	PM6			PM6-DH+			HF/aug-cc-pVDZ			B3LYP/aug-cc-pVDZ			MP2/aug-cc-pVDZ		
	$r(Cl\cdots H_{near})$	$r(Cl\cdots O)$	$\theta(Cl\cdots H\text{-}O)$	$r(Cl\cdots H_{near})$	$r(Cl\cdots O)$	$\theta(Cl\cdots H\text{-}O)$	$r(Cl\cdots H_{near})$	$r(Cl\cdots O)$	$\theta(Cl\cdots H\text{-}O)$	$r(Cl\cdots H_{near})$	$r(Cl\cdots O)$	$\theta(Cl\cdots H\text{-}O)$	$r(Cl\cdots H_{near})$	$r(Cl\cdots O)$	$\theta(Cl\cdots H\text{-}O)$
$1(C_s)$	1.833	2.815	153.7	1.833	2.817	153.9	2.362	3.283	161.0	2.143	3.124	168.5	2.159	3.137	168.0
$1(C_{2v})$	2.433	2.927	111.0	2.436	2.930	111.0	2.828	3.309	112.6	2.654	3.180	114.3	2.638	3.179	115.4
$2(C_1)$	1.692	2.757	160.8	1.668	2.750	162.0	2.318	3.244	162.1	2.122	3.102	167.8	2.128	3.105	167.3
	2.580	3.319	133.9	2.765	3.474	131.3	2.543	3.420	153.3	2.372	3.281	154.1	2.366	3.277	154.4
$2(C_2)$	2.315	2.932	120.3	2.312	2.935	120.8	2.405	3.313	158.5	2.204	3.166	164.1	2.217	3.174	163.2
$2(C_{2h})$	-	-	-	-	-	-	2.398	3.314	160.3	2.189	3.161	167.9	2.205	3.175	167.2
$2(C_{2v})$	-	-	-	-	-	-	2.402	3.314	159.4	2.190	3.161	166.7	2.204	3.171	166.2
$2(C_{2v'})$	2.461	2.949	110.8	2.464	2.952	110.9	2.819	3.333	115.2	2.671	3.210	115.5	2.658	3.205	115.9
$3(C_3)$	2.243	2.946	127.6	2.299	2.950	123.3	2.479	3.357	153.1	2.322	3.232	153.8	2.308	3.222	154.4
$3(C_s)$	2.422	2.897	109.5	2.429	2.898	109.1	2.321	3.253	164.2	2.129	3.112	169.9	2.131	3.111	169.5
$3(C_{3h})$	2.491	2.974	110.7	2.492	2.975	110.7	2.416	3.339	162.5	2.216	3.189	169.3	2.225	3.196	169.0
$4(C_4)$	2.334	2.958	121.3	2.411	2.951	114.8	2.540	3.408	151.7	2.411	3.294	150.0	2.375	3.268	151.3
$4(C_2)$	2.424	3.105	127.2	2.532	3.254	131.8	2.367	3.288	161.5	2.176	3.144	166.2	2.183	3.149	165.9
	2.464	2.900	107.0	2.457	2.872	105.3	2.642	3.501	150.6	2.520	3.390	148.8	2.463	3.350	151.1
$4(C_s')$	1.569	2.730	172.0	1.551	2.713	160.0	2.233	3.188	172.7	2.079	3.066	170.4	2.077	3.063	170.8
	2.664	3.473	141.8	2.795	3.504	131.2	2.506	3.389	154.3	2.327	3.251	156.6	2.308	3.235	157.2
$4(C_s)$	2.484	3.350	150.4	2.670	3.527	149.5	2.531	3.455	164.1	2.395	3.348	164.9	2.331	3.290	166.0
	1.905	2.822	147.0	1.899	2.818	147.0	2.339	3.262	161.8	2.158	3.128	166.0	2.163	3.127	164.5

Table 2-5. Negative frequencies (cm^{-1}) of the transition state structures

		PM6	PM6-DH+	PM6-DH2	HF/aug-cc-pVDZ	B3LYP/aug-cc-pVDZ	MP2/aug-cc-pVDZ
$F^-(H_2O)_n$	$1(C_{2v})$	-424.80	-424.80	-424.80	-479.73	-548.41	-535.84
	$2(C_2)$	-324.02	-328.22	-379.56	-	-	-
	$2(C_{2v})$	-49.28	-	-	-64.91	-84.64	-118.67
	$2(C_{2h})$	-	-	-	-	-	-22.57
	$3(C_s)$	-88.62	-139.72	-112.98	-	-	-
	$3(C_{3h})$	-	-	-	-22.80	-35.65	-48.32
	$4(C_s)$	-175.79	-151.30	-203.30	-	-	-
	$4(C_i)$	-20.10	-18.78	-20.43	-	-16.37	-14.44
$Cl^-(H_2O)_n$	$1(C_{2v})$	-	-	-	-230.04	-287.06	-289.97
	$2(C_2)$	-85.36	-122.11	-115.89	-119.46	-130.24	-136.81
	$3(C_s)$	-	-145.49	-12.60	-	-	-
	$3(C_{3h})$	-	-	-	-24.60	-20.12	-
	$4(C_s)$	-	-	-	-26.88	-37.07	-34.09

List of figure captions

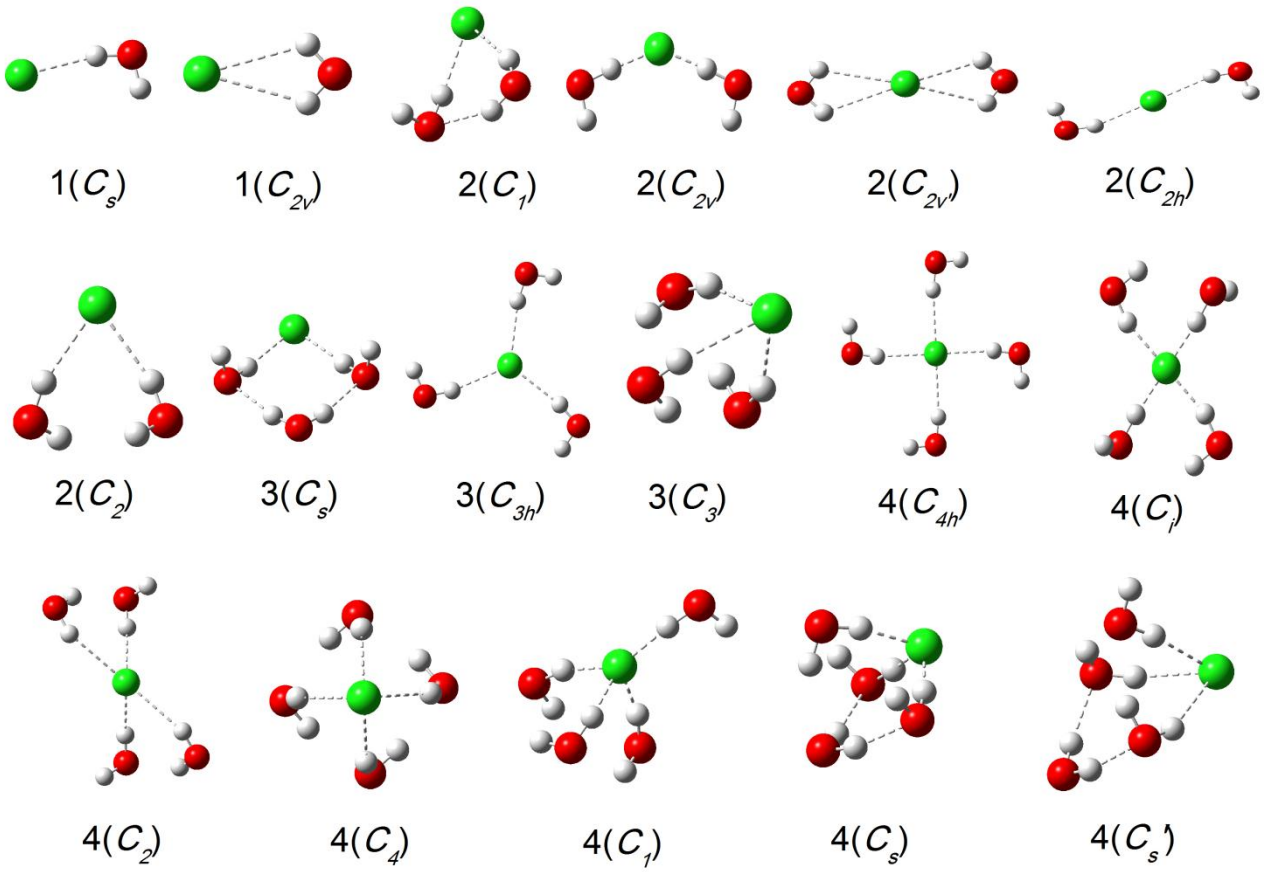

Figure 2-1. Optimized geometries of fluoride/chloride anion water clusters at MP2/aug-cc-pVDZ level. The colors of green, red and white represent fluoride/chloride, oxygen and hydrogen atoms, respectively.

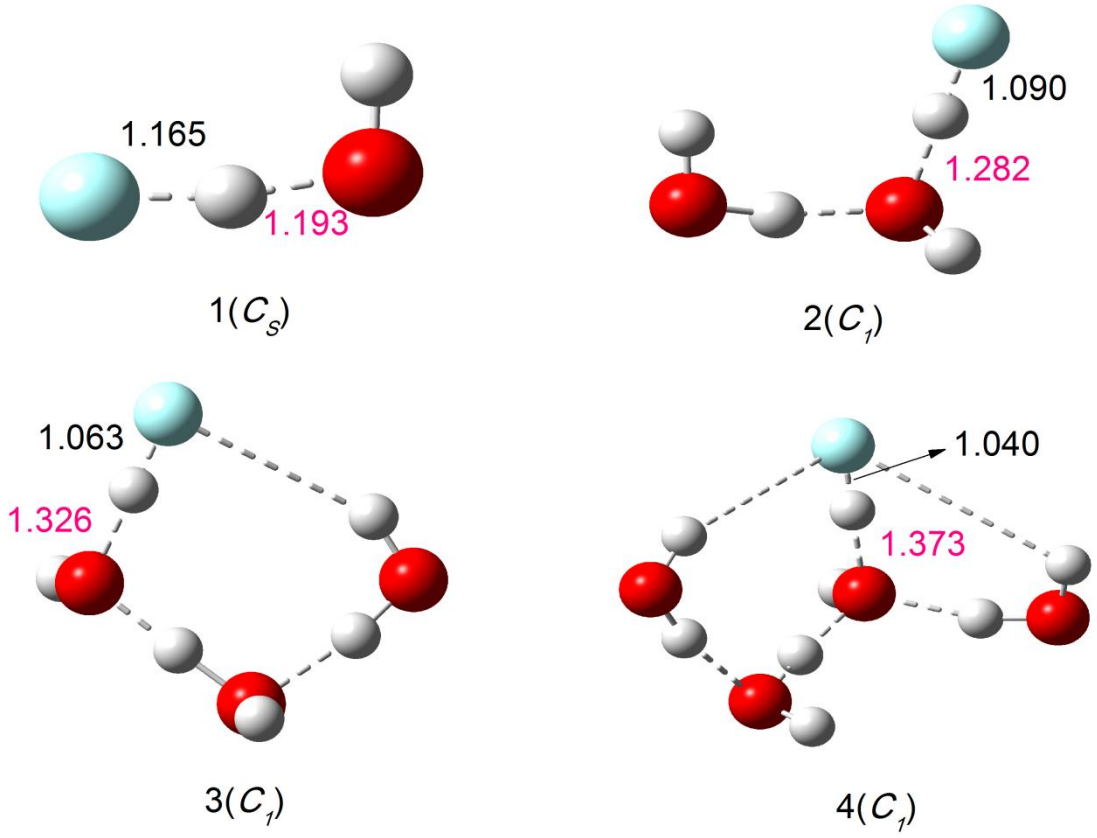

Figure 2-2. Optimized global minima of fluoride anion water clusters at PM6-DH+ level. The F….H and H…O distances in each clusters are shown in black and pink color, respectively. The optimized F…H and H…O distances in isolated HF and H_2O molecules are 0.966Å and 0.949Å at the same calculation level, respectively.

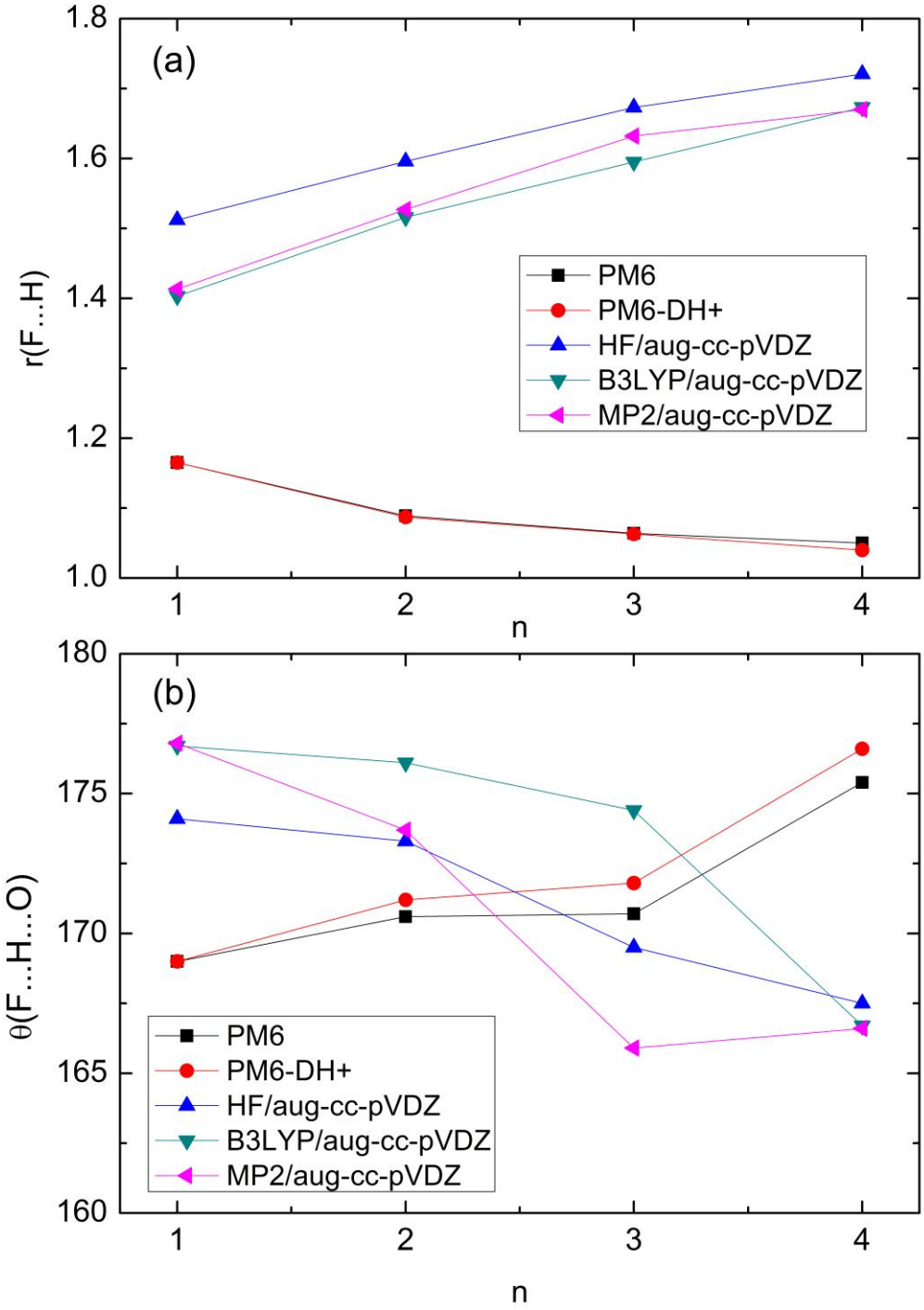

Figure 2-3. Comparison of semi-empirical and *ab initio*/DFT calculations on ionic hydrogen bonded structure of flouride anion water clusters. The horizontal axis represents the water numbers and the vertical axis represents (a) F…H distances (Angstrom) and (b) F…H…O angles (Degree).

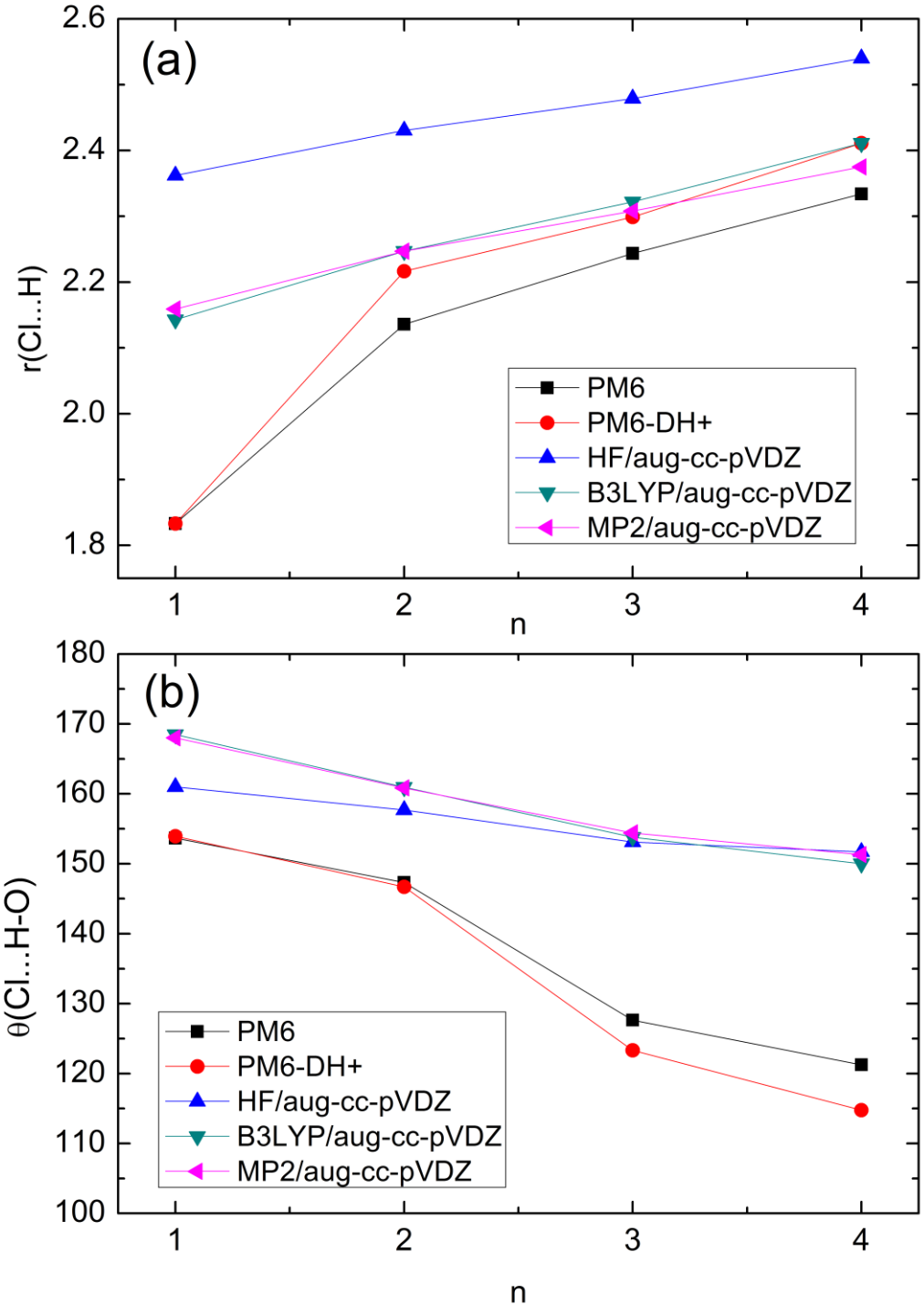

Figure 2-4. Comparison of semi-empirical and *ab initio*/DFT calculations on ionic hydrogen bonded structure of chloride anion water clusters. The horizontal axis represents the water numbers and the vertical axis represents (a) Cl…H distances (Angstrom) and (b) Cl…H-O angles (Degree).

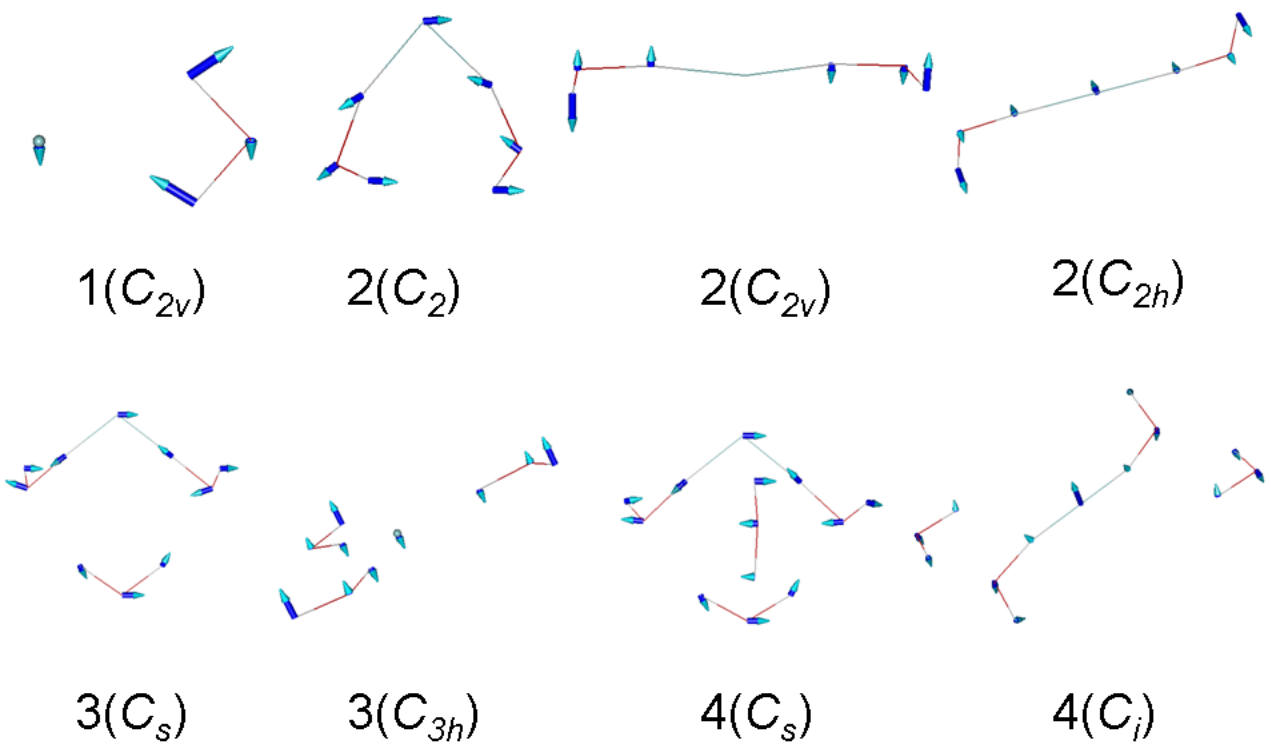

Figure 2-5. Schematically illustrations of the vibration directions of negative frequencies of transition state structures.

Chapter 3. Path Integral Molecular Dynamics Study of Nuclear Quantum Effect on Small Chloride Water Clusters of $Cl^-(H_2O)_{1-4}$

In this chapter, the nuclear quantum effects, which play important roles on ionic hydrogen bonded structures of $Cl^-(H_2O)_n$ (n=1-4) clusters, was explored by carrying out PIMD simulations. An outer shell coordinate r^l(Cl…O) is selected to display the rearrangement of single and multi hydration shell cluster structures. By incorporating the nuclear quantum effect, it is shown that the probability for single shell structures is decreased while the probability for multi shell structures is increased. On the other hand, the correlations between changing of bonded H* atom to Cl^- (defined as δ) and other cluster vibration coordinates are studied. I have found that δ strongly correlates with proton transfer motion while it has little correlation with ion-water stretching motion. Contrary to θ(H-O-H*) coordinate, the correlations between δ and other coordinates are decreased by inclusion of nuclear quantum effect. The results indicate that the water-water hydrogen bond interactions are encouraged by quantum simulations.

3.1. Introduction

Ion solvation in aqueous solution, which is a fundamental process in atmospheric chemistry and biochemistry, has attracted extensive attention of both theoretical and experimental studies [1, 2]. Specific ion effect, which also called Hofmeister effect, has significant impacts on the properties of the solution [3, 4]. For instance, the sign, size and polarizability of ion have been proved to be the major factors over various other possibilities to affect the cluster structures [5-8]. The simulations of monoatomic ion in small water clusters have demonstrated that large halide anions such as Cl^-, Br^-, I^- have an increasing propensity of surface solvation, while smaller halide anion F^- and cations prefer to reside in the interior of water clusters [9, 10].

The chloride ion is quite ubiquitous in nature and thus the structures of chloride ion water clusters have attracted intensive attention. Perera et al. firstly presented the surface preference of Cl^- solvation in the cluster composed of 20 water molecules by energetic considerations [11]. The subsequent photoelectron

spectroscopy experiments supported the surface solvation of Cl^- from the energetic point of view [12]. Afterwards, more experiments have brought insights to the effects of ion-water and water-water hydrogen bond interactions on the cluster structures. For example, Choi *et al.* [13] observed the hydrogen-bonded and free OH stretching motion of $Cl^-(H_2O)_n$ clusters with n up to 5 by vibrational predissociation spectroscopy. Their results showed no water-water hydrogen bond interaction in n=2 and n=3, which were different from *ab initio* predictions. However, the vibrational spectra using argon predissociation technique obtained by Ayotte *et al.* [14-16] have proved the existence of water-water hydrogen bond interactions in n=2 and n=3 at lower temperature. The temperature effect is thus considered to play important roles in understanding the differences between the experiments and the corresponding electronic structure calculations including *ab initio* MO and DFT methods [17-20]. These results show direct structural information of the clusters, such as bond lengths and bond angles, which are inaccessible for experiments especially for large cluster size.

In addition to the previously mentioned static MO studies, some classical MD [5-10, 21-23]simulations have also been performed. For example, Dorsett et al. probed the temperature effect on the hydrogen bonding network of $Cl^-(H_2O)_2$ cluster [24]. The computed vibrational spectra show the trend of decreasing of water-water interaction as temperature increases. Meanwhile, Tobias et al. reported results of Car-Parinello MD simulations for $Cl^-(H_2O)_6$ clusters with a focus on the importance of polarizable potentials on the surface solvation of Cl^- anion by comparing with nonpolarizable models [22].

On the other hand, the nuclear quantum effect also plays important roles in such hydrogen bonded systems [25-29]. However, up to now, there is little work on $Cl^-(H_2O)_n$ clusters which takes into account of both nuclear quantum effect and temperature effect. Thus we apply PIMD simulation, which is a standard treatment for investigating the quantum mechanical nature of nuclei [30-34], to study to ionic hydrogen bonded structures of $Cl^-(H_2O)_{1-4}$ clusters. A cyclic chain polymer composed of classical quasi particles (beads) is adopted to describe the quantum mechanical character of nuclei. The potential energy and its derivatives are calculated "on the fly" using *ab initio* or DFT electronic structure methods. The accuracy of PIMD simulation depends on the choice of potential level. The growing progress in computer power and in parallelizing technique has promoted the development *ab initio* PIMD calculations. However, it is still very time consuming to use *ab initio* or DFT potential to study the present $Cl^-(H_2O)_{1-4}$ clusters, in which the rearrangement of the hydrogen bond network happens frequently under thermal fluctuation.

As a compromise solution, semi-empirical potentials have been successfully applied with less accuracy but extremely cheap computation cost [35, 36]. For example, the PM6 semi-empirical potential has been successfully applied into the quantum chemistry study of neutral hydrogen bonded glycine-water clusters [37]. PM6 results show reasonable accurate structures and stabilization energies compared to *ab initio* calculations. Recently, new semi-empirical potentials PM6-DH [38], PM6-DH+ [39] and PM6-DH2 [40], which improve PM6 by including two important corrections of dispersion energy and hydrogen bonding, have shown promising results for extended hydrogen bonded complexes.

Thus, in this work, I carried out PIMD simulations on the $Cl^-(H_2O)_{1-4}$ clusters with semi-empirical PM6-DH+ potential for sake of the computational efficiency. Then I explored the nuclear quantum effects on the rearrangement single and multi shell structures of the clusters. On the other hand, the correlations between the changing of bonded H* atom to Cl^- and other cluster vibration motions, such as ion-water stretching motion and proton transfer motion, were also discussed with an emphasis on the nuclear quantum effects.

3.2. Computational details

Before starting PIMD simulations, it is very important to understand the features of ground state potential energy surfaces (PES) of $Cl^-(H_2O)_{1-4}$ clusters. To this end, the energetics and optimized structures by semi-empirical PM6-DH+ potential are compared with *ab initio* and DFT calculations. On the other hand, since r(Cl…O) coordinates play important roles in structural rearrangement of the clusters, the comparison of PM6-DH+ and MP2 potential energy surfaces along r(Cl…O) coordinates are presented for the $Cl^-(H_2O)_{1-2}$ clusters.

The thermal structures of $Cl^-(H_2O)_{1-4}$ clusters are obtained by using standard imaginary-time PIMD simulations on PM6-DH+ potential energy surface. In the path-integral formalism, a cyclic polymer chain consisting of classical quasi particles is utilized to describe the quantum character of nuclei. Thermal averages are calculated from time averages over fictitious molecular dynamics trajectories, which are generated from the equation of motions described in the normal mode coordinate representation [41]. The system temperature was controlled with a massive Nos é-Hoover chain technique [42, 43].

At each time step, the potential energy and gradient values were directly obtained “on the fly” using the

MOPAC2009 software package [44]. The PIMD run was performed with 16 beads at the temperature of T = 300 K. With time increment δt = 0.1fs, the total time steps were ranged 10^7. The Nos é-Hoover thermostat of length 4 combined with the velocity Verlet algorithm was used to control the system temperature.

3.3. Results and discussion

3.3.1. Potential energy surfaces

Before classical MD and PIMD simulations, the binding energies and optimized ionic hydrogen bonded structures of $Cl^-(H_2O)_{1-4}$ clusters by PM6-DH+ method are compared with MP2/B3LYP calculations and corresponding experimental values. The schematic illustration of optimized structures of $Cl^-(H_2O)_{1-4}$ clusters are shown in Fig. 3-1. As shown in Table 3-1, the binding energies by PM6-DH+ method are consistent with MP2/B3LYP results as well as experimental values. Topologically, PM6-DH+ method shows relative shorter r(Cl…O) distances in comparison with MP2/B3LYP calculations, while r(Cl…H) distances are consistent for PM6-DH+ and MP2/B3LYP calculations. On the other hand, the comparison between PM6-DH+ and MP2 methods on potential energy surfaces along r(Cl…O) coordinates are shown in Fig. 3-2. In Fig. 3-2(a) and Fig. 3-2(b), the results show that the minimum position of r(Cl…O) coordinates by PM6-DH+ is relative shorter than that by MP2, while the shapes of potential energy surfaces are relatively consistent. In Fig. 3-2(a), an extra local minimum for C_{2v} structure at 2.925 Å is presented by PM6-DH+ method. However, the low energy barrier (0.2 kcal/mol) is negligible for classical MD or PIMD simulations at 300K. As shown in Fig. 3-2(b), due to the asymmetric ionic hydrogen bonding in $Cl^-(H_2O)_2$ clusters, two minima are shown in the potential energy surfaces, which correspond to the r(Cl…O_1) and r(Cl…O_2) distances in the optimized $Cl^-(H_2O)_2$ structures, respectively. A peak appears at r_p=2.926/3.172 Å for PM6-DH+/MP2. The result means r(Cl…O_1) and r(Cl…O_2) are both equal to r_p at the peak position. For the region in the figure that r(Cl…O) distance is shorter or longer than r_p, the potential energy surface along r(Cl…O_1) or r(Cl…O_2) coordinate is lower, respectively. Thus, the r(Cl…O) coordinate shown in Fig. 3-2(b) represents r(Cl…O_1) or r(Cl…O_2) distance when it is shorter or longer than r_p, respectively. In addition, the peak height is 1.5/0.1 kcal/mol for PM6-DH+/MP2, which could be easily jumped over by thermal effect and nuclear quantum effect, as shown

later. Fig. 3-2(c) and Fig. 3-2(d) show the potential energy surfaces including the zero-point energies for n=1 and n=2, respectively. The zero points of potentials in Fig. 3-2(c) and Fig. 3-2(d) are selected to be the same as Fig. 3-2(a) and Fig. 3-2(b), respectively. It could be seen that the potential energy surfaces are significantly raised by zero-point energies. However, the sharp of the potential energy surfaces with zero-point energy corrections are close to the ones without corrections. In addition, one important difference by including zero-point energy corrections is that the r(Cl…O) distance in the minimum structures for n=1 is shortened by about 0.1A for PM6-DH+ potential, as shown in Fig. 3-2(a) and Fig. 3-2(c). Despite the optimized r(Cl…O) distances are about 0.3A shorter than the experiments, the shape of potential energy surface by PM6-DH+ is in agreement with that by MP2, which could well reflect the floppy nature of the cluster structures. Thus it is reasonable to use PM6-DH+ potential to investigate the nuclear quantum effects on structural rearrangement of $Cl^-(H_2O)_n$ clusters by comparison of classical MD and PIMD simulations.

3.3.2. Structural rearrangement

The structures of $Cl^-(H_2O)_{1-4}$ clusters are rather flexible and the rearrangement of ion-water and water-water hydrogen bond network is quite frequent within the simulation time. It could be expected that each geometrically equivalent coordinate would display the same statistical feature at the infinite time limit. For example, the n r(Cl…O) coordinates in $Cl^-(H_2O)_n$ clusters (n>1) would show the same probability distribution function (pdf). Thus, the average pdf of n r(Cl…O) coordinates, which is written as r^{aver}(Cl…O) below, was calculated to show the average cluster structures (Fig. 3-3(a)). At the same time, the longest r^l(Cl…O) (Fig. 3-3(b)) and the shortest r^s(Cl…O) coordinates (Fig. 3-3(c)) at each time step were also picked out to make comparison with the average value.

Unlike the well-known delocalization of the intramolecular covalent hydrogen bond stretching motion [45], other cluster coordinates with heavier atoms may display localized distributions by including the nuclear quantum effects [46]. Here the delocalization of the r(Cl…O) coordinate would be not so obvious as r(O-H*) coordinate due to the heavier mass of Cl. On the other hand, the intermolecular ionic hydrogen bond bending (θ(Cl…H*-O)) becomes more localized by including the nuclear quantum effects. The asymmetric ionic hydrogen bonded structures, which correspond to shorter r(Cl…O) distances, become more favorable

than the symmetric structures. Thus the quantum distributions of r(Cl…O) coordinates become shorter and more delocalized than the corresponding classical distributions.

It is shown in Fig. 3-3(a) that the average probability for one water molecule to reside in the first hydration shell ($r(Cl…O) < r_0$) is much larger than that in outer shells ($r(Cl…O) > r_0$). A typical r_0 is selected to be 3.9Å by following a previous MD study [47]. It is found that the peak position of $r^{aver}(Cl…O)$ remains almost the same as the cluster size increases. The quantum PIMD simulations show slightly larger (<0.1 Å) peak positions than the classical MD simulations. The differences arise from the changing of effective potential by incorporating the nuclear quantum effect.

To distinguish between single and multi hydration shell cluster structures, the $r^l(Cl…O)$ coordinate, which stands for the longest r(Cl…O) distance in $Cl^-(H_2O)_n$ clusters (n>2) at each time step, was selected and shown in Fig. 3-3(b). As no cluster dissociation occurred within the simulation time, the $r^l(Cl…O)$ distance, which is larger than r_0, can be viewed as an intuitive proof for the existence of water-water hydrogen bond interactions as well as the multi hydration shell cluster structures. In Fig. 3-3(b), the results show that the probability for the second shell structures is increasing with cluster size. It is interesting that for n=4, the probability of multi hydration shell structures is comparable to that of single shell structures. This feature is not presented from the previous obtained pdf of $r^{aver}(Cl…O)$. For each r(Cl…O) coordinate, the probability of residing in outer shell is much smaller than that in the first shell. However, when we pick out the $r^l(Cl…O)$ coordinate, any r(Cl…O) coordinates which resides in outer shell would make contributions to the probability. Thus the out shell probability of $r^l(Cl…O)$ is larger than that of $r^{aver}(Cl…O)$. These results indicate that the important structural information may be covered by doing statistical average. In contrast to trend of $r^{aver}(Cl…O)$, the first peak position of $r^l(Cl…O)$ is obviously increasing with the increasing cluster size, which is resulted from the weakening of ionic hydrogen bond strength. Comparing with classical MD, the quantum results show that the probability for single hydration shell structures is decreased while the probability for multi shell structures is slightly increased. The results imply that the water-water hydrogen bond interactions are encouraged by incorporating the nuclear quantum effect.

For the convenience of comparison, the coordinate $r^s(Cl…O)$, which represents the shortest r(Cl…O) distance at each time step, was also selected and shown in Fig. 3-3(c). The results reflect the ion-water stretching motion in the first hydration shell. In contrast to the trend of the outer shell, the peak positions of

r^s(Cl…O) coordinate get shorter as the cluster size increases. The results indicate that the ionic hydrogen bonds in the first shell become stronger due to the cooperation of water-water and ion-water hydrogen bond interactions. The quantum simulations show slightly shorter peak position values than the corresponding classical MD ones due to the inclusion of the nuclear quantum effect. Since the pdf difference between n=3 and n=4 are quite small, an asymptotic pdf could be expected for n>4. The results imply that the water molecules from outer shells would have little effect on the properties of the first shell.

3.3.3. Symmetric and asymmetric hydrogen bonding in the first shell

To describe the changing of bonded H* atom to the chloride ion, here we define a coordinate δ. For the two hydrogen atoms H_1 and H_2 in the same water molecule of the first hydration shell, δ represents the relative position of H_1 and H_2 atoms pointing towards the chloride ion.

$$\delta = \left| r(Cl...H_1) - r(Cl...H_2) \right|, \tag{3.1}$$

When δ=0, the two H atoms are symmetrically bonded to the ion. As δ increases, one H atom becomes non-bonded while the other H atom is still bonded to the ion. Then the coordinate δ could be used to recognize the symmetric and asymmetric hydrogen bonding structures in the first hydration shell. On the other hand, since larger δ corresponds to stronger ionic hydrogen bond, it could be viewed as a measure of ionic hydrogen bond strength.

In Fig. 3-4, both classical MD and PIMD results show that the ionic hydrogen bond in the first hydration shell is getting stronger with cluster size. The strengthening of ionic hydrogen bond is due to the rising cooperation effect of ion-water and water-water interactions. The results are consistent with previous presented r^s(Cl…O) coordinate. Comparing with classical MD, quantum simulations show smaller probability for symmetric hydrogen bond structures while larger probability for asymmetric ones. The results indicate that the intermolecular ionic hydrogen bond bending (θ(Cl…H*-O)) becomes more localized by incorporating the nuclear quantum effects, which tends to weaken the ionic hydrogen bonds. On the other hand, as an important feather of including the nuclear quantum effects, the intramolecular covalent hydrogen bond stretching motion (r(O-H*)) is delocalized, which tends to strengthen the water-water and ion-water hydrogen bond interactions. The two aspects of the nuclear quantum effects contribute to the hydrogen

bonded structures in a competitive manner. The water-water interactions are strengthened while the ion-water interactions are weakened by including the nuclear quantum effects, thus the multi shell structures are more favorable than the single shell structures of $Cl^-(H_2O)_n$ (n=1-4) clusters. Note that the peaks at δ=0 for symmetric hydrogen bond structures from classical MD results are due to the utilization of semi-empirical potential, in which the symmetric hydrogen bond is preferred due to an overestimation of coulombic interaction. However, when the nuclear quantum effect is incorporated, the peaks for symmetric hydrogen bond structures disappear. Instead, a broad distribution for $0<\delta<0.7$ Å comes up, which dues to the frequent water wagging motion.

3.3.4. The correlations between δ and other cluster coordinates

In this subsection, I would discuss the correlations between δ and other cluster vibration coordinates. The selected coordinates, such as ion-water stretching motions and proton transfer motions, are important in the ionic hydrogen bonded cluster structures. Note that all the coordinates are selected within the first hydration shell due to the definition of δ in Eq. 1.

First, I show the correlation between δ and ion-water stretching motion in Fig. 3-5. From the two dimensional distribution, it is clearly shown that the peak of asymmetric hydrogen bonded structures corresponds to a shorter r(Cl…O) distance, comparing with the one for symmetric hydrogen bonded structures. By incorporating the nuclear quantum effect, the proportion for asymmetric hydrogen bonded structures becomes larger in comparison of classical MD results. However, both classical and quantum simulations show that there is little correlation between δ and ion-water stretching motion. Thus it is concluded that the changing of bonded H* atom has little effect on the ion-water stretching motion of the clusters.

Next, I consider the correlation between δ and proton transfer motion in Fig. 3-6. The classical MD results show the r(O-H*) distances for symmetric structures is obviously smaller than the ones for asymmetric structures. Correspondingly, due to the nuclear quantum effect, the distribution of r(O-H*) coordinate is significantly broadened and the overlaps between symmetric and asymmetric structures appear in the quantum simulation results. Both the classical MD and PIMD results show that the correlation between

δ and r(O-H*) coordinate is strong for n=1, while it is decreasing with cluster size due to the addition of water-water hydrogen bond interactions. Besides, by incorporating the nuclear quantum effect, the correlation is slightly decreased in comparison of classical results, which is due to the preference of water-water hydrogen bond interactions by quantum simulations.

In addition, the cross correlation coefficients between δ and other coordinate were shown in Table 3-2. The coefficients were normalized to 1/-1, which means complete positive/negative correlation. The results show that the coefficient between δ and r(Cl…O) is almost half of the coefficient between δ and r(O-H*), which is consistent with previous analysis. Contrary to the θ(H-O-H*) coordinate, the absolute value of correlation coefficients between δ and other coordinates are all decreased by inclusion of nuclear quantum effect. The results indicate the vibration motions affected by the ion are weakened by nuclear quantum effect, which results from the preference of water-water hydrogen bond interactions by quantum simulation.

Previous experimental vibrational spectra has provide indirect structural information for each vibration mode of $Cl^-(H_2O)_1$ cluster [48]. For example, the experimental frequency of r(Cl…O) stretching motion is 210cm^{-1}, which is quite slow in comparison of r(O-H*) stretching motion (3130cm^{-1}). Together with the previous 2 dimensional distribution analysis, it is concluded that the changing of bonded H* atom would be much faster than ion-water stretching motion while it is comparable with proton transfer motion. When the cluster size increases, since the coupling of vibration modes becomes more complex, it is very difficult get information for each vibration mode from experimental spectra. However, the calculation results could provide such information and similar trends as n=1 are clearly shown for n=2-4.

3.4. Summary

In this chapter, the nuclear quantum effect on the ionic hydrogen bonded structures of $Cl^-(H_2O)_{1-4}$ clusters is examined by carrying out classical MD and PIMD simulations.

An outer shell coordinate r^l(Cl…O) is picked out to distinguish between single and multi shell structures and to display the rearrangement of the cluster structures. The proportion of the multi shell structures is increasing with cluster size. When n=4, the proportion of single and multi shell structures are very close. By

incorporating the nuclear quantum effect, it is shown that the probability for single hydration shell structures is decreased while the probability for multi shell structures is slightly increased.

As the cluster size increases, it is interesting to find that the ionic hydrogen bond strength in the first hydration shell is increasing. The results are due to the rising corporation of ion-water and water-water hydrogen bond interactions. Meanwhile, an asymptotic value of ionic hydrogen bond strength in the first shell could be expected for larger cluster size. On the contrary, the ionic hydrogen bond strength for single shell structures is decreasing with cluster size. By taking both aspects into consideration, the average ionic hydrogen bond strength remains approximately constant with the increasing of cluster size.

On the other hand, the correlations between changing of bonded H* atom to chloride ion and other cluster coordinates are presented. The results show that δ strongly correlates with proton transfer motion while it has little correlation with ion-water stretching motion. The results indicate that the frequency of δ is comparable to proton transfer motion while it is much faster than ion-water stretching motion. Besides, on the contrary to θ(H-O-H*) coordinate, the correlations between δ and other coordinates are all decreased by inclusion of nuclear quantum effect. The results indicate the vibration motions affected by the ion are weakened by nuclear quantum effect, which results from the preference of water-water hydrogen bond interactions by quantum simulation.

References in Chapter 3:

[1] K. A. Dill, T. M. Truskett, V. Vlachy, B. Hribar-Lee, *Annu Rev Bioph Biom* **34**, 173-199 (2005).

[2] J. E. Enderby, *Chem Soc Rev* **24**, 159-168 (1995).

[3] P. Lo Nostro, B. W. Ninham, *Chem Rev* **112**, 2286-2322 (2012).

[4] Y. Marcus, *Chem. Rev.* **109**, 1346-1370 (2009).

[5] D. M. Rogers, T. L. Beck, *J Chem Phys* **132**, 14505 (2010).

[6] P. Lopes, B. Roux, A. D. Mackerell, *Theor Chem Acc* **124**, 11-28 (2009).

[7] Z. Zhao, D. M. Rogers, T. L. Beck, *J Chem Phys* **132**, 14502 (2010).

[8] S. J. Stuart, B. J. Berne, *J. Phys. Chem.* **100**, 11934-11943 (1996).

[9] D. H. Herce, L. Perera, T. A. Darden, C. Sagui, *J. Chem. Phys.* **122**, 24513 (2005).

[10] C. Caleman, J. S. Hub, P. J. Van Maaren, D. Van Der Spoel, *P Natl Acad Sci Usa* **108**, 6838-6842 (2011).

[11] L. Perera, M. L. Berkowitz, *J Chem Phys* **96**, 8288-8294 (1992).

[12] G. Markovich, S. Pollack, R. Giniger, O. Cheshnovsky, *J Chem Phys* **101**, 9344-9353 (1994).

[13] J. H. Choi, K. T. Kuwata, Y. B. Cao, M. Okumura, *J. Phys. Chem. A* **102**, 503-507 (1998).

[14] P. Ayotte, S. B. Nielsen, G. H. Weddle, M. A. Johnson, S. S. Xantheas, *J Phys Chem A* **103**, 10665-10669 (1999).

[15] P. Ayotte, G. H. Weddle, M. A. Johnson, *J Chem Phys* **110**, 7129-7132 (1999).

[16] P. Ayotte, G. H. Weddle, J. Kim, M. A. Johnson, *J. Am. Chem. Soc.* **120**, 12361-12362 (1998).

[17] R. W. Gora, S. Roszak, J. Leszczynski, *Chem Phys Lett* **325**, 7-14 (2000).

[18] M. Masamura, *J Phys Chem A* **106**, 8925-8932 (2002).

[19] J. Kim, H. M. Lee, S. B. Suh, D. Majumdar, K. S. Kim, *J. Chem. Phys.* **113**, 5259-5272 (2000).

[20] H. M. Lee, D. Kim, K. S. Kim, *J. Chem. Phys.* **116**, 5509-5520 (2002).

[21] H. T. Dong, W. B. Liu, D. Doren, R. Wood, *J Phys Chem B* **110**, 18504-18514 (2006).

[22] D. J. Tobias, P. Jungwirth, M. Parrinello, *J Chem Phys* **114**, 7036-7044 (2001).

[23] S. J. Stuart, B. J. Berne, *J Phys Chem A* **103**, 10300-10307 (1999).

[24] H. E. Dorsett, R. O. Watts, S. S. Xantheas, *J Phys Chem A* **103**, 3351-3355 (1999).

[25] C. Swalina, Q. Wang, A. Chakraborty, S. Hammes-Schiffer, *J Phys Chem A* **111**, 2206-2212 (2007).

[26] J. A. Morrone, R. Car, *Phys Rev Lett* **101**, 17801 (2008).

[27] B. S. Gonzalez, E. G. Noya, C. Vega, L. M. Sese, *J Phys Chem B* **114**, 2484-2492 (2010).

[28] B. Walker, A. Michaelides, *J Chem Phys* **133**, 174306 (2010).

[29] X. Z. Li, B. Walker, A. Michaelides, *P Natl Acad Sci Usa* **108**, 6369-6373 (2011).

[30] D. Marx, M. Parrinello, *J. Chem. Phys.* **104**, 4077-4082 (1996).

[31] M. Shiga, M. Tachikawa, S. Miura, *Chem. Phys. Lett.* **332**, 396-402 (2000).

[32] M. J. Gillan, F. Christodoulos, *Int. J. Mod. Phys. C* **4**, 287-297 (1993).

[33] M. Shiga, M. Tachikawa, S. Miura, *J. Chem. Phys.* **115**, 9149-9159 (2001).

[34] B. J. Berne, D. Thirumalai, *Annu. Rev. Phys. Chem.* **37**, 401-424 (1986).

[35] M. E. Foster, K. Sohlberg, *Phys Chem Chem Phys* **12**, 307-322 (2010).

[36] K. E. Riley, P. Hobza, *WIREs Comput. Mol. Sci.* **1**, 3-17 (2011).

[37] T. Yoshikawa, H. Motegi, A. Kakizaki, T. Takayanagi, M. Shiga, M. Tachikawa, *Chem Phys* **365**, 60-68 (2009).

[38] J. R Eza C, J. I. Fanfrli K, D. Salahub, P. Hobza, *J. Chem. Theory Comput.* **5**, 1749-1760 (2009).

[39] M. Korth, *J. Chem. Theo. Compu.* **6**, 3808-3816 (2010).

[40] M. Korth, M. Pitonak, J. Rezac, P. Hobza, *J. Chem. Theo. Compu.* **6**, 344-352 (2010).

[41] M. E. Tuckerman, G. J. Martyna, *J Phys Chem B* **104**, 159-178 (2000).

[42] G. J. Martyna, M. L. Klein, M. Tuckerman, *J. Chem. Phys.* **97**, 2635-2643 (1992).

[43] S. Nose, *J. Chem. Phys.* **81**, 511-519 (1984).

[44] J. J. P. Stewart, *MOPAC2012, Stewart Computational Chemistry, Colorado Springs, CO, USA, HTTP://OpenMOPAC.net* (2012).

[45] K. Suzuki, M. Tachikawa, M. Shiga, *J. Chem. Phys.* **132**, 144108 (2010).

[46] S. Raugei, M. L. Klein, *J Am Chem Soc* **125**, 8992-8993 (2003).

[47] S. Chowdhuri, A. Chandra, *J Phys Chem B* **110**, 9674-9680 (2006).

[48] J. M. Lisy, *J. Chem. Phys.* **125**, 132302 (2006).

[49] K. Hiraoka, S. Mizuse, S. Yamabe, *J. Phys. Chem.* **92** 3943 (1988).

[50] H. Ohtaki, T. Radnai, *Chem. Rev.* **93** 1157 (1993).

Table 3-1 Optimized structures of chloride hydrates for n=1-4 water molecules

n	structure	PM6-DH+			B3LYP/aug-cc-pVDZ			MP2/aug-cc-pVDZ			Experiment	
		BE[a]	r(Cl…O)[b]	r(Cl…H*)	BE	r(Cl…O)	r(Cl…H*)	BE	r(Cl…O)	r(Cl…H*)	BE[c]	r(Cl…O)[d]
1	C_S	14.2	2.817	1.833	13.2	3.124	2.143	13.5	3.137	2.159	14.7	3.06-3.26
	C_{2v}	13.9	2.925	2.490	-	-	-	-	-	-		
2	C_1	28.1	2.750,3.474	1.668,2.765	24.5	3.102,3.281	2.122,2.372	26.2	3.105,3.277	2.128,2.366	27.7	
3	C_3	40.8	2.950	2.299	35.4	3.232	2.322	39.4	3.222	2.308	39.5	
4	C_4	52.5	2.951	2.411	45.1	3.294	2.411	51.1	3.268	2.375	51.1	
	$C_{S'}$	51.5	2.709, 3.413	1.560, 2.683	44.1	3.066,3.251	2.079,2.327	49.1	3.063,3.235	2.077,2.308		

a. BE represents binding energies (kcal/mol) with zero-point corrections; b. Distances are in Å. Degenerate distances are listed only once. c. ref. [49] d. ref. [50].

Table 3-2 Cross correlation coefficients[a] between δ and other coordinates

Coordinate	n=1		n=2		n=3		n=4	
	classical	quantum	classical	quantum	classical	quantum	classical	quantum
r(Cl…O)	-0.31	-0.31	-0.48	-0.42	-0.48	-0.41	-0.45	-0.39
r(Cl…H)	-0.84	-0.83	-0.92	-0.89	-0.93	-0.89	-0.93	-0.89
r(O-H*)	0.61	0.45	0.75	0.58	0.76	0.61	0.76	0.63
θ(Cl…H*-O)	0.97	0.90	0.96	0.90	0.95	0.88	0.94	0.87
θ(Cl…O-H*)	-0.97	-0.92	-0.97	-0.92	-0.96	-0.91	-0.95	-0.89
θ(H-O-H*)	0.13	0.15	0.12	0.14	0.12	0.14	0.14	0.15

a. The correlation coefficients have been normalized to 1/-1.

List of figure captions

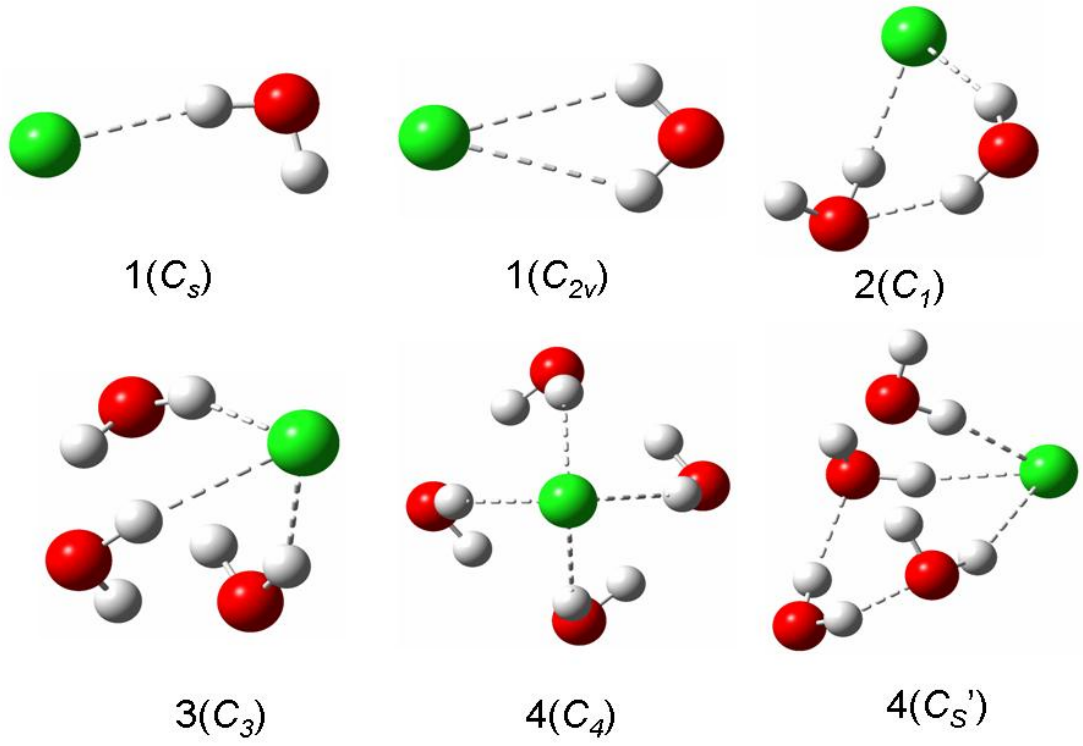

Figure 3-1. Schematically illustrations of optimized structures of $Cl^-(H_2O)_{1-4}$ clusters. The colors of green, red and white represent chloride, oxygen and hydrogen atoms, respectively.

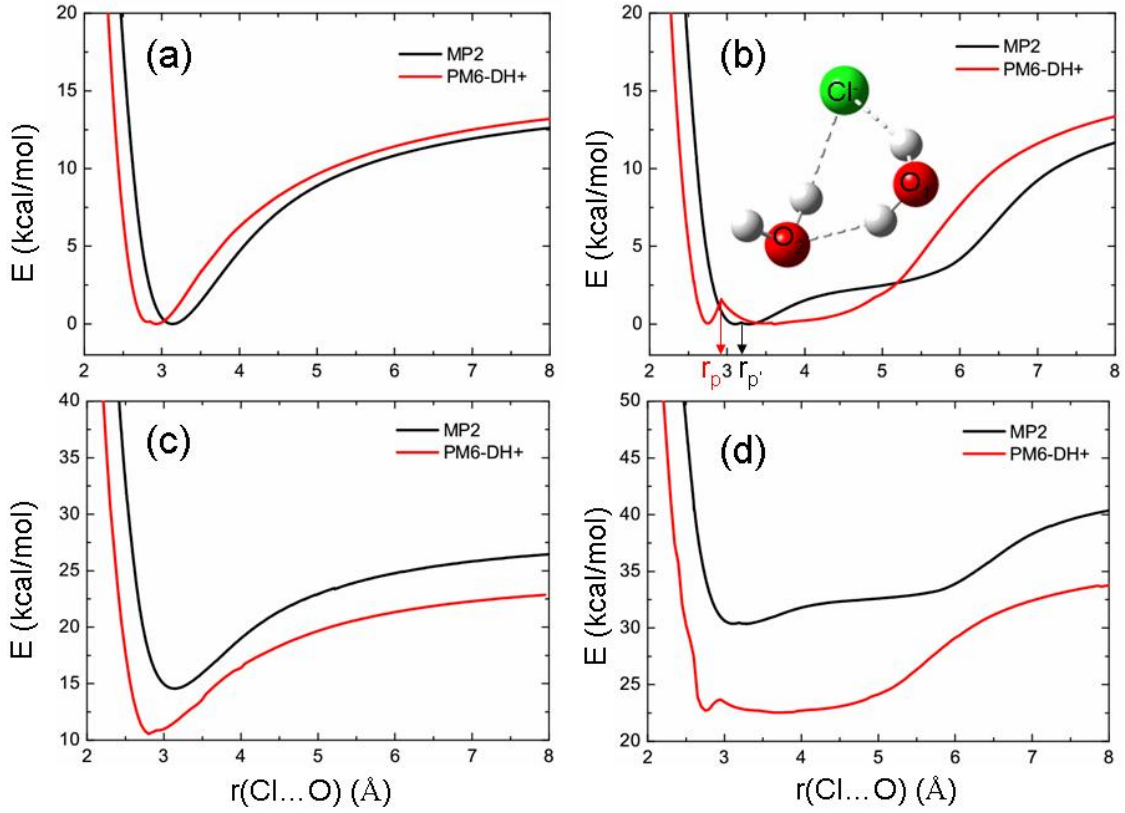

Figure 3-2. Potential energy surfaces of r(Cl…O) coordinates of (a) $Cl^-(H_2O)_1$ and (b) $Cl^-(H_2O)_2$ clusters without zero-point energies; (c) $Cl^-(H_2O)_1$ and (d) $Cl^-(H_2O)_2$ clusters with zero-point energies. The black and red lines represent MP2 and PM6-DH+ methods, respectively. The points r_p=2.926Å and $r_{p'}$ =3.172Å represent the peak position obtained by PM6-DH+ and MP2 methods, respectively.

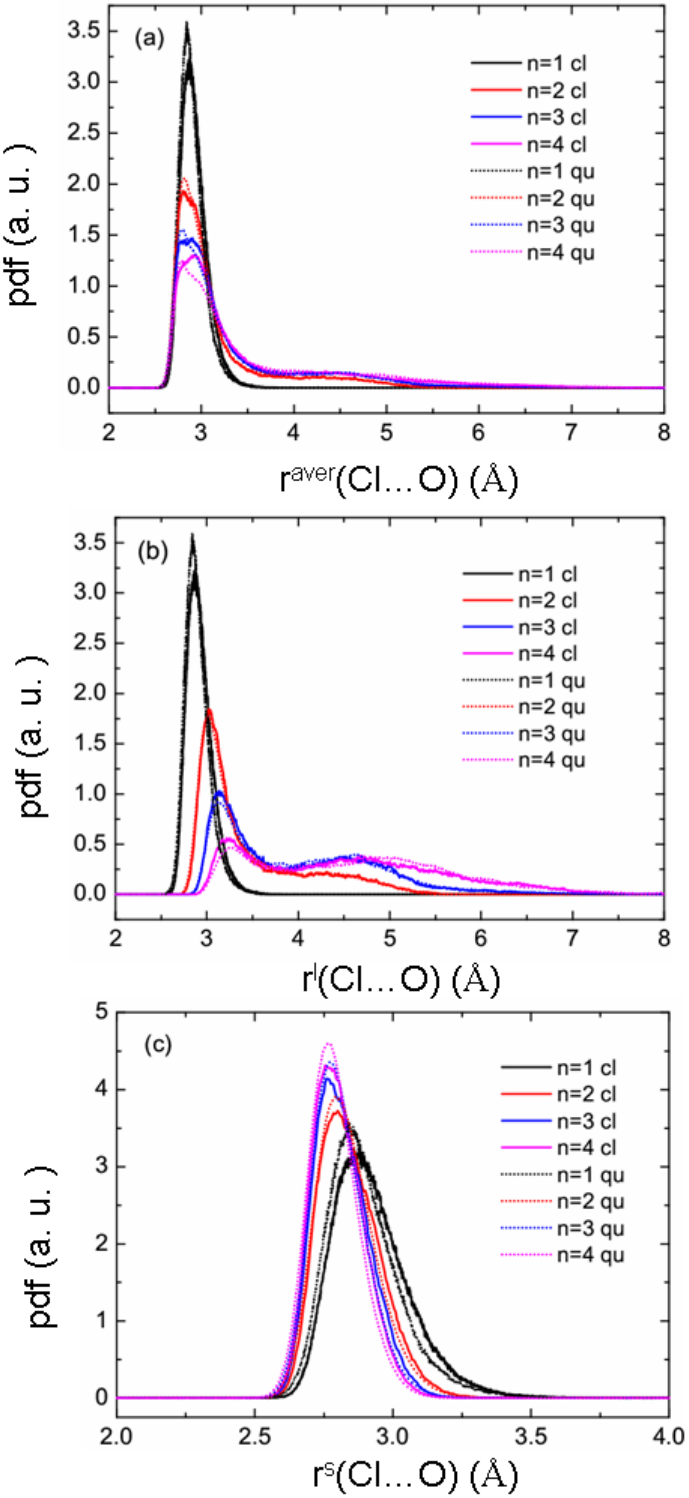

Figure 3-3. The probability distribution function of (a) the (average) r^{aver}(Cl…O); (b) the (longest) r^{l}(Cl…O); (c) the (shortest) r^{s}(Cl…O). The solid and dot lines represent the classical (cl) and quantum (qu) MD simulation results, respectively. The color of black, red, blue, magenta stands for the cluster size for n=1-4.

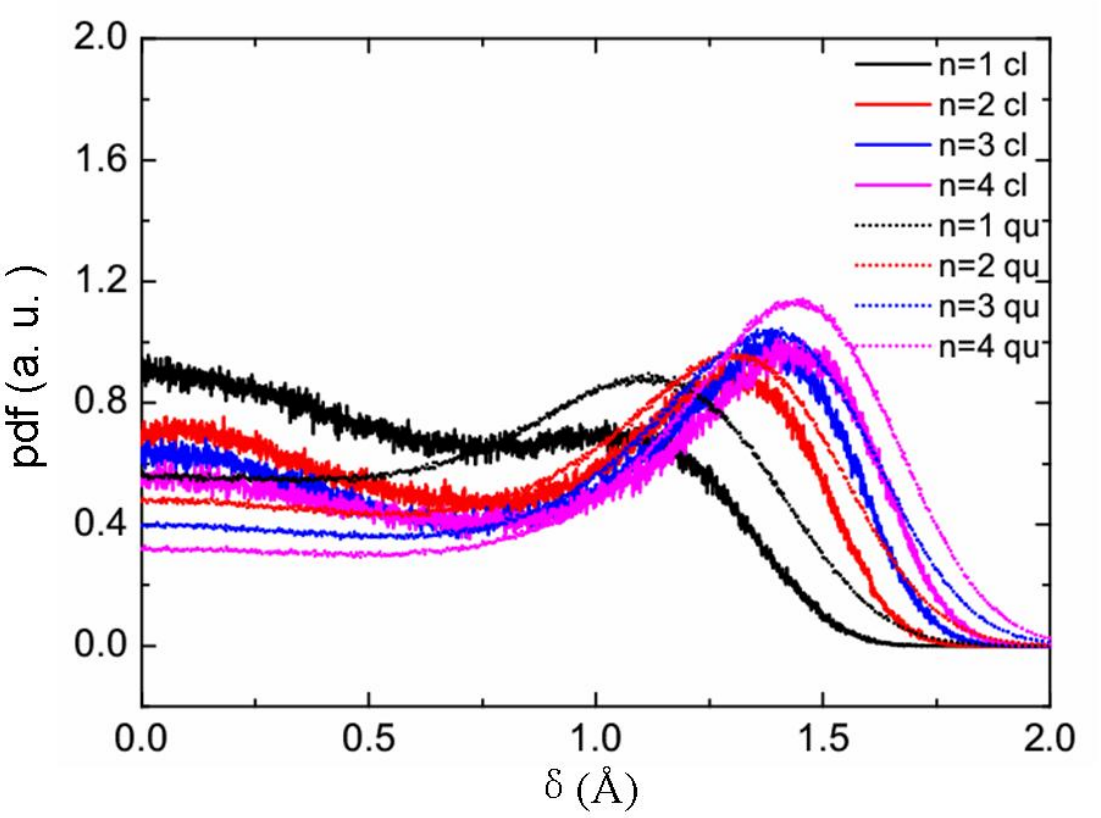

Figure 3-4. The probability distribution function of δ (The changing of bonded hydrogen atom pointed to chloride ion). The color of black, red, blue, magenta stands for the cluster size for n=1-4.

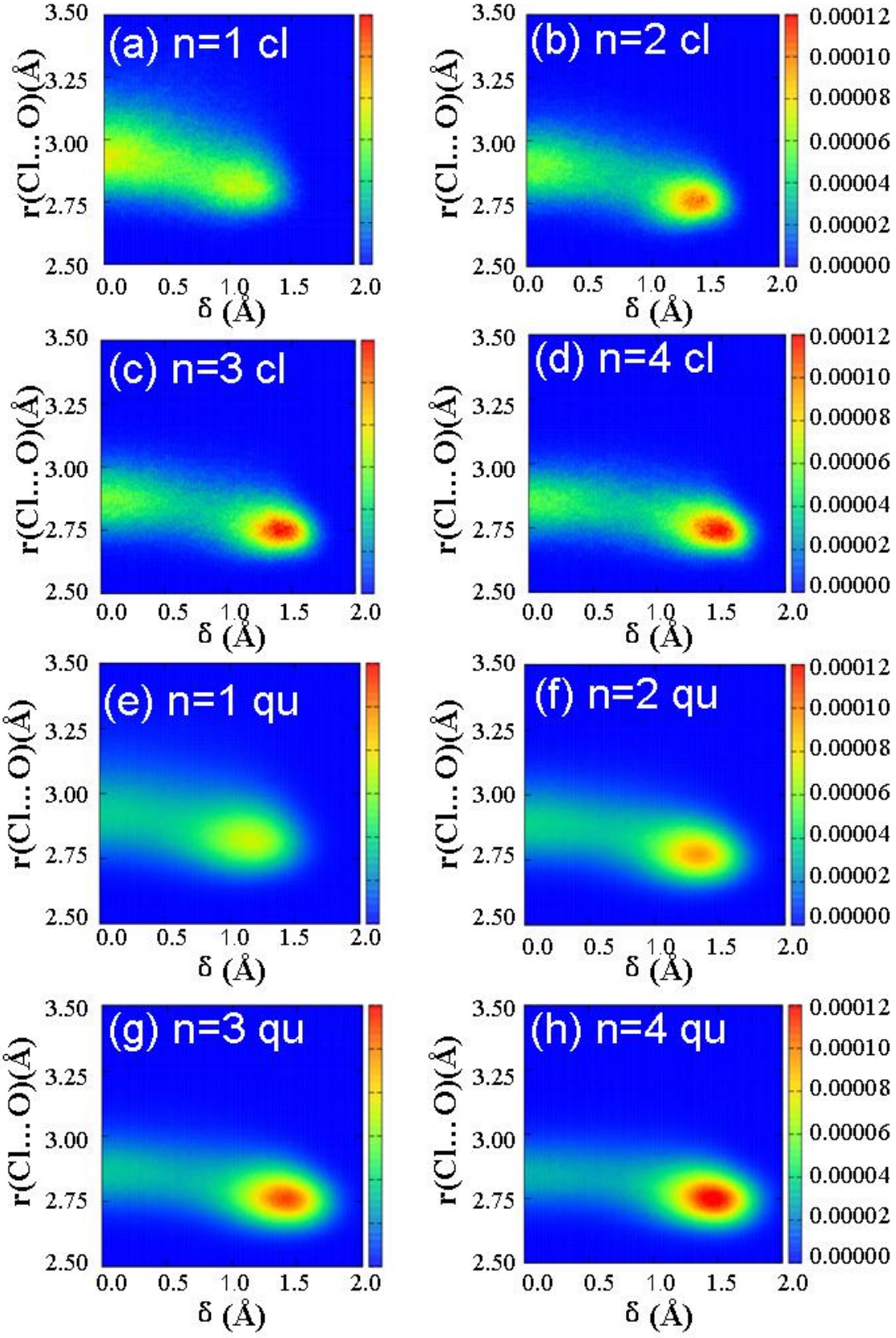

Figure 3-5. Correlation between δ and ion-water stretching motion. (a)-(d) and (e)-(h) show the classical and quantum simulation results, respectively.

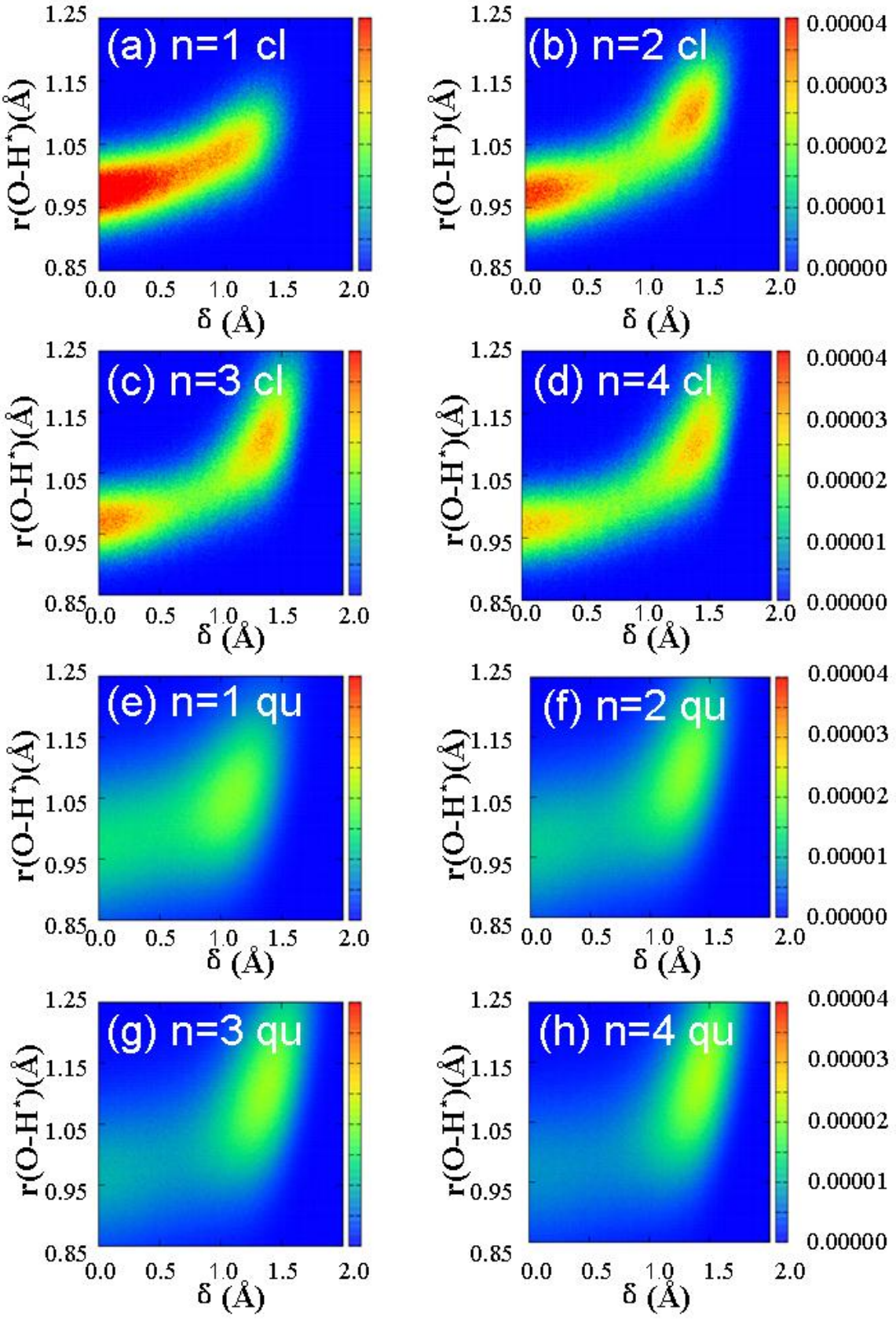

Figure 3-6. Correlation between δ and proton transfer motion. (a)-(d) and (e)-(h) show the classical and quantum simulation results, respectively.

Chapter 4. Geometric Isotope Effects on Small Chloride Ion Water Clusters with Path Integral Molecular Dynamics Simulations

In this chapter, I explored the geometric isotope effects on the structures of ionic hydrogen bonded clusters by carrying out PIMD simulations. First, an outer shell coordinate r^{l}(Cl…O) is selected to display the rearrangement of single and multi hydration shell cluster structures. Next, to show the competition of intramolecular and intermolecular nuclear quantum effects, the r(O-Y*) stretching and ion-water wagging motions are studied for single and multi shell structures, respectively. The results indicate that the intermolecular nuclear quantum effects stabilize the ionic hydrogen bonds in single shell structures, however, they are destabilized through the competition with intramolecular nuclear quantum effects in multi shell structures. In addition, the correlations between ion-water stretching motion and other cluster vibration coordinates are discussed. The results indicate that the intermolecular nuclear quantum effects on the cluster structures are strongly related to the cooperation of the water-water hydrogen bond interactions.

4.1. Introduction

The understanding of the nature of water has attracted intensive attentions since it is essential for life [1-5]. The effects of ion on the properties of water have been shown to be important both in the bulk and at vapor/water interface [6-9]. The structures of water clusters are significantly affected due to the formation of ionic hydrogen bonds. For instance, the simulations of halide ion in small water clusters have demonstrated that F^- prefers to reside in the interior of water clusters, while larger anions such as Cl^-, Br^-, I^- have an increasing propensity of surface solvation due to the decreasing ion-water interactions [10, 11].

The structures of chloride ion water clusters have attracted intensive attention for the ubiquitous existence of Cl^- in nature [12-14]. Perera et al. firstly presented that the Cl^- locates at the surface of the $Cl^-(H_2O)_{20}$ cluster [15], which is supported by the subsequent photoelectron spectroscopy experiments from the energetic point of view [16]. In addition, recent experiments have brought insights into the understanding of cooperation and competition effects of ion-water and water-water hydrogen bond interactions on the

cluster structures. For example, Choi *et al.* [17] observed the hydrogen-bonded and free OH stretching motion of small $Cl^-(H_2O)_n$ clusters by vibrational predissociation spectroscopy. Their results show no water-water hydrogen bond interaction in n=2 and n=3, which are different from the corresponding *ab initio* MO and DFT predictions [18-21]. However, the vibrational spectra using argon predissociation technique obtained at lower temperature by Ayotte *et al.* [13, 22, 23] have presented the existence of water-water hydrogen bond interactions in n=2 and n=3. Thus the temperature effect is considered to play important roles in understanding the differences. On the other hand, classical MD simulations [10, 11, 24-30], which take into account of the temperature effect, could show direct structural information of the clusters. The detailed bond lengths and bond angles are inaccessible for experiments especially for large cluster size. For example, Dorsett et al. probed the temperature effect on the hydrogen bonding network of $Cl^-(H_2O)_2$ cluster [31]. The computed vibrational spectra show a decreasing trend of water-water interactions when temperature increases.

On the other hand, strong quantum behavior is exhibited for the light atom at low temperature or even at room temperature. The nuclear quantum effects, such as zero-point motion and tunneling, are shown to be important in hydrogen-bonded systems [32-36]. For example, the macroscopic properties of water, such as the melting point and the temperature of maximum density (TMD), are increased by 3.8K and 7.2K in D_2O compared with H_2O, respectively [37-39]. From the microscopic point of view, the neutron diffraction experiments show that intramolecular r(O-D) distance is shorter than r(O-H) by about 0.5% [40]. In addition, the anomalous expansion of D_2O ice relative to H_2O is reported recently [41]. In our previous study [50], the geometric isotope effects on fluoride ion water clusters have been discussed. However, up to now, there is little work with respect to the geometrical isotope effects on the ionic hydrogen-bonded $Cl^-(H_2O)_n$ clusters, which shows quite different feature from the fluoride ion water clusters due to its relative weaker ionic hydrogen bonds.

To investigate the geometric effects of isotope substitution, the PIMD simulation is a standard treatment to investigate the quantum nature of nuclei [42-47]. The idea of path integral formulation of quantum mechanics was first developed by Feynman [48]. The only important assumption for PIMD simulation is the Born-Oppenheimer (BO) approximation, which is reasonable and effective to separate nuclear and electronic motions. The accuracy of the PIMD simulations depends on the application of potential level. Due to the

computer limitations, the empirical potentials are developed according to the experimental results or high-level *ab initio* calculations. Recently PIMD calculations using empirical potentials have shown consistent physical properties of water with experimental values [40]. Owing to the growing progress in computer power and in parallelizing technique, the potential energy and its derivatives could be calculated "on the fly" using *ab initio*/DFT electronic structure methods. The *ab initio*/DFT PIMD calculations have been successfully applied into the study of geometric isotope effects for the small charged clusters [49, 50]. However, it is still very time consuming to use *ab initio*/DFT potentials for systems with large size or with floppy structures, which require long simulation time to reach statistical convergence.

As a compromise of both calculation accuracy and efficiency, semi-empirical potentials [51, 52] have been applied to PIMD simulations. For example, the PM6 semi-empirical potential has shown reasonable accurate structures and stabilization energies of neutral hydrogen bonded glycine-water clusters [53] in comparison of *ab initio* calculations. Recently, new semi-empirical potentials PM6-DH [54], PM6-DH+ [55] and PM6-DH2 [56], which improve PM6 by including two important corrections of dispersion energy and hydrogen bonding, have shown promising results for extended hydrogen bonded complexes. In addition, the effectiveness of the semi-empirical potentials for small halide ion water clusters has been discussed in detail in our previous study [57].

In this chapter, I carry out PIMD simulations on the $Cl^-(H_2O)_{1-4}$ clusters with semi-empirical PM6-DH+ potential for the sake of the computational efficiency. Under thermal fluctuation, the frequent rearrangement of the ion-water and water-water hydrogen bond network makes the clusters to vary from the single to multi shell structures. Since the cluster structures are affected by the intramolecular and intermolecular nuclear quantum effect in a competitive way, I explore the geometric isotope effects on the single and multi shell structures of the $Cl^-(H_2O)_{1-4}$ clusters, respectively.

4.2. Computational details

Before PIMD simulations, it is necessary to understand the ground state potential energy surfaces of chloride ion water clusters. To this end, the energetics and optimized structures are compared between semi-empirical PM6-DH+ potential and *ab initio*/DFT calculations in detail in the previous chapters [57]. On the other hand, since r(Cl…O) coordinates play important roles in structural rearrangement of the clusters,

the potential energy surface of PM6-DH+ along r(Cl…O) coordinate is compared with MP2, B3LYP and CCSD levels of theory with the basis set of aug-cc-pVDZ (see Fig. 4-2).

The thermal structures of $Cl^-(H_2O)_{1-4}$ clusters are obtained by using standard imaginary-time PIMD simulations on PM6-DH+ potential energy surface. In the path-integral formalism, a cyclic polymer chain consisting of classical quasi particles is utilized to describe the quantum character of nuclei. Thermal averages are calculated from time averages over fictitious molecular dynamics trajectories, which are generated from the equation of motions described in the normal mode coordinate representation [58]. The system temperature was controlled with a massive Nosé-Hoover chain technique [59, 60].

At each time step, the potential energy and gradient values were directly obtained "on the fly" using the MOPAC2012 software package [61]. The PIMD run was performed with 16 beads at the temperature of T = 300K. With time increment δt = 0.1fs, the total time steps were ranged 10^7. The Nosé-Hoover thermostat of length 4 combined with the velocity Verlet algorithm was used to control the system temperature.

4.3. Results and discussion

In the previous study [50], the geometric isotope effects on strong ionic hydrogen bonded structures of fluoride ion water clusters have been discussed. However, the geometric isotope effects on relative weaker ionic hydrogen bond structures of chloride ion water clusters would show quite different features, as shown in the following subsections.

4.3.1. Potential energy surfaces

The schematic illustrations of the single shell and multi shell structures of $Cl^-(H_2O)_{2-4}$ clusters are shown in Fig. 4-1. The water molecules are directly bonded to the Cl^- via ion-water hydrogen bonds in single shell structures. While in multi shell structures, the outer shell water molecule is connected to the first hydration shell via water-water hydrogen bonds. Due to the relative weaker ionic hydrogen bond interactions, the rearrangement of single and multi shell structures are frequent in $Cl^-(H_2O)_{2-4}$ clusters.

Before classical MD and PIMD simulations, the comparisons of potential energy surfaces between

PM6-DH+ and high-level methods along r(Cl…O) coordinate of $Cl^-(H_2O)$ cluster are shown without and with zero-point energy (ZPE) corrections in Fig. 4-2 (a) and (b), respectively. The results show that PM6-DH+ represents relative shorter r(Cl…O) distances for the minimum position, while the shapes of potential energy surfaces are relatively consistent with high-level calculations. Note that an extra local minimum for C_{2v} structure at 2.925 Å is presented by PM6-DH+ method. However, the low energy barrier (0.2 kcal/mol) is negligible for classical MD or PIMD simulations at 300K.

The comparison of PM6-DH+ method with high-level methods on the optimized geometries of $Cl^-(H_2O)_{1-4}$ clusters are presented in detail in the previous chapters [57, 62]. Despite the optimized r(Cl…O) distances are about 0.3 Å shorter than the experiments, the shape of potential energy surface by PM6-DH+ is in agreement with high-level methods, which could well reflect the floppy nature of the cluster structures. Thus it is reasonable to use PM6-DH+ potential to investigate the geometric isotope effects on structural rearrangement of $Cl^-(H_2O)_n$ clusters by comparison of classical MD and PIMD simulations.

4.3.2. Rearrangement of single and multi shell structures

The structures of chloride ion water clusters are rather flexible and the rearrangement of ion-water and water-water hydrogen bond network is quite frequent within the simulation time. First, I apply a set of geometric criteria to recognize the ionic hydrogen-bonded structures by following a previous study [63].

$r(Cl\cdots O)<r_c(Cl\cdots O)$,

$r(Cl\cdots Y^*)<r_c(Cl\cdots Y^*)$,

$\theta(Cl\cdots O\text{-}Y^*)<\theta_c(Cl\cdots O\text{-}Y^*)$,

$\delta>\delta_c$ (4.1)

Here I define a new coordinate $\delta = | r(Cl\cdots Y_1)\text{-}r(Cl\cdots Y_2) |$, where Y_1 and Y_2 are the hydrogen atoms in the same water molecule. Y represents hydrogen (H) and its isotope deuterium (D). When $\delta=0$, the water molecule is symmetrically bonded to the ion. Larger δ corresponds to stronger ionic hydrogen bonds. The quantities with subscript "c" denote the cutoff values for the upper limit of the ionic hydrogen bond. The cutoff values for chloride-oxygen and chloride-hydrogen bond distances are chosen as $r_c(Cl\cdots O)=3.9$ Å and $r_c(Cl\cdots Y^*)=3.0$ Å, respectively. Here the coordinate of $\theta(Cl\cdots O\text{-}Y^*)$ is used instead of $\theta(Cl\cdots Y^*\text{-}O)$. By

following [63], we use θ_c(Cl…O-Y*)=30° for angular cutoff. The geometric criterion for δ coordinate is chosen as δ_c=0.5 Å.

By using the above mentioned geometric criteria, we firstly explored the probability distribution function (pdf) of the r(Cl…O) distance for n=1. In this case, no water-water hydrogen bond interaction exits since there is only one water molecule in the cluster. It is shown in Fig. 4-3 that the r(Cl…O) distances elongate in the sequence of H(qu), D(qu) and H(cl). In this work, qu and cl are short for quantum and classical, respectively. The results indicate that the ion-water stretching motion is strengthened by the quantum simulations of both H and D, while it is relative weaker for D due to its heavier mass than H.

Next, to show the rearrangement of single and multi hydration shell cluster structures, the r^l(Cl…O) coordinates are picked out as the longest r(Cl…O) distance at each time step for n>1 (see Fig. 4-4). When r^l(Cl…O)<r_c(Cl…O), all the water molecules are connected to Cl^- via ion-water hydrogen bond interactions and thus form the single shell cluster structures. Otherwise, when r^l(Cl…O)>r_c(Cl…O), the multi shell structures are formed and outer shell water molecules are connected via water-water hydrogen bond interactions. The corresponding typical structures of S1-S15 in Fig. 4-4 are selected with respect to the r^l(Cl…O) distance. The ion-water and water-water hydrogen bond interactions in the selected structures are schematically illustrated in Fig. 4-5.

As shown in Fig. 4-4, the proportion of multi shell structures is increased with the number of water molecules. The results indicate the increasing preference of water-water hydrogen bond interactions with the number of water molecules. For n=2, the proportion of single shell structures (S1, S2) is decreased for quantum simulations of H and D in comparison of the classical simulations. On the other hand, the proportion of multi shell structures (S3) is increased for the quantum simulations. However, it is interesting to find that the results of D(qu) looks more favored than H(qu) for multi shell structures (S3). When the proton is replaced by its isotope deuterium D, the ion-water and water-water hydrogen bonds are both weakened due to the heavier mass of D. However, the decrease of ion-water hydrogen bond is relative larger than the decrease of the water-water hydrogen bond. Thus the cluster behaves to favor the water-water hydrogen bond network. On the other hand, since the zero-point energy for D(qu) is smaller than that of H(qu), the hydrogen bonded cluster could be viewed as cooling down for D(qu) in comparison of H(qu). The water-water hydrogen bond interactions are more favored for the “lower” temperature. It is shown in the Fig.

4(a) that the probability difference between H(qu) and H(cl) is obviously smaller than that between H(qu) and D(qu). The results indicate that the effective potential is more sensitive to H/D isotope substitution. For the case of n=3 and n=4, the same trend caused by geometric isotope effects is obtained for single shell structures, while different trends are shown for n=3 and n=4 in the two regions of multi shell structures (see Fig. 4-4(b) and (c)). For n=3, D(qu) and H(qu) show close probability for S6 and S7 structures, while S8 structure is preferred by D(qu). It is interesting to find that S8 structure has more/less water-water hydrogen bonds than S7/S6 structure. For n=4, D(qu) increases the probabilities for S11-S13 structures, while decreases the ones for the S14 and S15 structures in comparison of H(qu). It is shown that the S11-S13 structures have more water-water hydrogen bond interactions than S14, S15 structures. The difference of n=3 and n=4 arises from the competition of ion-water and water-water hydrogen bond interactions in the structures. The results indicate the structures with more water-water hydrogen bond interactions are preferred for D(qu), which are consistent with the case of n=2.

In the next subsection, the geometric isotope effects on intramolecular r(O-Y*) stretching and intermolecular ion-water wagging motions would be discussed in detail for single and multi shell structures, respectively.

4.3.3. Intramolecular r(O-Y*) stretching and intermolecular ion-water wagging motions

Two competitive nuclear quantum effects are shown in the intramolecular r(O-Y*) stretching and intermolecular ion-water wagging motions by a recent study [64]. The intramolecular zero-point energy effect tends to stabilize the hydrogen bond network, which results a slower diffusion behavior. However, the intermolecular nuclear quantum effect disrupts the hydrogen bond network and thus leads a larger diffusion coefficient.

First, the geometric isotope effects on intramolecular r(O-Y*) stretching motion are shown in Fig. 4-6 for single and multi shell structures, respectively. The r(O-Y*) distances shrink in the sequence of H(qu), D(qu) and H(cl) for both single shell and multi shell structures. The average values are presented in Table 4-1. The results indicate that intramolecular nuclear quantum effect tends to stabilize the hydrogen bond network for both single and multi shell structures. However, the bond lengths are obviously longer in multi shell

structures than those in single shell structures. The results indicate the existence of additional outer shell water molecule makes the inner ionic hydrogen bond interactions stronger.

Next, the geometric isotope effects on intermolecular ion-water wagging motion are shown in Fig. 4-7 for single and multi shell structures, respectively. The θ(Cl…Y*-O) angles are becoming smaller for single shell structures in the sequence of H(qu), D(qu) and H(cl). However, they are becoming larger for multi shell structures in the same sequence. The average values are presented in Table 4-1. The results indicate that the intermolecular nuclear quantum effects stabilize the ionic hydrogen bonds in single shell structures, however, the ionic hydrogen bonds in multi shell structures are destabilized. The destabilization of ion-water hydrogen bond interactions in multi shell structures is due to competition with the intramolecular nuclear quantum effects, which stabilizes the water-water hydrogen bond network (see Fig. 4-6).

4.3.4. Correlations between ion-water stretching motion and other coordinates

In this subsection, I would discuss the correlations between the r(Cl…O) distances and other selected cluster vibration coordinates, such as r(O…O') and r(O-Y*) distances.

First, we show the correlations between ion-water stretching motion and the r(O…O') distances in Fig. 4-8. Here the r(O…O') coordinate represents the distance between the water molecule which is bonded to Cl^- and its nearest neighbor water molecule. The water-water hydrogen bond interactions between the two water molecules exist for r(O…O')<3.5 Å, while no such interactions exit for r(O…O')>3.5 Å. For single shell structures, as the number of water molecules increases, the probability for Cl^- to reside in the internal of the clusters is dramatically getting decreased. As shown in Fig 4-8(a)-(c), the r(Cl…O) distances are getting shorter in the sequence of H(qu), D(qu) and H(cl) for r(O…O')>3.5 Å. In this case, there is no cooperation of water-water hydrogen bond interactions and thus the result is consistent with the case of n=1 (see Fig. 4-3). However, the r(Cl…O) distances are getting longer for r(O…O')<3.5 Å in the same sequence. The results indicate that the ion-water stretching motions are strongly affected by the cooperation of water-water hydrogen bonds. On the other hand, for multi shell structures, the r(O…O') distances are always smaller than 3.5 Å. The results are due to that the outer shell water molecule is connected to the first shell via the water-water hydrogen bonds, which indicate Cl^- favors to locate at the surface of the clusters. For the same

reason, the ion-water stretching motion is more localized for multi shell structures than that for single shell structures. Thus, little correlation between the two coordinates is presented for the multi shell structures.

In addition, the correlations between ion-water stretching and r(O-Y*) stretching motions are shown in Fig. 4-9 for single and multi shell structures, respectively. For single shell structures, the correlations are getting smaller in the sequence of H(qu), D(qu) and H(cl), which are due to decreasing ion-water hydrogen bond interactions by the intermolecular nuclear quantum effects. On the other hand, there is little correlation between the coordinates for multi shell structures. The correlations between the two coordinates are much smaller in multi shell structures than those in single shell structures. With the addition of outer shell water molecule, the intermolecular ion-water stretching motion becomes localized, while the intramolecular r(O-Y*) stretching motion becomes delocalized. The results indicate that the ion-water hydrogen bond interactions in the first shell become stronger due to the cooperation of the water-water hydrogen bond interactions.

4.4. Summary

In this work, the geometric isotope effects on ionic hydrogen bonded $Cl^-(H_2O)_{1-4}$ clusters are examined by carrying out classical MD and PIMD simulations for the single and multi shell structures, respectively. First, a set of geometric criteria is applied to recognize the ionic hydrogen bonded structures. To display the rearrangement of single and multi shell cluster structures, an outer shell coordinate r^1(Cl…O) is picked out. As the cluster size increases, the proportion of the multi shell structures is increasing, which indicates the increasing preference of surface solvation of Cl^-. The results show that classical simulation of H prefers single shell structures, while quantum simulation of D favors multi shell structures. The results indicate that the cluster structures are affected by the competition of intramolecular and intermolecular nuclear quantum effects.

Next, to show the competitive intramolecular and intermolecular nuclear quantum effects, the r(O-Y*) stretching and ion-water wagging motions are studied in single shell and multi shell structures, respectively. The r(O-Y*) distances shrink in the sequence of H(qu), D(qu) and H(cl) for both single and multi shell structures. The results indicate that intramolecular nuclear quantum effects tend to stabilize the hydrogen

bond network for both single and multi shell structures. On the other hand, the θ(Cl…Y*-O) angles become smaller/larger for single/multi shell structures in the sequence of H(qu), D(qu) and H(cl). The results indicate that the intermolecular nuclear quantum effects stabilize the ionic hydrogen bonds in single shell structures, however, the ionic hydrogen bonds in multi shell structures are destabilized due to the competition of intramolecular and intramolecular nuclear quantum effects.

In addition, to explore the correlations between the ion-water stretching motion and the cooperation effects of water-water hydrogen bond interactions, two dimensional distributions of r(Cl…O) and r(O…O') coordinates are presented for single and multi shell structures, respectively. The results show that r(Cl…O) distances are getting shorter/longer in the sequence of H(qu), D(qu) and H(cl) without/with the presence of water-water hydrogen bond interactions. The results indicate that the intermolecular nuclear quantum effects on the cluster structures strongly related to the formation of second hydration shell. On the other hand, the correlations between ion-water stretching and r(O-Y*) stretching motions are also presented. It is shown that the correlations are much larger in single shell structures than those in multi shell structures. With the addition of outer shell water molecules, the intermolecular ion-water stretching motion becomes localized while the intramolecular r(O-Y*) stretching motion becomes delocalized. The results indicate that the ion-water hydrogen bond interactions in the first shell become stronger with the cooperation of the water-water hydrogen bond interactions.

References in Chapter 4:

[1] M. J. Shultz, T. H. Vu, B. Meyer, P. Bisson, *Accounts Chem Res* **45**, 15-22 (2012).

[2] L. Darré, M. R. Machado, S. Pantano, *WIREs Comput Mol Sci* **2**, 921-930 (2012).

[3] A. Striolo, *Adsorpt Sci Technol* **29**, 211-258 (2011).

[4] G. Clark, C. D. Cappa, J. D. Smith, R. J. Saykally, T. Head-Gordon, *Mol Phys* **108**, 1415-1433 (2010).

[5] R. Ludwig, *Angew Chem Int Edit* **40**, 1808-1827 (2001).

[6] R. R. Netz, D. Horinek, *Annu. Rev. Phys. Chem.* **63**, 401-418 (2012).

[7] P. Jungwirth, D. J. Tobias, *Chem Rev* **106**, 1259-1281 (2006).

[8] Y. Levin, A. P. Dos Santos, A. Diehl, *Phys. Rev. Lett.* **103**, 257802 (2009).

[9] K. D. Collins, G. W. Neilson, J. E. Enderby, *Biophys Chem* **128**, 95-104 (2007).

[10] D. H. Herce, L. Perera, T. A. Darden, C. Sagui, *J Chem Phys* **122**, 24513 (2005).

[11] C. Caleman, J. S. Hub, P. J. Van Maaren, D. Van Der Spoel, *P Natl Acad Sci Usa* **108**, 6838-6842 (2011).

[12] J. T. O'Brien, E. R. Williams, *J Am Chem Soc* **134**, 10228-10236 (2012).

[13] P. Ayotte, G. H. Weddle, J. Kim, M. A. Johnson, *J Am Chem Soc* **120**, 12361-12362 (1998).

[14] S. Cummings, J. E. Enderby, G. W. Neilson, J. R. Newsome, R. A. Howe, W. S. Howells, A. K. Soper, *Nature* **287**, 714-716 (1980).

[15] L. Perera, M. L. Berkowitz, *J Chem Phys* **96**, 8288-8294 (1992).

[16] G. Markovich, S. Pollack, R. Giniger, O. Cheshnovsky, *J Chem Phys* **101**, 9344-9353 (1994).

[17] J. H. Choi, K. T. Kuwata, Y. B. Cao, M. Okumura, *J Phys Chem A* **102**, 503-507 (1998).

[18] R. W. Gora, S. Roszak, J. Leszczynski, *Chem Phys Lett* **325**, 7-14 (2000).

[19] M. Masamura, *J Phys Chem A* **106**, 8925-8932 (2002).

[20] J. Kim, H. M. Lee, S. B. Suh, D. Majumdar, K. S. Kim, *J Chem Phys* **113**, 5259-5272 (2000).

[21] H. M. Lee, D. Kim, K. S. Kim, *J Chem Phys* **116**, 5509-5520 (2002).

[22] P. Ayotte, S. B. Nielsen, G. H. Weddle, M. A. Johnson, S. S. Xantheas, *J Phys Chem A* **103**, 10665-10669 (1999).

[23] P. Ayotte, G. H. Weddle, M. A. Johnson, *J Chem Phys* **110**, 7129-7132 (1999).

[24] D. M. Rogers, T. L. Beck, *J Chem Phys* **132**, 14505 (2010).

[25] P. Lopes, B. Roux, A. D. Mackerell, *Theor Chem Acc* **124**, 11-28 (2009).

[26] Z. Zhao, D. M. Rogers, T. L. Beck, *J Chem Phys* **132**, 14502 (2010).

[27] S. J. Stuart, B. J. Berne, *J. Phys. Chem.* **100**, 11934-11943 (1996).

[28] H. T. Dong, W. B. Liu, D. Doren, R. Wood, *J Phys Chem B* **110**, 18504-18514 (2006).

[29] D. J. Tobias, P. Jungwirth, M. Parrinello, *J Chem Phys* **114**, 7036-7044 (2001).

[30] S. J. Stuart, B. J. Berne, *J Phys Chem A* **103**, 10300-10307 (1999).

[31] H. E. Dorsett, R. O. Watts, S. S. Xantheas, *J Phys Chem A* **103**, 3351-3355 (1999).

[32] C. Swalina, Q. Wang, A. Chakraborty, S. Hammes-Schiffer, *J Phys Chem A* **111**, 2206-2212 (2007).

[33] J. A. Morrone, R. Car, *Phys Rev Lett* **101**, 17801 (2008).

[34] B. S. Gonzalez, E. G. Noya, C. Vega, L. M. Sese, *J Phys Chem B* **114**, 2484-2492 (2010).

[35] B. Walker, A. Michaelides, *J Chem Phys* **133**, 174306 (2010).

[36] X. Z. Li, B. Walker, A. Michaelides, *P Natl Acad Sci Usa* **108**, 6369-6373 (2011).

[37] C. Mcbride, J. L. Aragones, E. G. Noya, C. Vega, *Phys Chem Chem Phys* **14**, 15199-15205 (2012).

[38] R. Ramirez, C. P. Herrero, *J Chem Phys* **133**, 144511 (2010).

[39] E. G. Noya, C. Vega, L. M. Sese, R. Ramirez, *J. Chem. Phys.* **131**, 124518 (2009).

[40] A. Zeidler, P. S. Salmon, H. E. Fischer, J. C. Neuefeind, J. M. Simonson, T. E. Markland, *J. Phys. Condens. Matter* **24**, 284126 (2012).

[41] B. Pamuk, J. M. Soler, R. Ramirez, C. P. Herrero, P. W. Stephens, P. B. Allen, M. V. Fernandez-Serra, *Phys Rev Lett* **108**, 193003 (2012).

[42] K. Suzuki, M. Shiga, M. Tachikawa, *J. Chem. Phys.* **129**, 144310 (2008).

[43] D. Marx, M. Parrinello, *J Chem Phys* **104**, 4077-4082 (1996).

[44] M. Shiga, M. Tachikawa, S. Miura, *Chem Phys Lett* **332**, 396-402 (2000).

[45] M. J. Gillan, F. Christodoulos, *Int. J. Mod. Phys. C* **4**, 287-297 (1993).

[46] M. Shiga, M. Tachikawa, S. Miura, *J Chem Phys* **115**, 9149-9159 (2001).

[47] B. J. Berne, D. Thirumalai, *Annu Rev Phys Chem* **37**, 401-424 (1986).

[48] M. Ceriotti, T. E. Markland, *J. Chem. Phys.* **138**, 14112-14113 (2013).

[49] R. P. Feynman, *Rev Mod Phys* **20**, 367 (1948).

[50] M. Tachikawa, M. Shiga, *J Am Chem Soc* **127**, 11908-11909 (2005).

[51] M. E. Foster, K. Sohlberg, *Phys Chem Chem Phys* **12**, 307-322 (2010).

[52] K. E. Riley, P. Hobza, *WIREs Comput. Mol. Sci.* **1**, 3-17 (2011).

[53] T. Yoshikawa, H. Motegi, A. Kakizaki, T. Takayanagi, M. Shiga, M. Tachikawa, *Chem Phys* **365**, 60-68 (2009).

[54] J. R Eza C, J. I. Fanfrli K, D. Salahub, P. Hobza, *J. Chem. Theory Comput.* **5**, 1749-1760 (2009).

[55] M. Korth, *J. Chem. Theo. Compu.* **6**, 3808-3816 (2010).

[56] M. Korth, M. Pitonak, J. Rezac, P. Hobza, *J. Chem. Theo. Compu.* **6**, 344-352 (2010).

[57] Q. Wang, K. Suzuki, U. Nagashima, M. Tachikawa, S. Yan, *J. Theor. Appl. Phys.* **7**, 7 (2013).

[58] M. E. Tuckerman, G. J. Martyna, *J Phys Chem B* **104**, 159-178 (2000).

[59] G. J. Martyna, M. L. Klein, M. Tuckerman, *J Chem Phys* **97**, 2635-2643 (1992).

[60] S. Nose, *J Chem Phys* **81**, 511-519 (1984).

[61] J. J. P. Stewart, *MOPAC2012, Stewart Computational Chemistry, Colorado Springs, CO, USA, HTTP://OpenMOPAC.net* (2012).

[62] Q. Wang, K. Suzuki, U. Nagashima, M. Tachikawa, S. Yan, *Chem Phys* (2013). http://dx.doi.org/10.1016/j.chemphys.2013.02.025

[63] S. Chowdhuri, A. Chandra, *J Phys Chem B* **110**, 9674-9680 (2006).

[64] S. Habershon, T. E. Markland, D. E. Manolopoulos, *J Chem Phys* **131**, 24501 (2009).

Table 4-1. Average value of the r(O-Y*)[a] and θ(Cl…Y*-O)[b] coordinates for single and multi shell structures, respectively.

		Single shell structures			Multi shell structures		
	n	H(qu)	D(qu)	H(cl)	H(qu)	D(qu)	H(cl)
r(O-Y*)	2	1.056	1.053	1.042	1.136	1.131	1.120
	3	1.041	1.040	1.024	1.134	1.130	1.119
	4	1.029	1.023	1.017	1.133	1.116	1.112
θ(Cl…Y*-O)	2	154.3	153.0	152.2	158.8	159.4	160.2
	3	154.1	152.5	151.2	158.2	159.3	159.5
	4	151.5	151.2	150.3	157.4	157.9	158.6

a. Distances are in Å.

b. Angles are in degree.

List of figure captions

Figure 4-1. Schematically illustrations of single and multi shell structures of $Cl^-(H_2O)_{2-4}$ clusters. The colors of yellow, red and white represent chloride, oxygen and hydrogen atoms, respectively.

Figure 4-2. Potential energy surfaces of r(Cl…O) coordinates for $Cl^-(H_2O)_1$ clusters: (a)Without zero-point energy (ZPE) corrections; (b)With ZPE corrections. The black, blue, magenta and red lines represent MP2, B3LYP, CCSD and PM6-DH+ methods, respectively. The aug-cc-pVDZ basis set is used for MP2, B3LYP and CCSD calculations.

Figure 4-3. Probability distribution functions of the r(Cl…O) distances for n=1. The black, red and blue lines represent quantum H, quantum D and classical H simulations, respectively.

Figure 4-4. Probability distribution functions of the r^1(Cl…O) coordinates for (a)n=2; (b)n=3; (c)n=4. The black, red and blue lines represent quantum H, quantum D and classical H simulations, respectively. The structures of S1-S15 are shown in Fig. 4-5.

Figure 4-5. Schematically illustrations of $Cl^-(H_2O)_{2-4}$ structures (S1-S15) with respect to the r^1(Cl…O) coordinates. The bond distances are presented in the parentheses (in Angstrom). The ion-water and water-water hydrogen bond interactions are shown in black and red dot lines, respectively.

Figure 4-6. Probability distribution functions of r(O-Y*) coordinates (r(O-Y*) stretching motion) for (a)-(c)single shell structures; (d)-(f)multi shell structures. The black, red and blue lines represent quantum H, quantum D and classical H simulations, respectively.

Figure 4-7. Probability distribution functions of θ(Cl…Y*-O) coordinates (ion-water wagging motion) for (a)-(c)single shell structures; (d)-(f)multi shell structures. The black, red and blue lines represent quantum H, quantum D and classical H simulations, respectively.

Figure 4-8. Correlations between the r(Cl…O) and r(O…O') coordinates. (a)-(i) and (j)-(r) show the results for single shell and multi shell structures, respectively.

Figure 4-9. Correlations between the r(Cl…O) and r(O-Y*) coordinates. (a)-(i) and (j)-(r) show the results for single shell and multi shell structures, respectively.

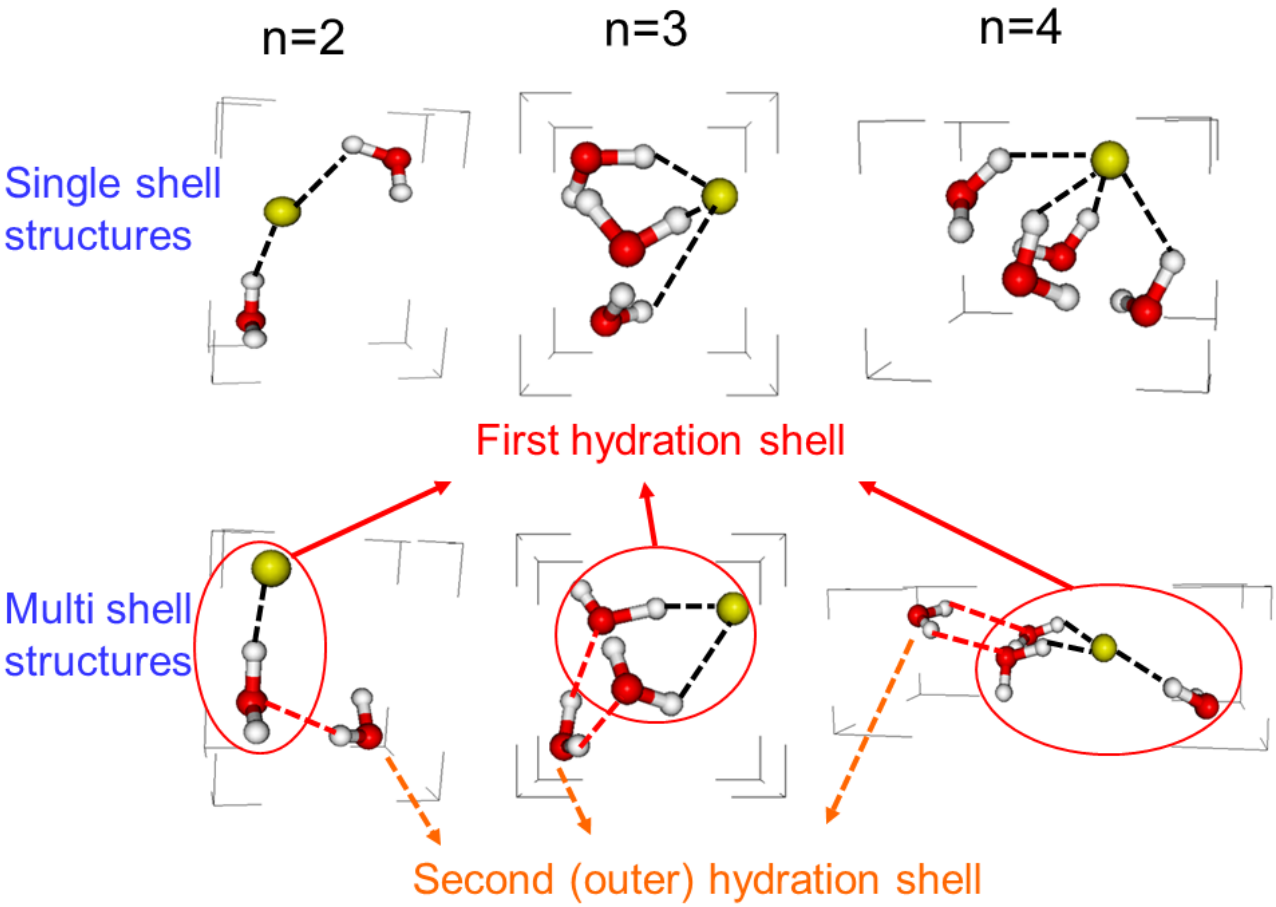

Figure 4-1. Schematically illustrations of single and multi shell structures of $Cl^-(H_2O)_{2-4}$ clusters. The colors of yellow, red and white represent chloride, oxygen and hydrogen atoms, respectively.

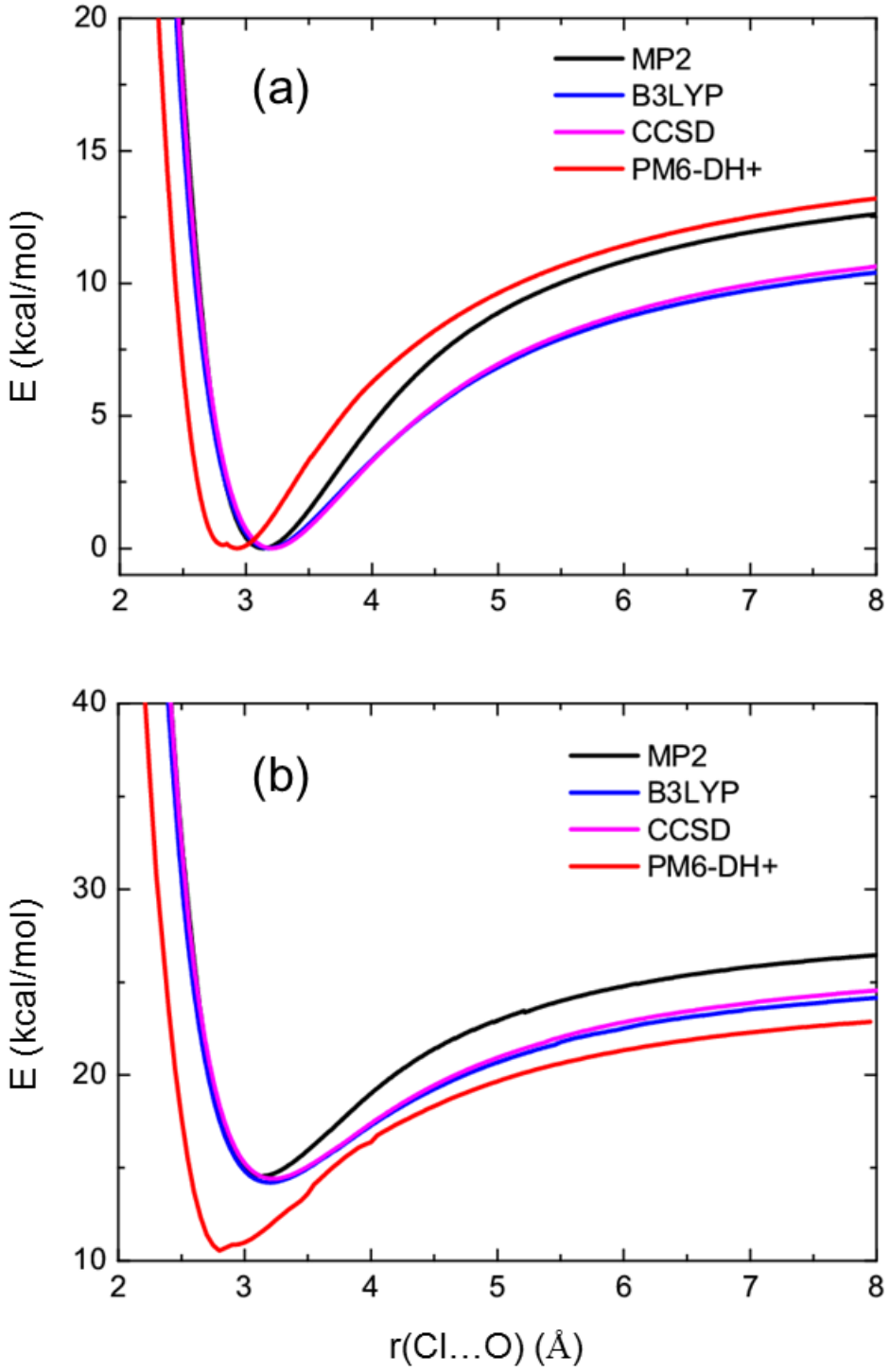

Figure 4-2. Potential energy surfaces of r(Cl…O) coordinates for $Cl^-(H_2O)_1$ clusters: (a)Without zero-point energy (ZPE) corrections; (b)With ZPE corrections. The black, blue, magenta and red lines represent MP2, B3LYP, CCSD and PM6-DH+ methods, respectively. The aug-cc-pVDZ basis set is used for MP2, B3LYP and CCSD calculations.

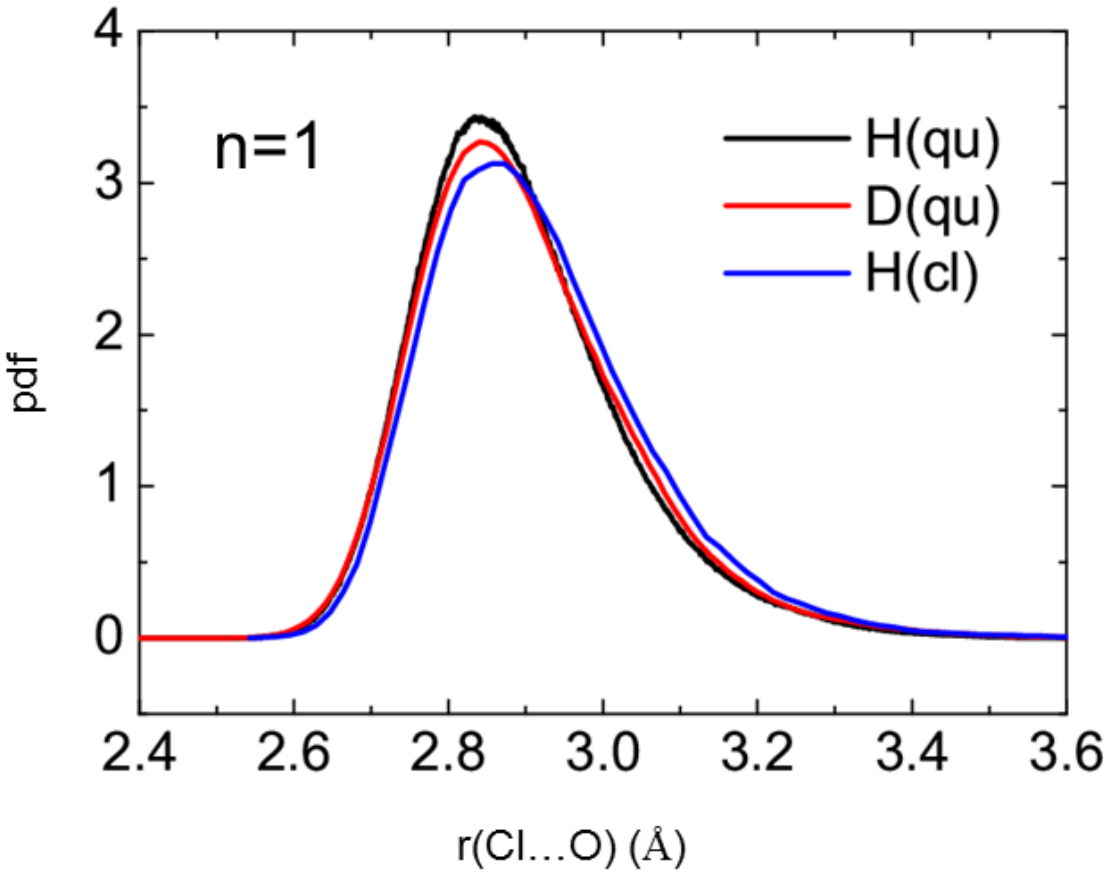

Figure 4-3. Probability distribution functions of the r(Cl…O) distances for n=1. The black, red and blue lines represent quantum H, quantum D and classical H simulations, respectively.

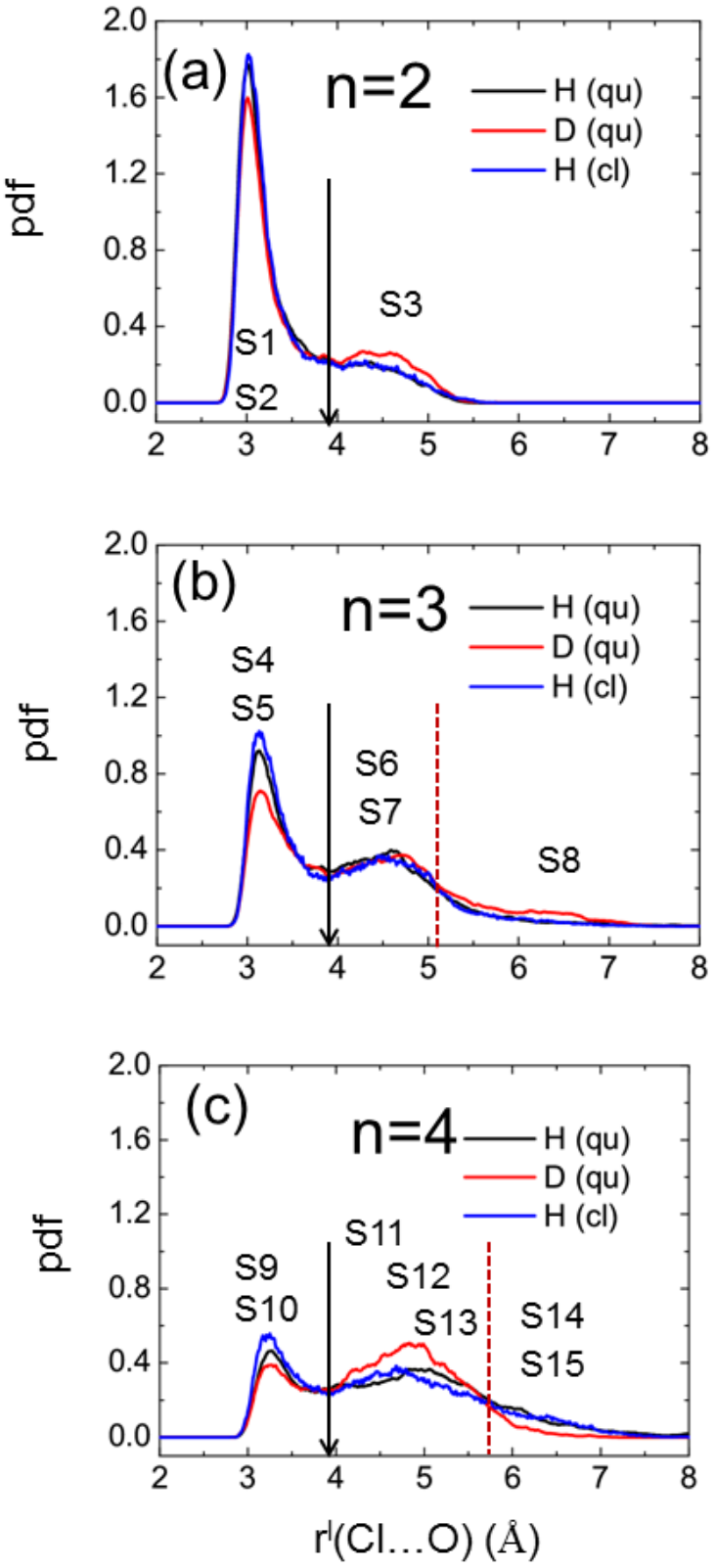

Figure 4-4. Probability distribution functions of the r^l(Cl…O) coordinates for (a)n=2; (b)n=3; (c)n=4. The black, red and blue lines represent quantum H, quantum D and classical H simulations, respectively. The structures of S1-S15 are shown in Fig. 4-5.

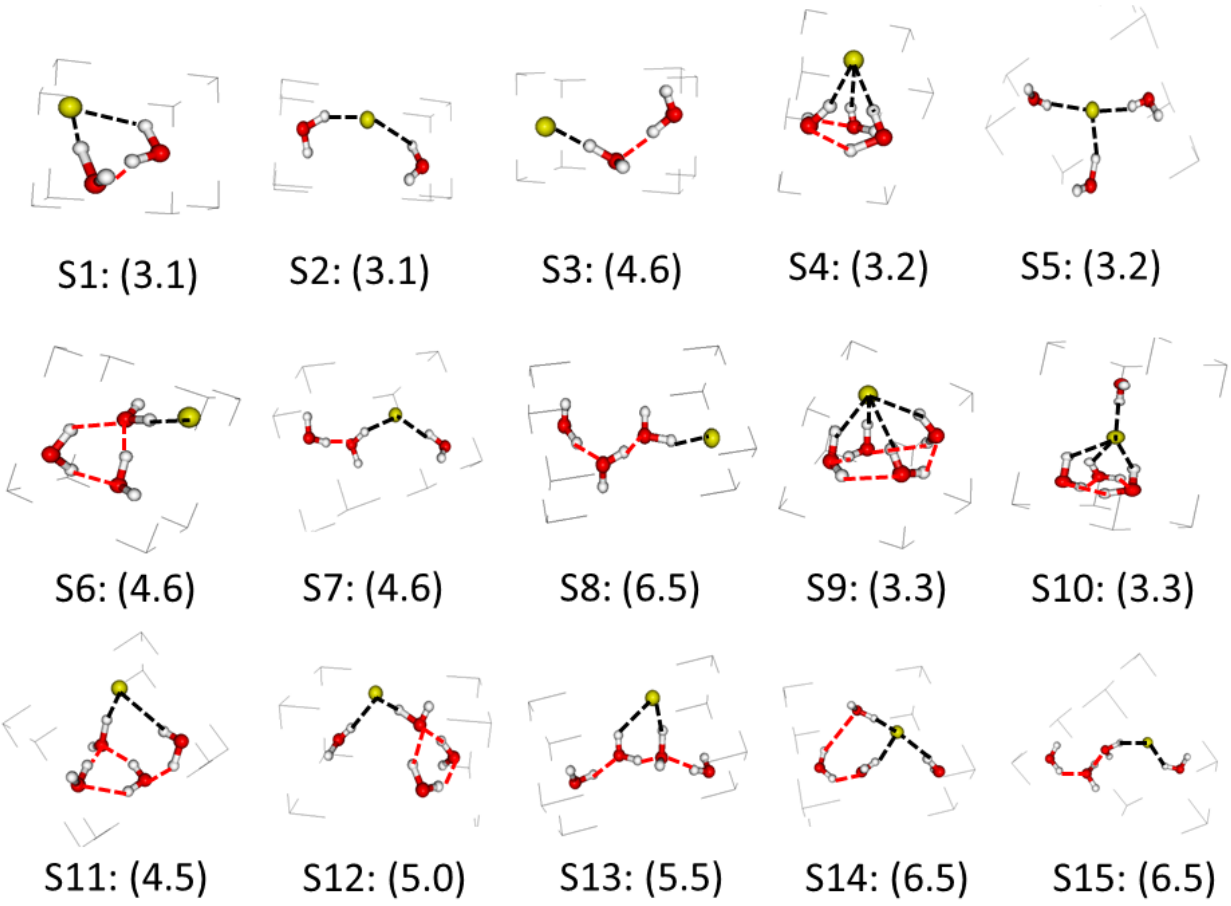

Figure 4-5. Schematically illustrations of $Cl^-(H_2O)_{2\text{-}4}$ structures (S1-S15) with respect to the r^l(Cl…O) coordinates. The bond distances are presented in the parentheses (in Angstrom). The ion-water and water-water hydrogen bond interactions are shown in black and red dot lines, respectively.

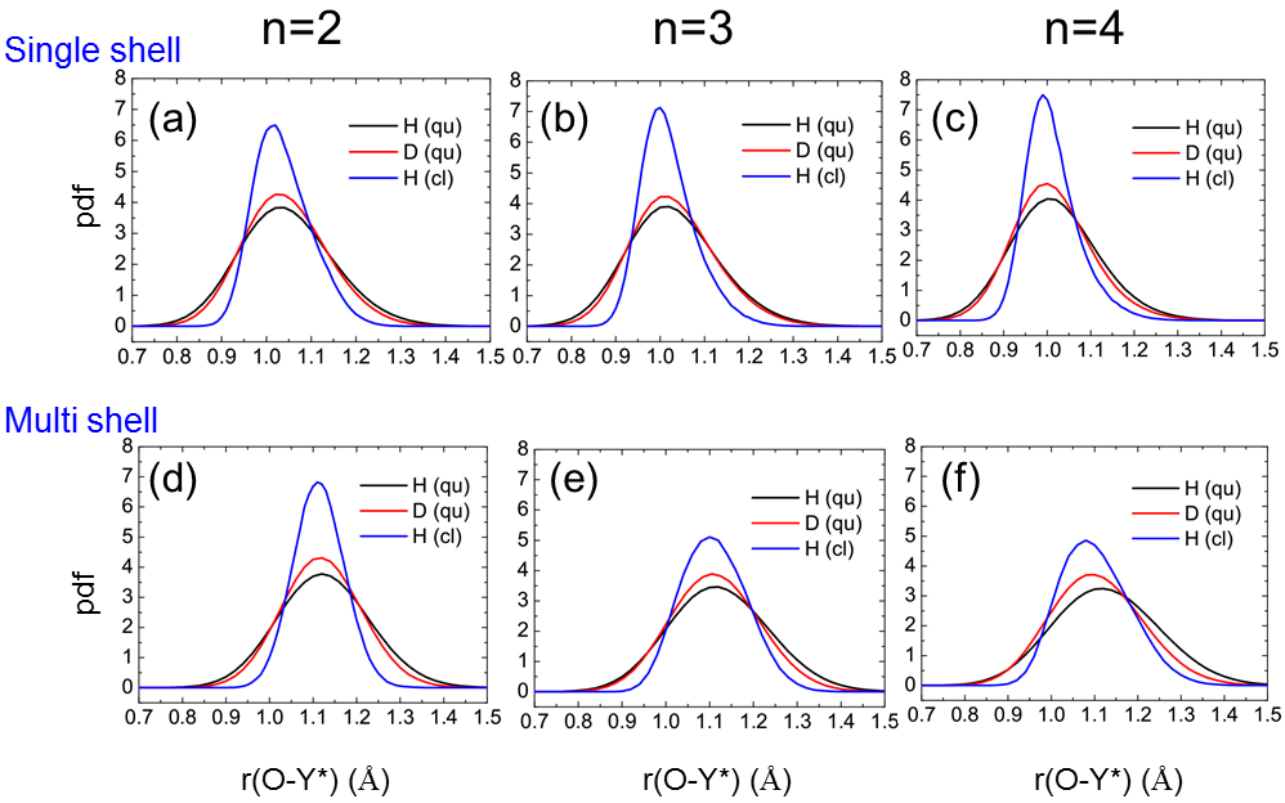

Figure 4-6. Probability distribution functions of r(O-Y*) coordinates (r(O-Y*) stretching motion) for (a)-(c)single shell structures; (d)-(f)multi shell structures. The black, red and blue lines represent quantum H, quantum D and classical H simulations, respectively.

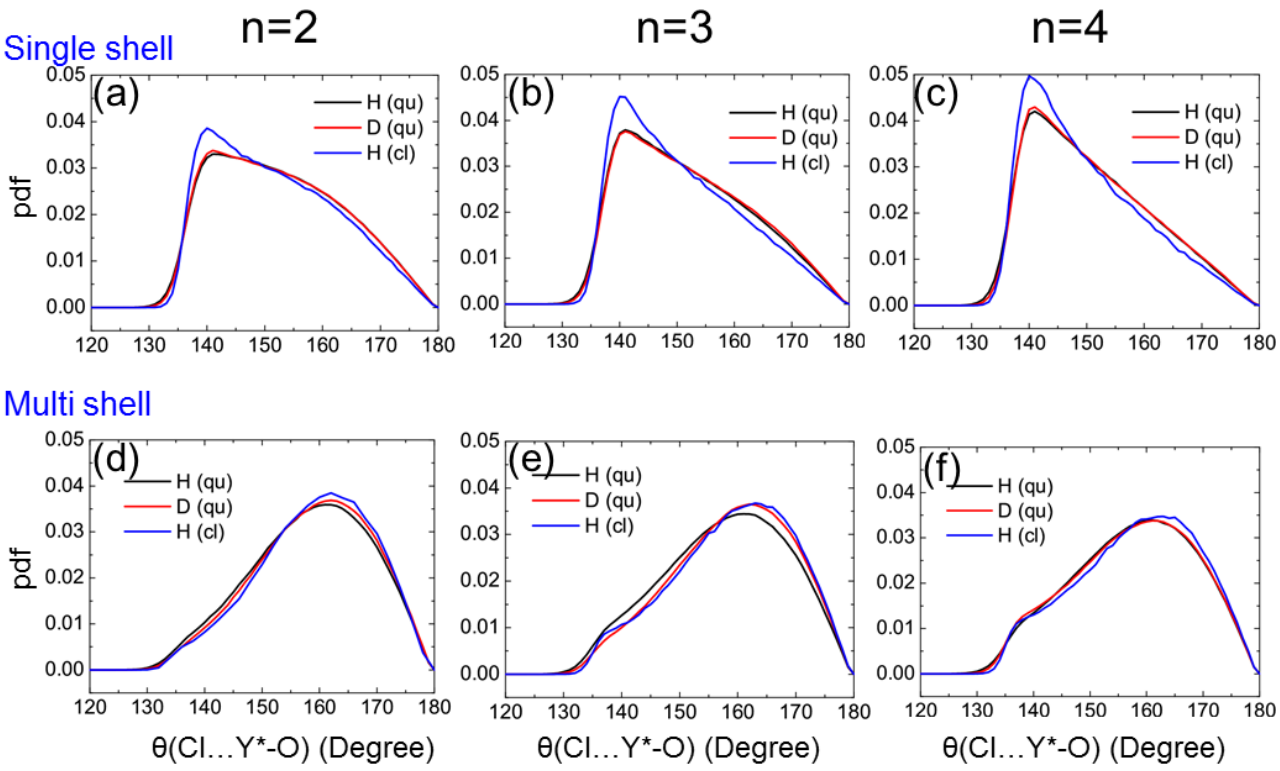

Figure 4-7. Probability distribution functions of θ(Cl…Y*-O) coordinates (ion-water wagging motion) for (a)-(c)single shell structures; (d)-(f)multi shell structures. The black, red and blue lines represent quantum H, quantum D and classical H simulations, respectively.

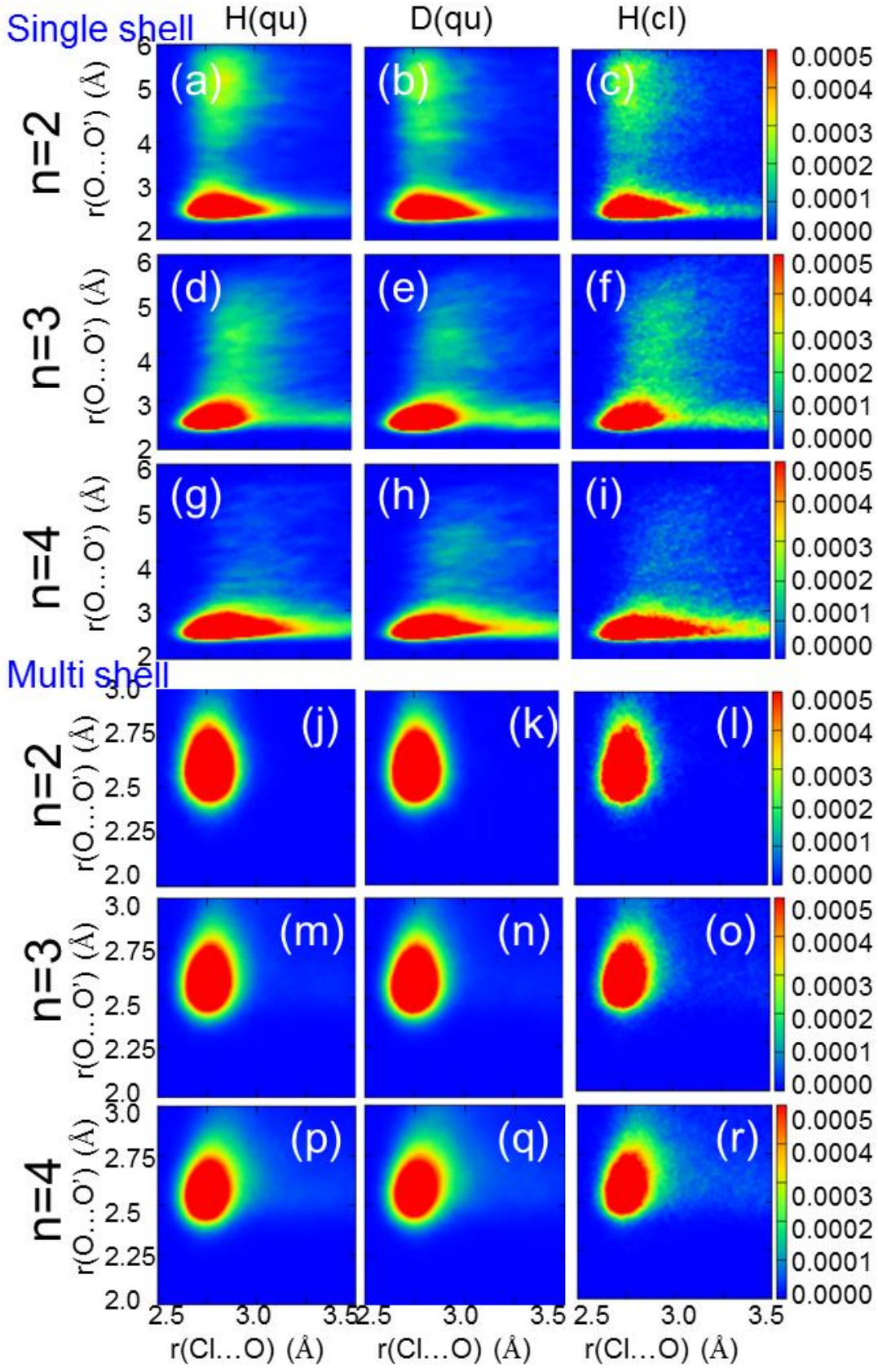

Figure 4-8. Correlations between the r(Cl…O) and r(O…O') coordinates. (a)-(i) and (j)-(r) show the results for single shell and multi shell structures, respectively.

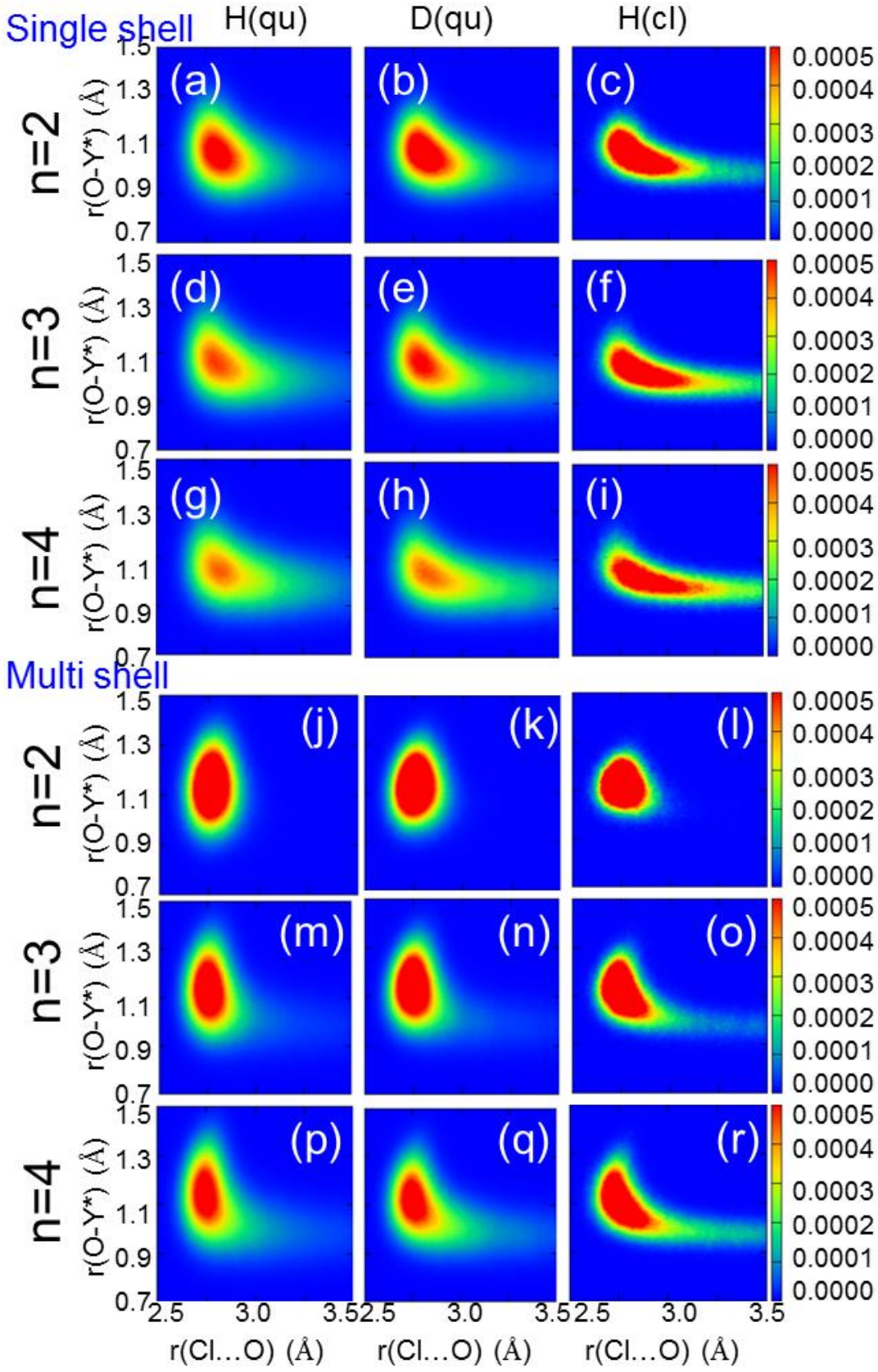

Figure 4-9. Correlations between the r(Cl…O) and r(O-Y*) coordinates. (a)-(i) and (j)-(r) show the results for single shell and multi shell structures, respectively.

Chapter 5. Conclusion

The understanding of ion solvation is an important subject for both chemical and biological science. The cooperation and competition of ionic hydrogen bonds and conventional water-water hydrogen bonds is a central issue due to its ubiquitous existence in nature. It is well known that the hydrogen bonds also play important roles in the structure of bio-molecules as well as the charged water clusters. However, the conventional MO calculations do not take into account of the nuclear quantum effects or geometric isotope effects, which are especially important in hydrogen bonded systems due to the small mass of hydrogen atom. To treat the hydrogen bonded systems with the nuclear quantum effects and the geometric isotope effects at finite temperature, the PIMD simulations were applied to obtain the quantum nature of hydrogen bonding.

In this thesis, I analyzed the nuclear quantum effects and geometric isotope effects on the structures of small halide-ion-water clusters with classical MD and PIMD simulations.

In the chapter 2, I utilized several semi-empirical methods to obtain the structures and stabilization energies of $X^-(H_2O)_n$ (X=F, Cl, n=1-4) clusters, which are compared with high-level *ab initio*/DFT MO results. The results show that the recently developed PM6-DH+ semi-empirical method can provide reasonable binding energies of hydrated fluoride and chloride ion clusters. The PM6-DH+ semi-empirical results are consistent stabilization energies with the corresponding experiments, and they dramatically reduce the calculation time. For the optimized geometries of X=F, however, the semi-empirical methods show that the global minima are close to $HF(OH)^-(H_2O)_{n-1}$ structures, which are different from *ab initio*/DFT calculations. Meanwhile, the topological characteristics for the global minima of X=Cl obtained by semi-empirical methods have the same symmetries with *ab initio* calculations, which take C_s, C_1, C_3 and C_4 symmetries for n=1-4, respectively. As the number of water molecules increases, the ionic hydrogen bond strength becomes weaker for $X^-(H_2O)_n$ clusters. The ionic hydrogen bond strength of fluoride cluster is stronger than that of chloride cluster with similar geometry. It is found that the emergence of the second hydration shell enhances the ionic hydrogen bond strengths, comparing with the structure that is without the additional water molecular. Meanwhile, I have reported new stable structure of $Cl^-(H_2O)_4$ with the second hydration shell. Based on the above results, thus, it is reasonable to use PM6-DH+ semi-empirical potential

for chloride ion water clusters in the following classical MD and PIMD simulations.

In the chapter 3, I examined the nuclear quantum effects on the ionic hydrogen bonded structures of $Cl^-(H_2O)_{1-4}$ clusters by carrying out classical MD and PIMD simulations. An outer shell coordinate r^l(Cl…O) is picked out to distinguish the single and multi shell structures and to display the rearrangement of the cluster structures. The proportion of the multi shell structures increases with the cluster size. By incorporating the nuclear quantum effects, it is shown that the probability for single hydration shell structures is decreased while the probability for multi shell structures is increased. As the cluster size increases, it is interesting to find that the ionic hydrogen bond strength in the first hydration shell increases. The results are due to the rising corporation of ion-water and water-water hydrogen bond interactions. Meanwhile, an asymptotic value of ionic hydrogen bond strength in the first shell could be expected for larger cluster size. On the contrary, the ionic hydrogen bond strength for single shell structures decreases with the cluster size. On the other hand, the correlations between changing of bonded H* atom to chloride ion and other cluster coordinates are presented. The results show that δ strongly correlates with proton transfer motion while it has little correlation with ion-water stretching motion. The results indicate that the frequency of δ is comparable to proton transfer motion while it is much faster than ion-water stretching motion. Besides, on the contrary to θ(H-O-H*) coordinate, the correlations between δ and other coordinates are all decreased by inclusion of the nuclear quantum effects. The results indicate that the vibration motions affected by the ion are weakened by the nuclear quantum effects, which results from the preference of water-water hydrogen bond interactions by PIMD simulation.

In the chapter 4, I examined the geometric isotope effects on ionic hydrogen bonded $Cl^-(H_2O)_{1-4}$ clusters for the single and multi shell structures, respectively. As the cluster size increases, the proportion of the multi shell structures increases, which indicates the increasing preference of surface solvation of Cl^-. The results show that the H(cl) and D(qu) take the highest proportion for single and multi shell structures, respectively. Due to H/D isotope substitution, both ion-water and water-water hydrogen bonds are weakened. Since the decrease of ion-water hydrogen bond strength is relative larger, the D(qu) results tend to favor the water-water hydrogen bond interactions. To show the competitive intramolecular and intermolecular nuclear quantum effects, the r(O-Y*) stretching and ion-water wagging motions are studied in single shell and multi shell structures, respectively. The r(O-Y*) distances shrink in the sequence of H(qu), D(qu) and H(cl) for

both single and multi shell structures. The results indicate that intramolecular nuclear quantum effects tend to stabilize the water-water hydrogen bond network for both single and multi shell structures. On the other hand, the θ(Cl…Y*-O) angles become smaller/larger for single/multi shell structures in the sequence of H(qu), D(qu) and H(cl). The results indicate that the intermolecular nuclear quantum effects stabilize the ionic hydrogen bonds in single shell structures, however, the ionic hydrogen bonds in multi shell structures are destabilized due to the competition of intramolecular and intramolecular nuclear quantum effects. In addition, the correlations between ion-water stretching motion and other cluster vibration coordinates are discussed. The results indicate that the intermolecular nuclear quantum effects on the cluster structures are strongly related to the cooperation of the water-water hydrogen bond interactions.

The PIMD simulations clearly show the nuclear quantum effects and geometric isotope effects of small halide-ion-water clusters at finite temperature. The PIMD method is a powerful tool to study the quantum nature of hydrogen bonded systems. I expect that the PIMD method contributes the understanding and progress in chemistry, physics as well as other interdisciplinary fields.

List of Publications

[1] Q. Wang, K. Suzuki, U. Nagashima, M. Tachikawa, S. Yan, Semiempirical Investigations on the Stabilization Energies and Ionic Hydrogen-Bonded Structures of $F^-(H_2O)_n$ and $Cl^-(H_2O)_n$ (n = 1-4) Clusters, J. Theor. Appl. Phys. 2013, 7, 7.

[2] Q. Wang, K. Suzuki, U. Nagashima, M. Tachikawa, S. Yan, Path Integral Molecular Dynamic Study of Nuclear Quantum Effect on Small Chloride Water Clusters of $Cl^-(H_2O)_{1\text{-}4}$, Chem. Phys. 2013, http://dx.doi.org/10.1016/j.chemphys.2013.02.025.

[3] Q. Wang, K. Suzuki, U. Nagashima, M. Tachikawa, S. Yan, Geometric Isotope Effects on Small Chloride Ion Water Clusters with Path Integral Molecular Dynamics Simulations, submitted to Chem. Phys.

Acknowledgements

The content in this dissertation summarizes my research from 2010 to 2013 at Department of Chemistry, Graduate School of Pure and Applied Sciences, University of Tsukuba, under the direction of Professor (Cooperative Graduate School Program) Umpei Nagashima at Research Institute for Computational Sciences, National Institute of Advanced Industrial Science and Technology (AIST).

First of all, I would like to express my great appreciation for Prof. Umpei Nagashima and all the professors in Department of Chemistry, Graduate School of Pure and Applied Sciences, University of Tsukuba to offer me such a precious opportunity for taking the Doctoral course.

I express my sincere gratitude to Prof. Umpei Nagashima for his thoughtful, patient, and hearty guidance over the three years. Under his guidance, I have received a good training and gained much in my academic sense. I was the most precious experience for me to be able to conduct research guided by his belief in science.

I am deeply grateful to Dr. Kimichi Suzuki at Research Institute for Computational Sciences, AIST for his guidance and continuous encouragement during my phD program. It is his hearty and excellent intellectual support that helps me with the dissertation.

I am extremely grateful to Prof. Mosanori Tachikawa at Quantum Chemistry Division, Graduate School of Science, Yokohama-City University for precious valuable academic advice and his hearty support. I also thank all of the members of Tachikawa group for the valuable and helpful discussions through group meetings. I would like to thank Ms. Haruko Takeshi for her assistance to my research activities in AIST.

I am also extremely indebted to Prof. Shiwei Yan at College of Nuclear Science and Technology, Beijing Normal University for his helpful suggestions of my research activities. I also thank all of the members of Yan group for the valuable discussions.

I thank to the financial support from the program of China Scholarships Council.

Finally, I am grateful to my parents Mr. Jingli Wang and Ms. Xiaoxia An for their patience and great understanding during the course of my phD program.

May 2013

Qi Wang

_____